



The  
University  
Of  
Sheffield.

# Time-dependent Resonant Damping in Coronal Loops

Alastair Williamson

Submitted for the degree of Doctor of  
Philosophy

School of Mathematics and Statistics

December 2, 2013

Supervisor: Róbertus von Fáy-Siebenbürgen

University of Sheffield



## ACKNOWLEDGEMENTS

I would like to thank my supervisor, Professor R. von Fáy-Siebenbürgen, for his help in guiding me through my PhD and for his invaluable support whilst writing my thesis.

I am also grateful to Prof. M. Ruderman for the help and advice given throughout the last 3 years.

I would also like to thank, for encouragement and general support, my family, friends and colleagues inside the department: Dad, Ben, Pete, Mark, Amy, Sam, Amy, Elizabeth, Ben, the H23a,c people and the Progress group. I would lastly like to thank my Mother who supported me throughout the years, but unfortunately did not get to see me make it to this point.

Thank you to everybody.

## ABSTRACT

This Thesis will extend the current theory of propagating, linear MHD waves into a cylindrical model containing a time-dependent background density. The current observations of propagating waves in the solar corona clearly show that the magnetic waveguides contain many time-dependent features which have, to date, been excluded from the majority of theoretical models investigating MHD wave propagation. Analysing a straight magnetic flux tube, to leading order in the WKB approximation, allows for the derivation of two governing equations describing the perturbed total pressure and the radial displacement. These governing equations allow for the formation of the general dispersion relation and, taking the thin-tube limit, a full expression for the wave phase can be determined. Using the wave phase, it is possible to calculate the dynamic frequency, dynamic wavenumber and amplitude of the various wave modes and then the temporal evolution of these quantities can be explored. By introducing a thin annular layer, smoothly joining the interior and exterior of the flux tube, an investigation into the resonant damping of the propagating MHD waves can be conducted. Analytical expressions for the resonant jump conditions and the damping coefficient for the fast MHD wave can be found and their temporal evolution explored.

# Contents

<b>1</b>	<b>Introduction</b>	<b>1</b>
1.1	Introduction to the Solar Atmosphere . . . . .	1
1.1.1	Solar Atmosphere . . . . .	1
1.2	Various Formations in the Solar Atmosphere . . . . .	4
1.2.1	Coronal Loops . . . . .	4
1.2.2	Prominences . . . . .	5
1.2.3	Coronal Holes . . . . .	7
1.3	Introduction to MHD . . . . .	8
1.3.1	MHD Equations . . . . .	9
1.3.2	Perturbation Theory . . . . .	13
1.4	Introduction to Linear MHD waves . . . . .	13
1.4.1	Wave in a Uniform Plasma . . . . .	14
1.4.2	Wave Propagation in Cylindrical Flux Tube . . . . .	17
1.4.3	Overview of Current Research . . . . .	22
1.5	Introduction to Resonant Absorption . . . . .	23
1.5.1	Resonance in the Alfvén Continuum . . . . .	25
1.5.2	Resonance in the Slow Continuum . . . . .	27
1.6	Wave Dissipation . . . . .	29
1.6.1	Overview of Resonant Absorption Investigations . . . . .	30
1.7	The WKB Approximation . . . . .	32
1.7.1	Introduction to WKB Analysis . . . . .	32
1.7.2	Example of the WKB Approximation . . . . .	34
1.7.3	WKB Approximation . . . . .	36
<b>2</b>	<b>MHD Wave Propagation in a Zero-beta Dynamic Plasma</b>	<b>37</b>
2.1	Introduction . . . . .	37
2.2	The Governing Equations . . . . .	38
2.3	Over-dense Loop Approximation . . . . .	41
2.3.1	Amplitude of the fast MHD wave . . . . .	44
2.3.2	Temporal Dependency of Individual Wave Modes . . . . .	44
2.3.3	Spatial Dependency of Wave Modes . . . . .	46

2.3.4	Increasing Density . . . . .	47
2.4	Moderate-Activity Approximation . . . . .	47
2.4.1	Temporal Evolution of the Individual Wave Modes . . . . .	52
2.5	Conclusion . . . . .	53
<b>3</b>	<b>MHD Wave Propagation in a Finite Plasma-beta</b>	<b>56</b>
3.1	Introduction . . . . .	56
3.2	Background Plasma . . . . .	57
3.3	Governing Equations . . . . .	58
3.4	Fast Wave Propagation . . . . .	61
3.4.1	Over-Dense Loop Approximation . . . . .	61
3.4.2	Moderate-Activity Approximation . . . . .	62
3.5	Slow Wave Propagation . . . . .	63
3.6	Conclusion . . . . .	65
<b>4</b>	<b>Leaky Wave Propagation in a Zero-beta Dynamic Plasma</b>	<b>67</b>
4.1	Introduction . . . . .	67
4.2	Introduction to leaky waves . . . . .	68
4.3	Governing Equations . . . . .	70
4.4	Leaky Wave Solution . . . . .	72
4.5	Conclusions . . . . .	78
<b>5</b>	<b>Resonant Damping of MHD Waves in a Zero-beta Plasma</b>	<b>81</b>
5.1	Introduction . . . . .	81
5.2	Governing Equations . . . . .	82
5.3	Evaluation around the Alfvén Resonant Point . . . . .	84
5.4	Wave Dissipation . . . . .	88
5.5	Resonance in the Moderate-Activity Approximation . . . . .	90
5.6	Conclusions . . . . .	92
<b>6</b>	<b>Resonant Damping of MHD Waves in a Finite Plasma-beta</b>	<b>94</b>
6.1	Introduction . . . . .	94
6.2	Background . . . . .	95
6.3	Governing Equations . . . . .	96
6.4	Alfvén Resonance . . . . .	97
6.5	Slow Resonance . . . . .	99
6.6	Dissipative Layer . . . . .	100
6.7	Conclusion . . . . .	101

<b>7 Discussion and Further Work</b>	<b>103</b>
7.1 Overview of Thesis and Summary of Results . . . . .	103
7.2 Further Work . . . . .	105
<b>Appendix A- SGRH Method of Asymptotics</b>	<b>108</b>
<b>Appendix B- Slab Geometry</b>	<b>113</b>
7.3 Background Geometry . . . . .	113
7.4 Application of the WKB Approximation . . . . .	114
7.5 Analysis of Kink Wave Mode with Different $k_y$ . . . . .	115
7.5.1 $k_y = 0$ . . . . .	116
7.5.2 $k_y \neq 0$ . . . . .	116
7.5.3 Solution Attempt . . . . .	117
<b>Appendix C-Application of the WKB Approximation</b>	<b>118</b>
<b>Bibliography</b>	<b>120</b>

# List of Figures

1.1	SDO/HMI magnetogram of the magnetic field in the photosphere. Image taken on 27th August 2011. Courtesy of NASA/SDO and the AIA, EVE, and HMI science teams. . . . .	4
1.2	This image of coronal loops over the eastern limb of the Sun was taken in the TRACE 171 pass band, characteristic of plasma at 1 MK, on November 6, 1999, at 02:30 UT. Image credit: TRACE Team, NASA . . . . .	6
1.3	Large, eruptive prominence in He II at $304\text{\AA}$ , with an image of the Earth added for size comparison. (Courtesy of SOHO consortium. SOHO is an international cooperation project between ESA and NASA.) . . . . .	7
1.4	Elongated coronal hole as observed on 27 <sup>th</sup> December 2005. Courtesy of NASA/SDO and the AIA, EVE, and HMI science teams. . . . .	7
2.1	$\Omega/\omega$ plotted for characteristic change periods ( $t/\tau_\rho$ ) against characteristic flow speeds ( $V_{0z}/V_{A0}$ ). . . . .	42
2.2	$K/K_0$ ( $K_0 = K(t = 0)$ ) plotted for characteristic change periods ( $t/\tau_\rho$ ) against characteristic flow speeds ( $V_{0z}/V_{A0}$ ). . . . .	43
2.3	Relative change in wave amplitude of the fast MHD kink waves for a fixed loop radius ( $R = 1/K_0$ ). . . . .	46
2.4	Relative change in wave amplitude of the $m = 2$ wave for a fixed loop radius ( $R = 1/K_0$ ). . . . .	47
2.5	Temporal evolution of the wave frequency under the moderate activity approximation. All quantities are the same as detailed in Figure 2.1. . . . .	50
2.6	Temporal evolution of the vertical wavenumber under the moderate activity approximation. All quantities are the same as detailed in Figure 2.2. . . . .	51
2.7	Relative change in the amplitude of the fast, $m = 1$ , MHD wave under the moderate activity approximation. . . . .	53

2.8	Relative change in the amplitude of the fast, $m = 2$ , MHD wave under the moderate activity approximation. . . . .	54
4.1	Dynamic frequency of propagating leaky waves. All quantities have the same description as given in Figure 2.1. . . . .	75
4.2	Dynamic wavenumber of propagating leaky waves. All quantities have the same description as given in Figure 2.2. . . . .	76
4.3	Relative change in the amplitude of the propagating $m = 1$ body waves. . . . .	77
4.4	Relative change in the amplitude of the propagating $m = 2$ body wave. . . . .	78
4.5	Evolution of dimensionless damping coefficient, i.e. $\gamma/\gamma(t = 0, z = 0)$ . . . . .	79
4.6	Damping coefficient in a static system plotted against density ratio. 80	
5.1	Evolution of the width of the dimensionless dissipative layer, i.e. $\delta_A/\delta_A(t = 0, z = 0)$ . . . . .	86
5.2	Evolution of the jump across the Alfvén resonant point as a function in time . . . . .	87
5.3	The evolution of the dimensionless wave dissipation, i.e. $\gamma/\gamma(t = 0, z = 0)$ . . . . .	89
5.4	Jump condition under the moderate-activity approximation . . .	90
5.5	Evolution of the width of the dissipative layer under the moderate-activity approximation. . . . .	91
5.6	Evolution of the dimensionless dissipation coefficient under the moderate-activity approximation. . . . .	92
6.1	Evolution of the dimensionless dissipative layer, $\delta_c/\delta_c(t = 0, z = 0)$ . 101	



# Chapter 1

## Introduction

### 1.1 Introduction to the Solar Atmosphere

#### 1.1.1 Solar Atmosphere

The solar atmosphere, and more specifically the solar corona, is an area containing high concentrations of magnetic field and plasma flow activity and as such has been a plentiful source of research areas into the nature of not only the Sun, but into magnetically dominated plasma-phenomenon in many astrophysical plasmas. The corona, as the one of the more easily observable astrophysical plasmas, gives a great deal of insight into how magnetic fields alter the flow of plasma and the energy transfer as a result of disturbances within the many and varied magnetic structures. The highly dynamic magnetic fields give rise to many structures within the corona of which the loop-like structures, that are anchored at the photosphere, will be the main, but not only, magnetic formation considered within this Thesis. Figure 1.1 highlights a small fraction of the activity that can be seen within the solar atmosphere and can only hint and the complexity of these events.

The density profile across the solar atmosphere is of paramount importance for the work that is to follow. The large density gradients created by the presence of the magnetically dominated structures give rise to the resonant damping of the propagating MHD waves, as considered later in this work. Now, we can evaluate the general form of the solar atmosphere, i.e. in the absence of the

magnetic structures, various properties of the solar atmosphere arise and can be evaluated. It can also be noted that the magnetic structures share many of these physical properties, e.g. gravitational stratification. However, several of the physical parameters are very different from the general background and will be discussed separately in Section 1.2. We can deduce that the density is stratified due to the gravitational effect of the Sun and hence different regions, where the variation in the physical parameters follow specific trends, can be defined for the purposes of further investigation. At the base of the solar atmosphere is the photosphere and is considered to be the outer surface of the Sun. The photosphere is kinetic pressure-dominated, i.e. the thermal pressure is much greater than the magnetic pressure (this ratio is referred to as the plasma-beta of the system). As a result much of the fluid flows take place under an approximately hydro-dynamic model with a small magnetically driven change. Above the photosphere is the chromosphere, a region of much lower density and a region where the magnetic and kinetic pressure forces are approximately equal (i.e, the plasma-beta is approximately 1). However, one of the more interesting aspects of the chromosphere is the increase in temperature with height above the photosphere, such an increase in temperature has posed one of the greatest problems in solar physics especially when considered in conjunction with a similar manner of temperature increase in the corona. Above the chromosphere is a thin layer known as the transition region where the magnetically generated forces, i.e. the magnetic pressure begins to dominate the thermal pressure and the rise in the temperature is extremely large. Investigations into modelling the transition region have not been as common as those that have taken place with regard to the photosphere, chromosphere and corona and hence this area is not well understood in comparison to other regions in the solar atmosphere. The last region of the solar atmosphere, and the region of greatest interest with respect to this Thesis, is the corona. Density levels within the corona are very low when compared to the other levels within the solar atmosphere, yet this region also contains the highest temperature. A table of typical values for the main physical parameters in the solar atmosphere is given in table (1.1).

The variation in temperature across the corona is an important part of the *coronal heating problem* and has occupied many researchers since its discovery,

Table 1.1: Approximate values of physical quantities at various points in the solar atmosphere.

Parameter	Photosphere	Chromosphere	Corona
Density ( $cm^{-3}$ )	$10^{23}$	$10^{15}$	$10^{12}$
Temperature (K)	$6 \times 10^3$	$25 \times 10^3$	$5 \times 10^6$
Magnetic Field (G)	500	50	10

therefore means of energy transport and release through and into the corona is of interest to many people. There are many competing theories of energy release into the corona, the two most common theories are magnetic reconnection and the damping of magnetohydrodynamic (MHD) waves. Magnetic reconnection is not under consideration here and will not be expanded upon further, however, an overview of the coronal heating problem is given by e.g. Erdélyi and Ballai (2007), Parnell and De Moortel (2012). Whilst the MHD waves are the main focus of the work, the heating (and therefore energy flux) associated with these waves will not be considered further, instead this work will focus upon the analytical forward modelling of these oscillations.

The dynamic nature of the magnetic field within the corona introduces continuous changes to the structures found therein. Many of the structures last for minutes whilst others have lifetimes of the order of days or even months. These temporal variations in the corona make the analysis of observational data more difficult. The work performed in this Thesis is a first step into creating analytical dynamic models that can improve our understanding of the current data. For the structures with large life-times equilibrium models are very good approximations to the true activity taking place within these structures. The shorter the lifetime, however, the less accurate these equilibrium models become, attempts into modelling these temporally varying structures has so far been limited.

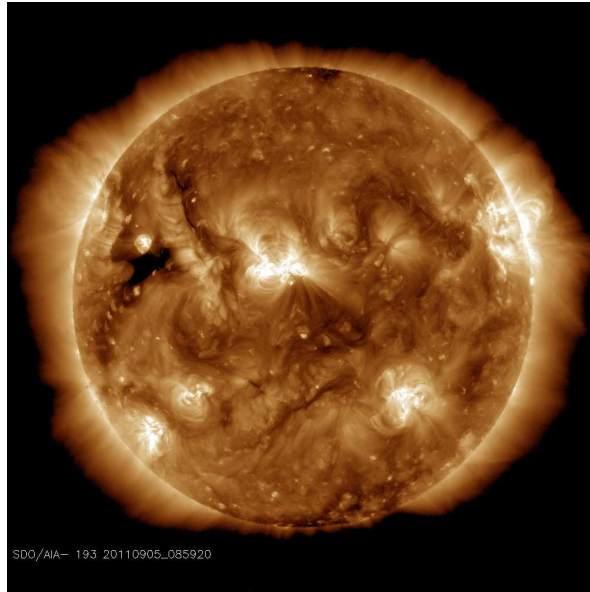


Figure 1.1: SDO/HMI magnetogram of the magnetic field in the photosphere. Image taken on 27th August 2011. Courtesy of NASA/SDO and the AIA, EVE, and HMI science teams.

## 1.2 Various Formations in the Solar Atmosphere

In this section we discuss a small number of the magnetic structures found in the solar atmosphere, the most important of which is the context of this Thesis is the coronal loop. Other structures are discussed in order to give a general background and for their possible use as an extension to the work done in this Thesis.

### 1.2.1 Coronal Loops

The magnetic structure known as the coronal loop is one of the most numerous and widely studied structures found in the solar corona, Figure (1.2) shows an image provided by the TRACE satellite displaying one of the clearest images of a series of loops in the solar atmosphere. Coronal loops are anchored, at their foot points, to the photosphere and consist of closed magnetic field lines stretching high into the solar atmosphere. This plasma is tied to these field lines through the ‘frozen in’ condition, discussed in Section 1.3.1 below, en-

abling us to observe these loops and hence gain further information on the Sun and solar atmosphere in general. The plasma within the loop is estimated to have a temperature of approximately  $2.5 \times 10^6 \text{K}$  with very little variation due to density, the density itself has been measured and found to be in the region of  $5 \times 10^{-14} \text{m}^{-3}$  to  $5 \times 10^{-15} \text{m}^{-3}$ , many times that of the typical coronal density (all values as stated by Aschwanden (2004)).

Since these closed loops are anchored in the photosphere, the change in the exterior atmosphere as they travel through the chromosphere and the corona necessarily implies that the structure of the loop, and the plasma tied to the field lines, must change as well. These inhomogeneities in coronal loops make the act of solar atmospheric magneto-seismology, determining various physical quantities from the observed properties of MHD waves, very difficult. The forward-modelling (determination of physical quantities for a theoretical investigation) of such loops is, therefore, of great importance to those who wish to gain further information on the composition and the activities within the corona. Of the various motions within the corona, the most relevant to this Thesis are the wave-like motion observed throughout the solar atmosphere. An overview of the current investigations into the modelling of the oscillations within coronal loops is given in Section 1.4.3 and an review of the observational evidence for these waves is given by e.g. Aschwanden and Title (2004), Nakariakov and Verwichte (2005) or De Moortel and Nakariakov (2012).

### 1.2.2 Prominences

A prominence is a highly dense structure high in the solar atmosphere consisting of plasma that is at a much lower temperature than the surrounding atmosphere. Prominences generally fall into one of two categories, active or quiescent, depending on the magnitude of the lifespan of the prominence. Active prominences generally contain highly dynamic events that may well result in large density losses through e.g. a Coronal Mass Ejection (CME), and, hence, dramatically reduce the lifespan of the prominence. In contrast, a quiescent prominence may well exist for a timescale of the order of several months which provides many questions about their continued stability. Figure 1.3 shows a



Figure 1.2: This image of coronal loops over the eastern limb of the Sun was taken in the TRACE 171 pass band, characteristic of plasma at 1 MK, on November 6, 1999, at 02:30 UT. Image credit: TRACE Team, NASA

large prominence as seen by SoHo and gives an indication of the size of these structures in relation to the others discussed here.

Quiescent prominences have a density of approximately  $10^{16} - 10^{17} \text{m}^{-3}$  with internal temperatures between 3000 – 6000K. Such values and the slowly changing nature of the prominence make such structures ideal candidates for an extension of the work and analysis performed within this Thesis. A review of the observational evidence for oscillations in prominences and the theoretical model associated with these oscillations is given by Arregui et al. (2012).

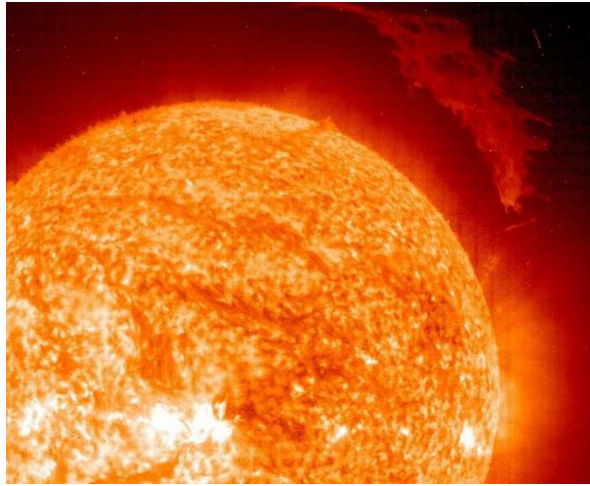


Figure 1.3: Large, eruptive prominence in He II at  $304\text{\AA}$ , with an image of the Earth added for size comparison. (Courtesy of SOHO consortium. SOHO is an international cooperation project between ESA and NASA.)

### 1.2.3 Coronal Holes

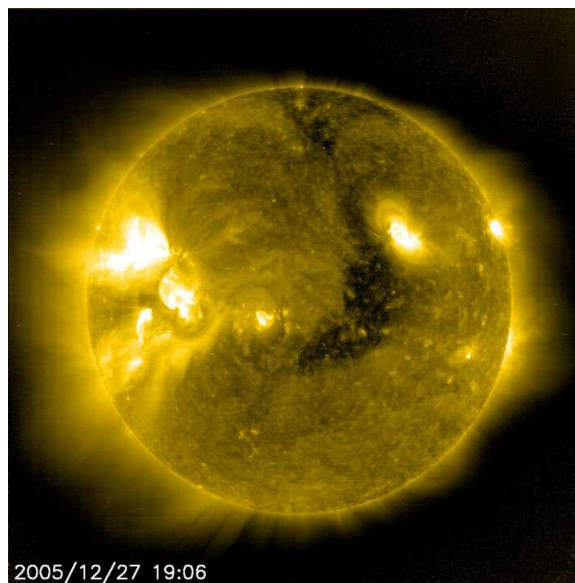


Figure 1.4: Elongated coronal hole as observed on  $27^{\text{th}}$  December 2005. Courtesy of NASA/SDO and the AIA, EVE, and HMI science teams.

Coronal holes are regions on the solar surface where an open magnetic field stretches out through the corona into open space. In order to ensure that no magnetic monopoles exist (i.e.  $\nabla \cdot \mathbf{B} = 0$ , see Section 1.3.1) the field lines are assumed to close beyond the solar atmosphere. The open field lines allow high velocity plasma to escape the solar atmosphere and, hence, is the source of the fast solar wind. Within these regions the density and temperature are of the order of three times less than the surrounding atmosphere and, as a result, is of interest in the study of oscillations where energy is lost to the surrounding atmosphere, see Chapter 4 for further details. Coronal holes are typically found at the northern and southern poles of the Sun, however, at the solar maximum they can occur at most point on the solar surface. The large, dark region in Figure 1.4 is a coronal hole that was observed in late 2005 and is one the largest coronal holes to have been detected. A review of the current observations of propagating MHD waves in coronal loops is given by Banerjee et al. (2011).

### 1.3 Introduction to MHD

Magnetohydrodynamics (MHD) is the the study of how the presence of a magnetic field influences the flow of a highly ionised fluid. A combination of the equations of fluid dynamics and Maxwell's equations of electromagnetism allows for a description of the bulk plasma flow, a plasma is here defined as a continuous fluid with a high level of ionisation. The derivation of Maxwell's equations of electromagnetism from first principles as well as the continued derivation of the equation of MHD are not considered here and can be found in many previous works, e.g. Goossens (2003) or Goedbloed and Poedts (2004).

Whilst the MHD equations are a very good description of magnetically influenced fluid flows, there are a number of potential areas where MHD can be considered to be a potentially flawed investigative tool. Whilst these problems are (in general) not applicable to MHD within the solar atmosphere, and MHD waves observed currently, they do give an indication into limitations of MHD applications in other research areas and physical applications.

The first of the assumptions made in constructed the MHD equations, is that the plasma is strongly collisional, i.e. that the plasma is a perfect con-

ductor. However, it can also be assumed that the typical length and velocity scales are much greater than the Debye radius and, hence, the plasma can be assumed to move as a single fluid. Models can be built which do account for the collisional effects of electron flow and indeed there are many two, or three (neutral atoms), fluid models, see again e.g. Goedbloed and Poedts (2004). The rate of ionisation and the energy loss as a result of electrons colliding with the positively charged and neutral atoms should not be ignored in a truly accurate model. In the corona, however, the rate of ionisation is approximately 97% and as such the neutral ions can be ignored.

These are just a small sample of the problems faced by MHD in all situations, but given the conditions of the solar atmosphere the use of the MHD equations is justified in order to make mathematical investigations into the magnetically generated phenomena therein. The MHD equations, as used at all further points in this Thesis, are given below.

### 1.3.1 MHD Equations

The MHD equations relate the magnetic field vector ( $\mathbf{B}$ ), the plasma density ( $\rho$ ), plasma pressure ( $p$ ), plasma temperature ( $T$ ) and the velocity vector ( $\mathbf{V}$ ). The recurring constant  $\mu_0$  is the permeability of free space. The following equations are at the heart of the of MHD.

#### Equation of Mass Conservation

The equation of mass conservation, also known as the continuity equation, states that the volume of fluid entering a volume must be equal to the volume leaving and can be expressed as

$$\frac{\partial \rho}{\partial t} + \nabla \cdot (\rho \mathbf{V}) = 0. \quad (1.1)$$

If the fluid density is constant everywhere the equation of mass conservation reduces to

$$\nabla \cdot \mathbf{V} = 0,$$

and as such is the expression for incompressible fluids.

### Induction Equation

The induction equation, equation (1.2), can be formed by eliminating the electric field components from Maxwell's electromagnetic equations. As stated earlier, the derivation has been done in many places and will not be shown here.

$$\frac{\partial \mathbf{B}}{\partial t} = \nabla \times (\mathbf{V} \times \mathbf{B}) + \eta \nabla^2 \mathbf{B} \quad (1.2)$$

Comparing the typical length scales of the convective component,  $\nabla \times (\mathbf{V} \times \mathbf{B})$ , and the diffusive component,  $\eta \nabla^2 \mathbf{B}$ , allows us to write the dimensionless magnetic Reynolds number,  $R_m$ , where

$$R_m = \frac{vl}{\eta}.$$

$R_m$  describes the relative magnitudes of the typical velocity ( $v$ ) and length ( $l$ ) scales to the magnetic diffusivity ( $\eta$ ). Like its equivalent in fluid dynamics, the magnetic Reynolds number gives an indication of the relative importance of dissipative force within the flow of plasma. For a flow with a large magnetic Reynolds number, i.e.  $R_m \gg 1$ , the dissipation is only important on small length scales. The magnetic field can be said to be ideal when plasma flows over typical length scale are considered. This limit represents plasma which is essentially 'frozen' to the magnetic field lines and is a good approximation for MHD in the corona. The frozen in condition states that the plasma is 'tied' to the magnetic field lines and will move with the field lines when a force is applied.

### Momentum Equation

The momentum equation is a version of the Navier-Stokes Equation of Fluid Dynamics, where a magnetic force component has been included. The Navier-Stokes equation models packets of fluid (Lagrangian description) as they move under external forces. The momentum equation as most commonly used in MHD has a pressure gradient and a combination of magnetic tension and mag-

netic pressure. The momentum equation is most commonly written as

$$\rho \frac{D\mathbf{V}}{Dt} = -\nabla p + (\nabla \times \mathbf{B}) \times \frac{\mathbf{B}}{\mu_0}, \quad (1.3)$$

where the magnetic component can be rewritten as

$$(\nabla \times \mathbf{B}) \times \frac{\mathbf{B}}{\mu_0} = \frac{1}{\mu_0} (\mathbf{B} \cdot \nabla) \mathbf{B} - \nabla \left( \frac{\mathbf{B}^2}{2\mu_0} \right).$$

The first term on the right hand side represents the magnetic tension and the second term the magnetic pressure. The magnetic pressure is sometimes combined with the plasma pressure and written as

$$P = p + \frac{\mathbf{B} \cdot \mathbf{B}}{2\mu_0},$$

where  $P$  is the total pressure of the system. Equation (1.3) can therefore, with the expansion of the material derivative, be rewritten as

$$\rho_0 \left( \frac{\partial}{\partial t} + \mathbf{V} \cdot \nabla \right) \mathbf{V} = -\nabla P + \frac{1}{\mu_0} (\mathbf{B} \cdot \nabla) \mathbf{B}. \quad (1.4)$$

If any other forces, e.g. gravitational or viscous, are considered their combined effects can be included by a simple summation of the additional forces.

### Energy Equation

The energy equation relates the change in the energy contained within a volume to the presence of heat sources or sinks within the same volume. Here,  $\gamma$  is the ratio of specific heats, also called the adiabatic invariant, and  $L$  is the total heat loss function

$$\rho^\gamma \frac{D}{Dt} \left( \frac{p}{\rho^\gamma} \right) = -L, \quad (1.5)$$

$L$  represents the various heat sources and sinks within the field, usually these taking the form of energy losses through particle collisions, radiative losses or background heating. If ideal energy conservation is applied  $L = 0$  the energy

equation then reduces to

$$\frac{\partial p}{\partial t} + \mathbf{V} \cdot \nabla p = -\gamma p \nabla \cdot \mathbf{V}. \quad (1.6)$$

Equation (1.6) is the the form of the energy equation that will be used throughout the work presented here and represents an adiabatic plasma.

Viscous or dissipative effects have been neglected from this formulation of the energy equation as in ideal, or approximately ideal, MHD these effects are negligible to leading order.

### Gauss'e Law of Magnetism

Magnetic flux through a closed surface ( $A$ ), in the absence of magnetic monopoles, is a conserved quantity and as such can be expressed by

$$\int_A \mathbf{B} \cdot \mathbf{S} = 0.$$

This expression can be written in a differential form, using Gauss's theorem, as

$$\nabla \cdot \mathbf{B} = 0, \quad (1.7)$$

which will be the form of the conservation law applied hereafter.

### Ideal Gas Law

The above equations are joined by the ideal gas law of thermodynamics which relate the plasma pressure, density and temperature.

$$p = \frac{R}{\hat{\mu}} \rho T \quad (1.8)$$

In equation (1.8)  $R$  and  $\hat{\mu}$  are the gas constant and mean atomic weight respectively.

### 1.3.2 Perturbation Theory

Perturbation theory is a method of analysing a system that is disturbed from its equilibrium state. This disturbance is usually considered to be small so that the background state is not destroyed. These perturbations often give rise to wave activity in flux tubes and therefore will be used as the starting point for further calculations. The basis of perturbation theory is as follows: taking the MHD equations (1.3)-(1.8) each variable will be written in the form,

$$f \rightarrow f_0 + f_1 \text{nonumber} \quad (1.9)$$

where  $f_0$  is the background state of the system and  $f_1$  is the small perturbation.  $f_1$  is now considered to be much less than the background values, enough so that  $f_1^2$  can be classed as insignificant. Using these perturbed variables it is possible to form equations to describe wave activity within the system. To clarify the future notation, all perturbed variables will not use the subscript 1 but all background values will continue with the 0 subscript.

## 1.4 Introduction to Linear MHD waves

Perturbations in a plasma can cause variations in e.g. the density, pressure, temperature, velocity field and magnetic field. The frozen-in condition of the magnetic field in ideal MHD scenarios implies that the fluctuations in the magnetic field cause the plasma to be dragged with the magnetic field. For plasmas in which the displacement has a length-scale such that the square of the displacement can be neglected with respect to the background parameters. The periodic perturbations are called linear waves and have been the focus of much study. In the absence of gravity or a buoyancy force, waves and oscillations in the magnetic field can be divided into three distinct wave modes with three distinct propagation speeds.

Using the fundamental equations of ideal MHD as discussed in the last section it is possible to form the wave equation in a uniform magnetised plasma. In a static equilibrium the three wave modes can be most clearly determined and therefore the most logical starting point to start a review of MHD wave

theory. We note that the derivation discussed below does not represent MHD waves in a fully arbitrary system. However, it is relevant to the work performed later in this Thesis.

### 1.4.1 Wave in a Uniform Plasma

For the initial investigation into linear wave propagation we consider an infinite, uniform plasma with constant vertical magnetic field, constant plasma pressure and constant density. We assume a time-independent perturbation and as such every perturbation is proportional to  $\exp[-i\omega t]$ , thus reducing the linearised, ideal MHD equations reduce to

$$\begin{aligned} -i\omega\rho &= -\nabla \cdot (\rho_0\mathbf{V}), \\ -i\omega\mathbf{B} &= \nabla \times (\mathbf{V} \times \mathbf{B}), \\ -i\omega\rho_0\mathbf{V} &= -\nabla \left( p + \nabla \left( \frac{\mathbf{B}^2}{2\mu_0} \right) \right) + \frac{1}{\mu_0}(\mathbf{B} \cdot \nabla)\mathbf{B}, \\ -i\omega p &= -\rho_0 c^2 \nabla \cdot \mathbf{V}. \end{aligned}$$

Algebraically combining these equations for the perturbed velocity component allows for the following to be written

$$\omega(\omega^2 - (B \cdot \nabla)^2) \left( \omega^4 - (c^2 + V_A^2)\omega^2 \nabla^2 + c^2 V_A^2 \frac{\partial^2}{\partial z^2} \nabla^2 \right) \mathbf{V} = 0.$$

By expressing the spatial derivatives using Fourier decomposition (or normal mode analysis), i.e.  $\exp[i(k_x \hat{\mathbf{x}} + k_y \hat{\mathbf{y}} + k_z \hat{\mathbf{z}})]$ , where  $k_i$  is the constant wavenumber in the  $i^{\text{th}}$  direction, thus reducing the dispersion relation to

$$\omega(\omega^2 - \omega_A^2)(\omega^4 - k^2(c^2 + V_A^2)\omega^2 + k_z^2 k^2 c^2 V_A^2) = 0, \quad (1.10)$$

where

$$k = \sqrt{k_x^2 + k_y^2 + k_z^2}, \quad \omega_A = V_A k_z, \quad V_A = \sqrt{\frac{B_0^2}{\mu_0 \rho_0}}, \quad \text{and} \quad c = \sqrt{\gamma \frac{p_0}{\rho_0}},$$

are the magnitude of the wavenumbers, the Alfvén frequency, Alfvén speed and sound speed, respectively. Equation (1.10) is the dispersion relation for MHD waves in an unbounded, uniform medium. It is clear that there exist four distinct solutions to the dispersion relation (if a single propagation direction is considered), each relating to a different wave mode that can be considered separately. The most obvious solution is that where  $\omega = 0$ . This solution represents the entropy wave and is considered a null solution for the purposes of this investigation into MHD wave modes and as such only three MHD wave modes will be referred to.

The solution  $\omega = V_A k_z$  is the second solution to equation (1.10) and describes the incompressible Alfvén wave. The unit eigenvector associated with the Alfvén wave in this plasma is in the  $y$  direction and therefore the perturbations associated with Alfvén wave can be considered to purely transverse to the background magnetic field. Alfvén waves are also important in the context of solar wave theory in that they propagate independently of the plasma pressure and therefore will be present in the low-pressure regions of the solar corona.

The last two solutions are the two magneto-acoustic wave modes and the propagation frequencies are given by

$$\omega_{f,s}^2 = \frac{k^2}{2}(V_A^2 + c^2) \pm \frac{k^2}{2}\sqrt{(V_A^2 + c^2)^2 - 4\frac{V_A^2 c^2 k_z^2}{k^2}},$$

where the '+' is the fast mode and the '-' is the slow mode. The fast and slow wave modes oscillate at orthogonal angles to each other, the slow wave oscillates parallel to the field, i.e. with a unit eigenvector in the  $z$  direction and the fast wave oscillates perpendicular to the magnetic field, i.e. in the  $x$ -direction. The phase speeds of these waves can be written as

$$V_{ph}^2 = \frac{\omega^2}{k_x^2} \approx V_A^2 + c^2, \quad \text{when } k^2 = k_x^2, \text{ i.e for perpendicular propagation,}$$

for the fast MHD wave and

$$V_{ph}^2 = \frac{\omega^2}{k^2} \approx \frac{V_A^2 c^2}{c^2 + V_A^2}, \quad \text{when } k^2 = k_x^2, \text{ i.e for parallel propagation,}$$

for the slow MHD wave. We can use these results to define an Alfvén frequency and a *cusp*, or *tube*, frequency at which the Alfvén and the slow wave would propagate in an unbounded infinite medium. The squares of the Alfvén and cusp frequencies are given by

$$\omega_A^2 = V_A^2 k_z^2, \quad \omega_c^2 = \frac{V_A^2 c^2 k_z^2}{c^2 + V_A^2}.$$

The slow MHD wave has certain properties that make it of interest when analysing data from the solar corona. If the cold-plasma limit is taken, the plasma pressure,  $p_0$  tends to 0 and the slow wave ceases to exist. In a low-pressure environment, more typical of the solar corona, the slow MHD wave acts like a modified sound wave traveling within a wave guide defined by the magnetic field. The slow wave ceases to propagate within the opposite limit, when the sound speed becomes infinitely large the plasma can be considered to be incompressible and the wave frequency tends to 0.

In contrast to the slow MHD wave, the fast wave continues to propagate in the cold-plasma limit albeit at a much reduced phase speed. The fast wave frequency tends to the Alfvén frequency although continues to oscillate in an orthogonal direction to the Alfvén wave, which is itself completely unaffected by the change in plasma pressure. Equally, the fast wave propagates differently in the incompressible limit. If the sound speed is again taken to an infinite value, the fast wave would propagate at an infinite speed, whilst this is obviously an unphysical solution, the continuation of propagation is worthy of note. Given that the fast wave continues to propagate in both these limits, the wave is sometimes called the *compressible* Alfvén wave which is modified by the plasma pressure.

Whilst the basic properties of the three main wave modes are revealed in this way, physical systems are not uniform or unbounded in magnitude. A series of works by Roberts (and later with Edwin and Benz) developed mathematical models with increasing levels of sophistication in order to describe the wave propagation around regions with discontinuities in the magnetic field. The wave propagation within a cylindrical flux tube is the most relevant to the work

done in later chapters and was detailed within, Edwin and Roberts (1983b), the analysis below will follow their work.

### 1.4.2 Wave Propagation in Cylindrical Flux Tube

The following work is conducted in a cylindrical coordinate system described by  $(r, \phi, z)$  for the radial, azimuthal and vertical components. A magnetic flux tube of constant radius  $R$  is embedded in a magnetised atmosphere of constant density and plasma pressure. We now introduce a twisted component to the magnetic field, i.e.  $B_{0\phi}$  is now finite, as well as the vertical magnetic field,  $B_{0z}$ . We assume that there exists a discontinuity between all interior and exterior values allowing for a variety of propagating MHD wave modes. We will assume the presence of trapped waves only, i.e. that the wave propagation in the exterior region does not transfer energy away from the flux tube. We start from the linearised MHD equations as given previously, except now the normal mode analysis is no longer valid in the radial direction, i.e.  $\partial/\partial r \neq ik_r$ . Therefore we can write the linearised, perturbed, MHD equations as

$$\begin{aligned}\rho &= -\nabla \cdot (\rho_0 \xi), \\ \rho_0 \frac{\partial^2 \xi}{\partial t^2} &= -\nabla P + \frac{\mathbf{B}_0}{\mu_0} \cdot \nabla \mathbf{B}, \\ \mathbf{B} &= (\mathbf{B}_0 \cdot \nabla) \xi, \\ p &= -\rho_0 c^2 \nabla \cdot \xi, \\ P &= p + \frac{\mathbf{B}_0}{\mu_0} \cdot \mathbf{B}.\end{aligned}$$

Using the linearised MHD equations it is possible to write, after normal mode analysis (i.e. perturbations proportional to  $\exp[-i\omega t + m\phi + kz]$ ), two governing equations (sometimes called the Hain-Lüst Equations) by isolating the total pressure perturbation,  $P$  and the radial displacement,  $\xi_r$ . The following equations have been derived in their current form in many works, see e.g. Sakurai

et al. (1991), Tirry and Goossens (1996) or Goossens (2003),

$$D \frac{1}{r} \frac{d(r\xi_r)}{dr} = C_1 \xi_r - C_2 P, \quad (1.11)$$

and

$$D \frac{dP}{dr} = C_3 \xi_r - C_1 P, \quad (1.12)$$

where

$$\begin{aligned} D &= \rho_0(\omega^2 - \omega_A^2)(\omega^2 - \omega_c^2)(c^2 + V_A^2), \\ C_1 &= 2 \frac{B_{0\phi}^2 \omega^4}{\mu_0 r} - 2 \frac{m}{r^2} f_B B_{0\phi} (\omega^2 - \omega_c^2)(c^2 + V_A^2), \\ C_2 &= \omega^4 - (\omega^2 - \omega_c^2)(c^2 + V_A^2) \left( \frac{m^2}{r^2} + k^2 \right), \\ C_3 &= D \left[ \rho_0(\omega^2 - \omega_A^2) + 2 \frac{B_{0\phi}}{\mu_0} \frac{d}{dr} \left( \frac{B_{0\phi}}{r} \right) \right] + \\ &\quad + 4 \frac{\omega^4 B_{0\phi}^4}{\mu_0^2} - 4(\omega^2 - \omega_c^2)(c^2 + V_A^2) \frac{B_{0\phi}}{\mu_0 r^2} \omega_A^2, \\ f_B &= \mathbf{k} \cdot \mathbf{B}_0, \quad g_B = \frac{m}{r} B_{0z} - k B_{0\phi}, \quad \omega_A^2 = \frac{f_B^2}{\mu_0 \rho_0}, \end{aligned}$$

and  $m$  and  $k$  are the azimuthal and vertical wavenumbers respectively. At this point, for the discontinuous magnetic field, we exclude the singular solutions which occur when the wave frequency matches that of the Alfvén frequency,  $\omega_A$  or the cusp frequency,  $\omega_c$ . When a more realistic model is considered, i.e. a transitional region is included, these solutions become feasible and the solutions in the region of the singularities are discussed in the next section. Unless a specific form of the azimuthal magnetic field component is specified it is difficult to make analytical progress from this point. Therefore, for the rest of this section we will reduce the problem to a constant, vertical magnetic field and hence the governing equations reduce to

$$D \frac{1}{r} \frac{d(r\xi_r)}{dr} = - \left[ \omega^2 - (c^2 + V_A^2)(\omega^2 - \omega_c^2) \left( \frac{m^2}{r^2} + k^2 \right) \right] P, \quad (1.13)$$

and

$$\frac{dP}{dr} = \rho_0(\omega^2 - \omega_A^2)\xi_r. \quad (1.14)$$

We now consider the two distinct regions, the interior and exterior atmosphere. Within these regions it is possible to combine equations (1.13) and (1.14) into the following equation for the total pressure

$$\left[ \frac{d^2}{dr^2} + \frac{1}{r} \frac{d}{dr} - \left( \frac{m^2}{r^2} + m_0^2 \right) \right] P = 0.$$

If we consider the interior of the flux tube this equation has to have a solution regular at  $r = 0$ , as such we write

$$P_i = A_i \begin{cases} I_{|m|}(m_i r) & r < R, \\ J_{|m|}(n_i r) & r < R, \end{cases}$$

where  $A_i$  is a constant,  $I_m$  and  $J_m$  are Bessel functions of order  $m$ , details of which can be found in e.g. Abramowitz and Stegun (1972). Here the radial wavenumbers,  $m_i^2$  or  $n_i^2$ , is given by

$$m_i^2 = -n_i^2 = -\frac{(\omega^2 - \omega_A^2)(\omega^2 - c^2 k^2)}{(c^2 + V_A^2)(\omega^2 - \omega_c^2)}.$$

If  $m_i^2 > 0$  the resulting wave is classed as a '*surface wave*', i.e. the displacement is localised on the boundary of the flux tube and propagates along the discontinuity; for  $m_i^2 < 0$  the resulting wave is called a '*body wave*', i.e. the wave propagates throughout the medium and contains maxima at various radial points, not just at the discontinuity. In the magnetised atmosphere we require the solution to be evanescent as  $r \rightarrow \infty$ , therefore we require that

$$P_e = A_e K_m(m_e r), \quad r > R.$$

Here  $K_m$  is the modified Bessel function of the second kind of order  $m$  and  $m_e$  is given by

$$m_e^2 = -\frac{(\omega^2 - \omega_{Ae}^2)(\omega^2 - c_e^2 k^2)}{(c_e^2 + V_{Ae}^2)(\omega^2 - \omega_c^2)}$$

and is the radial wavenumber for the magnetised atmosphere.

Thus, the expression for the radial displacement within the flux tube can be written, using equation (1.14), as

$$\xi_{ri} = \frac{1}{\rho_0(\omega^2 - \omega_A^2)} \frac{d}{dr} \left( A_i \begin{cases} I_{|m|}(m_i r) & m_i^2 > 0, \\ J_{|m|}(n_i r) & n_i^2 > 0, \end{cases} \right), \quad (1.15)$$

and the external perturbation is given by

$$\xi_{re} = \frac{A_e}{\rho_e(\omega^2 - \omega_{Ae}^2)} \frac{dK(m_e r)}{dr}. \quad (1.16)$$

Using both of these perturbations it is possible to write the dispersion relation for wave propagation in a cylindrical flux tube. We require that the radial displacement and the total pressure perturbation across the discontinuity are conserved, i.e.

$$[\xi_r] = \xi_{ri} \Big|_{r=R} - \xi_{re} \Big|_{r=R} = 0, \quad [P] = P_i \Big|_{r=R} - P_e \Big|_{r=R} = 0. \quad (1.17)$$

Therefore it is possible to write

$$\begin{aligned} \xi_{ri} &= \xi_{re}, \\ \Rightarrow \frac{P'_i}{\rho_i(\omega^2 - \omega_A^2)} &= \frac{P'_e}{\rho_e(\omega^2 - \omega_{Ae}^2)}, \end{aligned}$$

where a prime indicates a radial derivative. At this point we use the explicit form of the perturbed total pressure and the conservation law above to determine the ratio of the constants  $A_i$  and  $A_e$ .

$$\frac{A_i}{A_e} = \frac{K_m}{J_m \text{ or } I_m} \Big|_{r=R}$$

with this ratio it is possible to write the dispersion relation as

$$\rho_i(\omega^2 - \omega_A^2) m_e \frac{K'_m(m_e R)}{K_m(m_e R)} = \rho_e(\omega^2 - \omega_{Ae}^2) m_i \frac{I'_m(m_i R)}{I_m(m_i R)} \quad (1.18)$$

for surface waves and

$$\rho_i(\omega^2 - \omega_A^2)m_e \frac{K'_m(m_e R)}{K_m(n_e R)} = \rho_e(\omega^2 - \omega_{Ae}^2)n_i \frac{J'_m(n_i R)}{J_m(n_i R)} \quad (1.19)$$

for body waves. At this point we will neglect the discussion on propagating surface waves as, under conditions typical of coronal loops and other magnetically dominated coronal structures, only body waves propagate within the structures. The surface waves are prevented from propagating under these conditions due to the ratio of the sound and Alfvén speeds, i.e. the radial wavenumber  $m_i^2 < 0$  for typical values. As the surface wave does not propagate in these conditions, all the work presented after this point will focus on the body waves, see Edwin and Roberts (1983b) for further details on the propagation of surface waves.

The dispersion relation for propagating body waves can be reduced further if we use the thin-tube approximation (TT), which is sometimes called the long wavelength approximation. We assume that  $n_i R \ll 1$  the dispersion relation can be reduced to

$$\rho_i(\omega^2 - \omega_A^2) + \rho_e(\omega^2 - \omega_{Ae}^2) = 0. \quad (1.20)$$

The thin-tube assumption reduces the number of wave modes to the  $m \geq 1$  fast MHD wave modes. Rearranging equation (1.20) it is possible to write the phase speed of the wave and the 'kink' frequency of the transverse oscillations. The phase speed can be written as

$$V_{ph} = \frac{\omega}{k} = \sqrt{\frac{\rho_i V_A^2 + \rho_e V_{Ae}^2}{\rho_i + \rho_e}}, \quad (1.21)$$

and the frequency can be written as

$$\omega_k^2 = \frac{\rho_i V_A^2 + \rho_e V_{Ae}^2}{\rho_i + \rho_e} k^2. \quad (1.22)$$

Whilst the two quantities are intimately connected, they both represent important quantities in solar magneto-seismology as they are two of the most easily acquired values from observations of propagating MHD waves in the solar corona.

### 1.4.3 Overview of Current Research

Over the years there have been many studies that have dedicated themselves to wave propagation in the solar atmosphere. Early investigations by Defouw (1976), Hollweg (1978) and Spruit (1982) was directed to describe the propagation of the magneto-sonic wave modes under conditions typical of the disparate areas of the solar atmosphere. However, the foundation of the current theory of MHD wave propagation took place in the series of works by Roberts (1981a, 1981b) and Edwin and Roberts (1983b) for Cartesian geometry, which has since been extended to different geometries and even into steady systems in many later works (see *e.g.* Narayanan 1991, Goossens et al. (1992a), Terra-Homem, Erdélyi and Ballai 2003). The extension into cylindrical geometry was considered by Edwin and Roberts (1983a) and has since become a fundamental paper on which most studies of propagating MHD waves in the solar atmosphere are based. More recently, observations made by *Transition Region and Coronal Explorer* (TRACE), *Solar and Heliospheric Observatory* (SoHO) and *Hinode* have extensively indicated the complexity of the magnetic loops in the solar atmosphere and therefore the complexity of wave propagation in highly dynamic loops.

A result of this myriad of observational data, has been a series of investigations into MHD wave propagation where spatial or temporal variation has been taken into account. Spatial variation has been the more common of these models, Andries *et al.* 2005, Dymova and Ruderman (2006), and Erdélyi and Verth (2007) have all considered density stratification with magnetic flux tubes. The alteration to the eigenfrequencies for longitudinal variation in density was considered both numerically and analytically. The difference in eigenfrequencies using these techniques was found to be less than 1% for thin magnetic flux tubes. In order to model the observed expansion of magnetic flux tubes Verth and Erdélyi (2008) derived governing equations for symmetrically expanding loops, hence, determining the change to the fast kink wave as the loop expands. The inclusion of an azimuthal component to the background magnetic field i.e. a twisted magnetic field, was considered by Erdélyi and Fedun (2010b) and a dispersion relation for wave propagation was found. For an overview of

MHD wave theory in magnetically structured loops see Roberts (2000), Andries *et al* (2009), or Ruderman and Erdélyi (2009) for transverse oscillations, e.g. Roberts (2006), de Moortel (2009) or Wang (2011) for longitudinal oscillations and Mathioudakis *et al.* (2012) for a review of Alfvén waves.

This Thesis will concentrate on dynamic MHD wave propagation in the high solar atmosphere, however, some the work performed later is applicable to lower regions. As such we refer to Hasan (2008) for an overview of the dynamics currently under discussion within the chromosphere. The work performed in Chapters 3 and 6, in particular, may be of interest to people wishing to investigate the lower solar atmosphere.

## 1.5 Introduction to Resonant Absorption

Resonant absorption was initially discussed as a means of heating fusion plasmas, see e.g. Tataronis and Grossmann (1973) or Hasegawa and Chen (1974), and was introduced to the coronal heating debate by Ionson (1978). Hollweg (1988) and Erdélyi and Goossens (1994), among others, have discussed resonant absorption as a means of damping the numerous MHD waves observed in the corona. The concept of resonant absorption explores the idea, previously discounted in section (1.3.2), that the frequency of the transverse motions,  $\omega$ , is equal to the local Alfvén frequency,  $\omega_A$ , and/or the cusp frequency,  $\omega_c$ . In the two governing equations, (1.11) and (1.12), we note that singularities exist at these points. In a model containing a radial discontinuity this is not a problem as we only consider magnetic flux tubes for which these frequencies are irrelevant. However, a more realistic model of naturally occurring plasmas has a transitional layer smoothly joining the interior and exterior values across the boundary. Such a model allows for these singular frequencies to be present. If, however, we investigate the displacement either side of this singularity we find that there is a drop in amplitude across the resonant point. The drop in amplitude across this point is commonly referred to as the jump condition. The expression for this jump in the amplitude is derived in Section 1.5.1 below.

For the purposes of this Thesis, the transitional layer is assumed to be thin in comparison with the flux tube and the density is assumed to be monotonically

decreasing across the layer, thus reducing the number of singular points, called resonant points hereafter, to one per continuum. Whilst investigations into multiple resonant points have taken place see, e.g. Ruderman (2011), the possibility of overlapping dissipative layers may complicate the underlying physics. For simplicity this work will restrict itself to a single resonant point per continuum.

In physical terms the propagating fast MHD waves, oscillating with a frequency close to that of the local Alfvén frequency, will couple to local Alfvén waves producing quasi-modes. The energy loss, indicated by the negative jump in wave amplitude (as demonstrated in Section 1.5.1), is a result of the energy stored within the fast MHD wave being converted into local continuum waves. These locally generated waves have a much lower magnetic Reynolds number, i.e. the diffusivity length scale is more important, causing the locally generated waves to be damped and hence release the energy into the magnetised atmosphere.

At this point a model analogous to that discussed in Section 1.4.2, i.e. a stationary cylindrical model with a twisted magnetic field, however, we now introduce a magnetic diffusion term in order to create a physical means of distorting the singularity that exists in ideal MHD, as the linear wave theory, as described in the previous section, is only valid in ideal MHD we only consider the dissipation to be important in narrow bands in the neighborhood of the resonant points. We, then, form the governing equations in the same manner as in the case of no transition layer, except that with the inclusion of the dissipation, the coefficient  $D$ , as given in equations (1.10) and (1.11), now becomes the operator  $D_\eta$  which is given by

$$D_\eta = (\omega_\eta^2 - \omega_A^2)(\omega_\eta^2 - \omega_c^2)(c^2 + V_A^2), \quad \omega_\eta^2 = \omega^2 \left( 1 - i \frac{\eta}{\omega} \frac{d^2}{dr^2} \right).$$

We now note that when  $\omega = \pm\omega_A$  and  $\omega = \pm\omega_c$  the singularities that existed in ideal MHD no longer exist. Given that the magnetic diffusivity is only important in narrow bands around the two (formerly) singular points, we can approach the problem in a similar manner as for ideal MHD. The jump conditions in ideal MHD are not discussed here, but details may be found in e.g. Sakurai et al.

(1991), Goossens et al. (2011). The derivation below will focus on the jump conditions as derived by Goossens et al. (1995) in dissipative MHD. It should be noted that the jump conditions in both ideal and dissipative MHD can be shown to be identical.

### 1.5.1 Resonance in the Alfvén Continuum

We first consider the region where  $\omega = \pm\omega_A$ . We designate the radial point at which the resonance occurs as  $r_A$  and a new radial variable  $s = r - r_A$ . Following the method outlined by Goossens et al. (1995), we can now Taylor expand around the point  $s$  and take the first non-zero term, the leading order terms are given by

$$\begin{aligned} D_1 &= \rho_0 V_A^2 \omega_A^2 \Delta, \\ C_{10} &= -2B_{0\phi} B_{0z} \omega_A^2 f_B g_B / \rho_0 r \mu_0^2, \\ C_{20} &= -\omega_A^2 g_B^2 / \rho_0 \mu_0, \\ C_{30} &= -4B_{0\phi}^2 B_{0z}^2 \omega_A^2 / r^2 \mu_0^2, \end{aligned}$$

where

$$\Delta_A = \frac{d}{dr}(\omega^2 - \omega_A^2)|_{r=r_A},$$

and a subscript 'A' indicates an evaluation at the resonant point. These expressions reduce the governing equations (1.10)-(1.11) to

$$\left( s\Delta - i\eta\omega \frac{d^2}{ds^2} \right) \frac{d\xi_r}{ds} = \frac{g_B}{\rho_A B_0^2} C_A(s), \quad (1.23)$$

and

$$\left( s\Delta - i\eta\omega \frac{d^2}{ds^2} \right) \frac{dP}{ds} = 2 \frac{f_B B_{0\phi} B_{0z}}{\mu_0 r_A \rho_A B_0^2} C_A(s), \quad (1.24)$$

where

$$C_A(s) = g_B P - 2 \frac{f_B B_{0\phi} B_{0z}}{\mu_0 s} \xi_s = \text{const.} \quad (1.25)$$

Condition (1.25) is the fundamental conservation law for the Alfvén resonance across the region where the Taylor expansion is valid. In ideal MHD  $C_A$  is

exactly conserved and, to leading order, in dissipative MHD  $C_A$  can be shown to be conserved, see Appendix A for details. An equivalent value can be derived for the slow resonance and is discussed later.

Given that  $C_A$  is constant, further progress can be made towards deriving an analytic solution for the jump conditions across the point  $s = 0$ , hereafter the jump conditions refers to the loss of amplitude across the resonant point. A new radial variable,  $\tau_A$ , is introduced and is scaled over the region in which the dissipation,  $\eta$  is important, i.e. the area where  $s\Delta$  and  $\eta\omega d^2/ds^2$  are of comparable magnitude. This dissipative layer is designated  $\delta_A$  and both  $\tau_A$  and  $\delta_A$  are defined as

$$\tau_A = \frac{s}{\delta_A}, \quad \delta_A = \left( \eta \frac{\omega}{|\Delta_A|} \right)^{1/3}. \quad (1.26)$$

The governing equations can, once again, be rewritten as

$$\left( \frac{d^2}{d\tau^2} + i \operatorname{sign}(\Delta_A) \tau \right) \frac{d\xi_r}{d\tau} = i \frac{g_B}{\rho_A B_0^2 |\Delta_A|} C_A, \quad (1.27)$$

and

$$\left( \frac{d^2}{d\tau^2} + i \operatorname{sign}(\Delta_A) \tau \right) \frac{dP}{d\tau} = 2i \frac{f_B B_{0\phi} B_{0z}}{\rho_A B_0^2 \mu_0 r_A |\Delta_A|} C_A. \quad (1.28)$$

Equations (1.26) and (1.27) can be solved in terms of two functions  $F(\tau)$  and  $G(\tau)$ , as shown by e.g. Erdélyi et al. (1995b), Goossens et al. (1995) or Goossens et al. (2011), describing the asymptotic behavior of the perturbations at the point  $\tau_A = 0$ . The full derivation for both functions can be found in Appendix A. Using the two functions, the full form of  $\xi_r$  and  $P$  in the region of the resonant point can be expressed as

$$\xi_r \approx \frac{g_B C_A}{\rho_A B_0^2 \Delta_A} \left( \ln |\tau| + \frac{2\nu}{3} + \frac{1}{3} \ln 3 - i \frac{\pi}{2} \operatorname{sign}(\Delta\tau) \right) + C_\xi, \quad (1.29)$$

$$P \approx 2 \frac{f_B B_{0\phi} B_{0z} C_A}{\mu_0 r_A \rho_A \Delta_A B_0^2} \left( \ln |\tau| + \frac{2\nu}{3} + \frac{1}{3} \ln 3 - i \frac{\pi}{2} \operatorname{sign}(\Delta\tau) \right) + C_P, \quad (1.30)$$

where the constant  $\nu$  is the Euler constant. The presence of the signum function indicates a jump in wave amplitude across the resonant point. The jumps across

this point can be written as

$$[\xi_r] = -i\pi \frac{g_B}{\rho_A B_0^2 |\Delta_A|} C_A, \quad [P] = -2i\pi \frac{f_B B_{0\phi} B_{0z}}{\rho_A B_0^2 \mu_0 r_A |\Delta_A|} C_A. \quad (1.31)$$

It is interesting to note that the jump is independent of the dissipative constant  $\eta$  and, instead, only depends upon the background plasma values as found in ideal MHD. In the case of a purely vertical magnetic field the jump conditions reduce to

$$[\xi_r] = -i\pi \frac{m^2}{r_A^2 \rho_A |\Delta_A|} P, \quad [P] = 0. \quad (1.32)$$

The most interesting result of this reduction is that the jump in the total pressure perturbation disappears and the resonance in the radial displacement is simplified. The straight magnetic field is an important reduction to make at this point, since the relative twist in the magnetic field in coronal, loop-like, structures is very low and as such this approximation is accurate to leading order. The second reason for this reduction is that the work conducted in chapters 4 and 5 takes places in the presence of a straight magnetic field. Further analysis using these jump conditions can be performed, however, first a similar investigation into the resonance around the cusp frequency will be presented.

### 1.5.2 Resonance in the Slow Continuum

Now, we turn our attention to the singularity in the region of the cusp frequency, i.e. when  $\omega = \pm\omega_c$ . For the slow MHD wave, such damping is only effective given the compressible nature of the slow MHD wave and the radial motion of a result of this compression. Given the relatively small (in comparison to the Alfvén speed) magnitude of the sound speed in the corona, the damping is generally considered less important than that found in the Alfvén continuum, however, Chapter 5 will show that it is possible, under certain conditions, for the resonant damping of a slow MHD wave to become more important.

By Taylor expanding around the radial point where  $\omega = \pm\omega_c$ , i.e. when  $s = r - r_c = 0$ , and taking the first non-zero term we find that the governing

equations reduce to

$$\left( s\Delta_c - i\frac{\eta}{\omega} \frac{\omega_c^2}{\omega_A^2} \frac{d^2}{ds^2} \right) \frac{d\xi_r}{ds} = \frac{\mu_0\omega_c^4}{B_0^2\omega_A^2} C_s(s), \quad (1.33)$$

and

$$\left( s\Delta_c - i\frac{\eta}{\omega} \frac{\omega_c^2}{\omega_A^2} \frac{d^2}{ds^2} \right) \frac{dP}{ds} = \frac{2\omega_c^2}{r_c B_0^2 \omega_A^2} C_s(s), \quad (1.34)$$

where  $\Delta_c$  and  $C_s$  are given by

$$\Delta_C = \left. \frac{d}{dr} \left( \omega^2 - \omega_c^2 \right) \right|_{r=r_c}, \quad C_s = P - 2 \frac{B_{0\phi}^2 \xi_r}{\mu_0 s} = \text{const.}$$

The conserved quantity,  $C_s$  is comparable to the conserved value  $C_A$  as found in the Alfvén continuum and can be derived in the same way (see e.g. Sakurai et al. (1991), Erdélyi 1998). Such solutions are only valid in the dissipative region designated  $\delta_c$ , whose width is given by

$$\delta_c = \left( \eta \frac{\omega\omega_c^2}{|\Delta_c|\omega_A^2} \right)^{1/3}.$$

Given that  $C_s$  is conserved, we can seek solutions across the dissipative layer in the same manner as in the previous section, see Appendix A for details. The asymptotic solutions for the two functions  $F(\tau)$  and  $G(\tau)$  can be applied in a similar manner to that of the resonant Alfvén wave, giving jump conditions as

$$[\xi_r] = -i\pi \frac{\mu_0\omega_c^4}{B_0^2|\Delta_c|\omega_A^2} C_s, \quad [P] = -2i\pi \frac{B_{0\phi}^2\omega_c^2}{B_0^2 r_c \omega_A^2 |\Delta_c|} C_s. \quad (1.35)$$

Unlike in the case of the resonant Alfvén wave we find that in the case of a straight magnetic field, resonance exist for the slow,  $m = 0$ , sausage wave. If we, again, consider a straight magnetic field the jump conditions reduce to

$$[\xi_r] = -i\pi \frac{\mu_0\omega_c^4}{B_0^2|\Delta_c|\omega_A^2} P, \quad [P] = 0. \quad (1.36)$$

Similar to the Alfvén resonance in the case of a straight magnetic field in the total pressure perturbation. Once again the jump across the resonant point is

independent of the magnetic diffusivity. For full details on the derivation of jump conditions in the slow continuum, see Erdélyi (1998) or Goossens et al. (2011) for a full review.

## 1.6 Wave Dissipation

Now, that the jump conditions in both the Alfvén and slow regimes have been introduced, we will use the resulting jump condition in the Alfvén continuum to calculate the dissipation rate of the coupled fast and Alfvén wave. The derivation below follows the work carried out by Goossens et al. (1992a) and exploits the assumption of a thin tube.

We return to the dispersion relation for the fast kink wave in a thin, straight magnetic flux tube. In the case of a discontinuity in the magnetic field, as presented in Section 1.5.1, there is no jump in either the radial displacement or the perturbed pressure and as such the dispersion relation found in equation (1.19) holds. With the introduction of the transitional layer and, hence, the jump in the radial displacement, the dispersion relation can be derived as follows,

$$\xi_{ri} - \xi_{re} = -i\pi \frac{m^2}{r_A^2 \rho_A |\Delta|} P,$$

$$\rho_e(\omega^2 - \omega_{Ae}^2)P'_i - \rho_i(\omega^2 - \omega_A^2)P'_e = -i\pi \rho_i \rho_e (\omega^2 - \omega_A^2)(\omega^2 - \omega_{Ae}^2) \frac{m^2}{r_A^2 \rho_A |\Delta|} P_i.$$

Now, by applying the thin tube approximation this expression can be reduced to

$$\rho_i(\omega^2 - \omega_A^2) + \rho_e(\omega^2 - \omega_{Ae}^2) = i\pi \frac{m\rho_i\rho_e}{r_A\rho_A|\Delta|}. \quad (1.37)$$

The dissipation rate can now be determined by either algebraically rearranging the dispersion relation, as in the manner of Terradas, Goossens and Verth (2010), or by using the method as laid out by e.g. Krall and Trivelpiece (1973). The method followed here will use the second method, however, both methods will start by defining a complex frequency  $\omega = \omega_r + i\gamma$ . The imaginary component  $\gamma$  is assumed to be small in comparison to the real component  $\omega_r$ . Using

the method of Krall and Trivelpiece (1973),  $\gamma$  is given by

$$\gamma = -\frac{D_i(\omega_r, k)}{\partial D_r / \partial \omega_r}, \quad (1.38)$$

where  $D_r$  and  $D_i$  are the real and imaginary parts of the dispersion relation. In this example, where there is no background flow,  $\gamma$  has the following form

$$\gamma = -\frac{|m|\pi}{2r_A} \frac{\rho_i^2 \rho_e^2}{\rho_A (\rho_i + \rho_e)^3} \frac{|\omega_A^2 - \omega_{Ae}^2|}{\omega_k |\Delta|}, \quad (1.39)$$

where  $\omega_k$  is the kink frequency as stated in equation (1.21). This dissipation is, again, independent of the magnetic diffusivity,  $\eta$  and indicates the need for a large density gradient across the transitional layer. If the density gradient were small, i.e.  $\rho_i \approx \rho_e \approx \rho_A$ , the dissipation would reduce to the difference in magnetic fields, which in the approximately zero plasma- $\beta$  magnetic environment typical of the corona diminishes the resonance to insignificant levels.

### 1.6.1 Overview of Resonant Absorption Investigations

Propagating waves in coronal loops have been identified by analysis of data gained from the space satellites (see *e.g.* Berghmans and Clette, 1999, De Moortel, Ireland and Walsh, 2000, O'Shea *et al.*, 2001). The majority of the observed waves are heavily damped, most within 4-5 periods, several studies (see *e.g.* Ruderman and Roberts (2002), Terradas (2009) for a theoretical investigation of the damping period and Goossens *et al.* (2002), Verth *et al.* (2010) for the observational detection of the resonant damping) have interpreted this as due to resonant damping. In order to explain this rapid damping, development of the resonant absorption model has continued apace. We know that resonance appears in both the Alfvén and slow continua and that in different regions of the solar atmosphere the different magneto-acoustic wave modes have different levels of relative importance. Therefore, the investigations into both phenomenon have been numerous and some of these are detailed below.

The jump in amplitude across the resonant point were first found by Sakurai, Goossens and Hollweg (1991) by evaluating solutions around the singularity

at the resonant point. Goossens, Ruderman and Hollweg (1995) expanded on this method by finding analytic solutions across a scaled static dissipative layer. The solution found therein is then expanded to more complicated systems, i.e. systems containing both vertical and azimuthal flows see e.g. Goossens et al. (1992a), Erdélyi et al. (1995b). A longitudinally stratified background density was considered by Andries et al. (2005), where it was found that to leading order the stratification has no impact upon the damping time, i.e.  $\tau_{damping}/P$ . However, only a small longitudinal variation was considered. This work was then extended to numerical analysis which included a thick transitional layer in Arregui et al. (2005), showing that not only did the stratification have a minimal effect on the resonance, but that the thin tube thin boundary approximation under estimates the damping by a factor of approximately 2. Ballai and Ruderman (2011) reviews the recent advancements in the non-linear studies of resonant absorption. These investigations have indicated that many instabilities can occur and either enhance or disrupt the damping due to the resonance. Given the volume of non-linear MHD waves in the solar corona such research needs to be continued in order to expand our understanding of the observed wave damping.

The importance of resonant absorption in slow continuum, as a means of heating the corona, is an area of debate. Hollweg and Yang (1998) found the jump conditions for compressible waves and found that in the low-beta environments typical of the solar corona the slow resonance is not as important as other damping mechanisms. In a system with a larger plasma-beta the slow resonance takes on a greater importance in the damping of the slow MHD wave. Cadez and Ballester (1996) explored an arcade-model and showed that the resonance in the vicinity of the cusp frequency can lead to a continuous slow mode spectra. It is also worth noting that in the current work a variable background flow is considered, such a flow must be considered in the context of the analytical works done in e.g. Erdélyi, Goossens and Ruderman (1995a) and the numerical analysis of Csík, Erdélyi and Cadez (1997). The jump conditions for a steady background as found by e.g. Erdélyi *et al.* (1995a) showed only an algebraic difference between the static case and the steady case, however the analytic work was inconclusive on the effects of the flow under coronal conditions. Analysis of

these new jump conditions by e.g. Erdélyi and Goossens (1996) or Caik *et al.* (1997) showed that the flow can cause a strong enhancement of the resonance under the correct circumstances.

Non-linear investigations into the analogous jump conditions have been carried out by Ballai and Erdélyi (1998) who introduced a small non-linear parameter and recover a jump condition comparable to that found in the linear works discussed above. Erdélyi and Ballai (1999) then expanded upon this work with the introduction of a shear flow to the non-linear parameter in the first part of the work.

A full summary of the current research into the resonant absorption phenomenon, including aspects of theory not discussed here, is given by Goossens *et al.* (2011).

## 1.7 The WKB Approximation

### 1.7.1 Introduction to WKB Analysis

The WKB approximation was named after the three physicists (Wentzel, Kramers and Brillouin) who first formalised its use as a method for approximating the solution to linear differential equations. However, work had previously been done by Liouville and Green prompting an alternative name of Liouville-Green Theory. The WKB approximation isolates terms to orders of magnitude with respect to a small parameter,  $\delta$ , and removes all terms of a lesser magnitude. This approximation is very useful for the work I will be presenting later due to its ability to approximate a slowly changing background, if the background changes with the same order as the parameter  $\delta$ . The derivations below follow the style of Bender and Orszag (1978).

#### Formal WKB Expansion

The formal WKB approximation is an ansatz of the form

$$y(x) \approx \exp \left[ \frac{1}{\delta} \sum_{n=0}^{\infty} \delta^n S_n(x) \right], \quad \delta \rightarrow 0.$$

As higher orders of  $S_n$  are calculated the solution becomes increasingly accurate. However, a full solution to a problem, using this method, would require a solution for every order of magnitude within the problem. Therefore, in order to save time, only the first two orders of magnitude need be calculated in order to give an accurate representation whilst keeping calculations to a minimum. The first two orders of magnitude can be expressed in a concise manner by using the exponential approximation to the WKB method, as detailed below.

### The Exponential Approximation

The form of the WKB approximation that is considered to be most useful, is the Exponential Approximation, the form of which is below:

$$y(x) \approx \exp \left[ \frac{S_0}{\delta} + S_1 \right] = Q(x) \exp \left[ \frac{\hat{S}(x)}{\delta} \right].$$

Where

$$Q(x) = \exp[S_1], \quad \text{and,} \quad \hat{S}_1(x) = S_0.$$

The function  $\hat{S}(x)$  is assumed to be a non-constant function. When  $\hat{S}(x)$  is a real function the approximation represents a boundary layer problem. The boundary layer will then have a thickness of  $\delta$ .

If the function  $\hat{S}(x)$  is imaginary, then the system can be shown to represent a wave form with a wavelength  $\delta$ . In this form  $\hat{S}(x)$  represents the phase of the wave and  $Q(x)$  is the amplitude of the wave. In all further work a waveform solution will be sought and  $\hat{S}(x) \in \mathbf{R}$  will be assumed. Therefore, the standard WKB approximation used will be of the form

$$y(x) \approx Q(x) \exp \left[ \frac{i}{\delta} S(x) \right],$$

where the  $\hat{\phantom{x}}$  notation has now been dropped for convenience.

### Extension into Multiple Variables

Due to the relation between the spatial and time variable indicated by the mass conservation equation, each of the variables will need to vary over the same slow

time period. For simpler problems, like the ones solved below, it is useful to scale the wave numbers such that they vary over the timescale,  $\delta$ . However, in more complex problems it is not so simple and the Exponential Approximation must be altered in order to account for this. The multi-variable approximation is therefore as follows.

$$y(\mathbf{x}, t) \approx Q(\mathbf{x}, t) \exp \left[ \frac{i}{\delta} S(\mathbf{x}, t) \right],$$

where  $\mathbf{x}$  is the position vector.

### 1.7.2 Example of the WKB Approximation

To demonstrate the applicability of the WKB approximation we choose the one-dimensional wave equation with a vertically stratified, static, fluid. The standard wave equation for wave propagation in an infinite inhomogeneous medium is known to be

$$\frac{\partial^2 u}{\partial t^2} - \frac{\partial}{\partial z} \left[ c^2 \frac{\partial u}{\partial z} \right] = 0, \quad c = c(z).$$

The WKB approximation is now applied, the form of which is

$$u = U(t, z) \exp \left[ \frac{i}{\delta} \Theta(t, z) \right], \quad (1.40)$$

where  $\delta$  is the relative size of the wavelength in comparison to the change in the medium. The derivatives can be represented as

$$\begin{aligned} u_t &= \left[ U_t + \frac{i}{\delta} \Theta_t U \right] \exp \left[ \frac{i}{\delta} \Theta(t, z) \right], & u_z &= \left[ U_z + \frac{i}{\delta} \Theta_z U \right] \exp \left[ \frac{i}{\delta} \Theta(t, z) \right], \\ u_{tt} &= \left[ U_{tt} + \frac{2i}{\delta} \Theta_t U_t + \frac{i}{\delta} \Theta_{tt} U - \frac{U}{\delta^2} \Theta_t^2 \right] \exp \left[ \frac{i}{\delta} \Theta(t, z) \right], \\ u_{zz} &= \left[ U_{zz} + \frac{2i}{\delta} \Theta_t U_z + \frac{i}{\delta} \Theta_{zz} U - \frac{U}{\delta^2} \Theta_z^2 \right] \exp \left[ \frac{i}{\delta} \Theta(t, z) \right]. \end{aligned}$$

Therefore, to lowest order in  $\delta$

$$-\Theta_t^2 + c^2 \Theta_z^2 = 0,$$

$$\Rightarrow \Theta_t = \pm c\Theta_z. \quad (1.41)$$

The positive sign is taken in order to evaluate a single wave traveling in the positive direction. The second lowest order of  $\delta$  produces the following equation,

$$\Theta_{tt}U + 2\Theta_tU_t - c^2\Theta_{zz}U - 2c^2\Theta_zU_z - (c^2)_z\Theta_zU = 0. \quad (1.42)$$

A solution for  $\Theta$  is now sought

$$\Theta = \lambda t + \int \frac{\lambda}{c} dz,$$

where  $\lambda$  is a separation constant. Equation (1.41) can now be reduced to

$$\begin{aligned} \lambda U + 2U_t &= U[\lambda - c_z] + 2cU_z + 2c_zU, \\ \Rightarrow U_t &= cU_z + \frac{1}{2}c_zU. \end{aligned} \quad (1.43)$$

Equation (1.42) can be solved to give

$$U = \frac{\hat{B}}{c} \exp \left[ \psi t + \int \frac{\psi}{c} dz \right]. \quad (1.44)$$

The full solution is therefore given by

$$u = \frac{\hat{B}}{c} \exp \left[ \psi t + \int \frac{\psi}{c} dz \right] \exp \left[ \frac{i\hat{A}}{\delta} \left( \lambda t + \int \frac{\lambda}{c} dz \right) \right], \quad (1.45)$$

where  $\hat{A}$  and  $\hat{B}$  are arbitrary constants of integration. Equation (1.43) can be written in the form of d'Alembert's solution for a single wave traveling in the positive direction as

$$u(z, t) = \frac{\hat{B}}{c} \exp \left[ \psi f(z, t) + \frac{i\hat{A}}{\delta} \lambda f(z, t) \right], \quad (1.46)$$

where

$$f = t + \int \frac{1}{c} dz,$$

which can be compared to d'Alembert's solution of

$$f = z + ct, \quad \text{for} \quad c = \text{const.}$$

### 1.7.3 WKB Approximation

The WKB approximation, that is used in the following chapters, will take the following form,

$$F = Q_F \left( \frac{r}{\epsilon}, z, t \right) \exp \left[ \frac{i}{\epsilon} \left( \theta(t, z) + m\phi \right) \right]. \quad (1.47)$$

In equation (1.47)  $F$  is any perturbed function,  $m$  is the azimuthal wave number and  $\epsilon$  is a small parameter, defined as the ratio of the period of oscillation and the characteristic time of background density change within the loop. For more details on the WKB approximation see e.g. Bender and Orszag (1978). At this point it is also useful to define the following quantities

$$\Omega_w = -\frac{\partial \theta}{\partial t}, \quad K_w = \frac{\partial \theta}{\partial z}, \quad \varpi = \Omega_w - V_{0z} K_w. \quad (1.48)$$

The subscript ' $w$ ' indicates the individual MHD wave being considered. An ' $f$ ' will indicate the fast wave mode and an ' $s$ ' will indicate the slow wave mode.  $\Omega_w$  will represent the dynamic frequency and  $K_w$  will represent the dynamic wavenumber. The perturbation amplitude,  $Q$ , will appear with different indices in the following chapters.  $Q_P$  will represent the amplitude of the total pressure perturbation,  $Q_{\xi, r}$  will represent the radial displacement amplitude and  $Q_z$  will represent the vertical displacement amplitude.

# Chapter 2

## MHD Wave Propagation in a Zero-beta Dynamic Plasma

### 2.1 Introduction

MHD waves and oscillations in sharply structured magnetic plasmas have been studied for static and steady systems in the thin tube approximation over many years. This chapter will generalise these studies by introducing a slowly varying background density in time. We determine the changes to the wave parameters introduced by this temporally varying equilibrium. We investigate the amplitude, frequency and wavenumber for the kink and higher-order propagating fast magnetohydrodynamic wave in the leading order approximation to the WKB approach in a zero- $\beta$  plasma representing the upper solar atmosphere. In order to progress the thin tube approximation is made, after which application of the over-dense loop approximation and the moderate-activity approximation allow for two separate methods of solution representing different physical systems. Using such approximations it is shown that the amplitude of the kink wave is enhanced in a manner proportional to the square of the Alfvén speed and the frequency of the wave tends to the driving frequency of the system for an over-dense scenario and to zero for a moderate-activity approximation as time progresses. The over-dense loop has a wavenumber that approaches zero after a large multiple of the characteristic density change timescale, indicating an ever

increasing wavelength. In a similar manner it can be shown that the wavenumber in the moderate-activity approximation decreases in an exponential manner over time toward a constant level.

For the higher-order fluting modes the changes in amplitude are dependent upon the wave mode; for the  $m = 2$  mode the wave is amplified to a constant level, however, for all  $m \geq 3$  the fast MHD wave is damped within a relatively small multiple of the characteristic density change timescale. The changes in the amplitude of the various fast MHD wave modes are similar in nature and, therefore, the two results can be said to support each other.

The over-dense loop approximation and the analysis that goes along with this approximation is based upon the work carried out by Williamson and Erdélyi (2013-in Press).

## 2.2 The Governing Equations

An open cylinder of constant radius  $R$  and magnetic field  $B_{0zi}\hat{\mathbf{z}}$  is now constructed inside an exterior region of constant, vertical magnetic field,  $B_{0ze}\hat{\mathbf{z}}$ . The interior density of the cylinder is designated  $\rho_i$  and is decreasing in time with a constant exponential factor  $A$ . Due to the decrease in density a background flow is required to maintain mass conservation. The background flow  $\mathbf{V}=(0,0,V_{0z})$  is applied where the vertical component can be determined by the use of mass conservation and is given by  $V_{0z} = Az$ . The cold-plasma approximation is applied, the use of which implies that the thermal pressure,  $p_0 \approx 0$ , of the cylinder can be neglected when compared to the magnetic pressure. The application of the cold-plasma approximation gives a pressure balance across the flux tube boundary which can only be satisfied by imposing a non-distinct magnetic field, i.e.  $B_{0zi} = B_{0ze}$ . The exterior of the the cylinder is defined as a constant density with no flow. The cylinder is excited at the base, i.e.  $z = 0$ , with a constant driving frequency  $\omega$ .

The ideal linearised, perturbed MHD equations can be written as

$$\frac{\partial \rho}{\partial t} + \nabla \cdot (\rho_0 \mathbf{V} + \rho \mathbf{V}_0) = 0, \quad (2.1)$$

$$\rho_0 \left[ \frac{\partial \mathbf{V}}{\partial t} + \mathbf{V} \cdot \nabla \mathbf{V}_0 + V_{0z} \frac{\partial \mathbf{V}}{\partial z} \right] + \rho V_{0z} \frac{\partial \mathbf{V}_0}{\partial z} = -\nabla p + \frac{1}{\mu} (\nabla \times \mathbf{B}) \times \mathbf{B}_0, \quad (2.2)$$

$$\frac{\partial \mathbf{B}}{\partial t} = \nabla \times (\mathbf{V}_0 \times \mathbf{B}) + \nabla \times (\mathbf{V} \times \mathbf{B}_0), \quad (2.3)$$

$$\frac{\partial p}{\partial t} + \mathbf{V}_0 \cdot \nabla p = -\gamma \left( p \frac{\partial V_{0z}}{\partial z} \right). \quad (2.4)$$

The radial components of equations (2.2) and (2.3) can be combined to give the first governing equation, equation (2.5). The second governing equation can be formed by taking the equation for the perturbed total pressure,  $P \approx B_{0z} B_z / \mu$ , and eliminating all perturbed variables except  $P$  and  $V_r$ . Here  $P$  is given only by the magnetic pressure as a result of the cold plasma assumption. The set of governing equations, in operator form, are given by

$$\rho_0 \left( \hat{\omega} \left( \hat{\omega} + \frac{dV_{0z}}{dz} \right) - \hat{\omega}_A^2 \right) V_r = - \left( \hat{\omega} + 2 \frac{dV_{0z}}{dz} \right) \frac{\partial P}{\partial r}, \quad (2.5)$$

and

$$\begin{aligned} & \rho_0 V_A^2 \left( \hat{\omega} \left( \hat{\omega} + \frac{dV_{0z}}{dz} \right) - \hat{\omega}_A^2 \right) \frac{1}{r} \frac{\partial (r V_r)}{\partial r} = \\ & - \left[ \left( \hat{\omega} \left( \hat{\omega} + \frac{dV_{0z}}{dz} \right) - \hat{\omega}_A^2 \right) \hat{\omega} - \frac{V_A^2}{r^2} \left( \hat{\omega} + 2 \frac{dV_{0z}}{dz} \right) \frac{\partial^2}{\partial \phi^2} \right] P, \end{aligned} \quad (2.6)$$

where

$$V_A^2 = \frac{B_0^2}{\mu \rho_0}, \quad \hat{\omega} = \frac{\partial}{\partial t} + V_{0z} \frac{\partial}{\partial z}, \quad \hat{\omega}_A^2 = V_A^2 \frac{\partial^2}{\partial z^2}.$$

Here,  $\hat{\omega}_A$  is the Alfvén operator and  $\hat{\omega}$  is the convective operator. These will transform into frequencies if a harmonic dependence of the form  $\exp[i(\mathbf{k} \cdot \mathbf{r} - \omega t)]$  is assumed.

At this point the WKB approximation, as detailed in section 1.7, can be applied allowing for algebraic manipulation of the governing equations. As shown in Appendix 3, Equations (2.5) and (2.6) can now be combined into two equations, in terms of the radial displacement,  $\xi_r = -i\varpi V_r$ , and the perturbed total pressure,  $P$ , as

$$\frac{\rho_0}{r} (\varpi^2 - \varpi_A^2) V_A^2 \frac{\partial (r \xi_r)}{\partial r} = - \left[ \varpi^2 - V_A^2 \left( \frac{m^2}{r^2} + K^2 \right) \right] P, \quad (2.7)$$

and

$$\frac{\partial P}{\partial r} = \rho_0(\varpi^2 - \varpi_A^2)\xi_r. \quad (2.8)$$

Where  $\Omega$  and  $K$  are the dynamic frequency and wavenumber respectively. The operator forms of the Doppler-shifted frequency and the Alfvén frequency,  $\hat{\varpi}$  and  $\hat{\varpi}_A$ , are now replaced by the eikonal form of their respective values and are indicated by the drop of the hat notation. The Doppler-shifted frequency and the Alfvén frequency are now given by the following expressions

$$\varpi = \Omega - V_{0z}K, \quad \varpi_A^2 = V_A^2 K^2.$$

Equations (2.7) and (2.8) are in agreement with the results found by Edwin and Roberts (1983a) for plane wave solutions in a magnetic cylinder. Now, equations (2.7) and (2.8) can be evaluated for values inside and outside the cylinder. The following equation is to be solved for interior and exterior values of  $V_A$  and  $\varpi$ ;

$$\frac{V_A^2}{r} \frac{\partial}{\partial r} \left( r \frac{\partial Q_P}{\partial r} \right) = - \left[ \varpi^2 - V_A^2 \left( \frac{m^2}{r^2} + K^2 \right) \right] Q_P. \quad (2.9)$$

The most general solution to equation (2.9) is a linear combination of the Bessel functions of first and second kinds. As indicated in section (1.4) we only consider the body wave solution, as under coronal conditions surface waves will no longer propagate. Therefore the solution to equation (2.9), for evanescent waves in the exterior region and interior waves regular at  $r=0$ , is given below

$$Q_P = \begin{cases} A_i J_{|m|}(M_0 r) & r < R, \\ A_e K_{|m|}(M_e r) & r > R, \end{cases} \quad (2.10)$$

where

$$M_0^2 = \frac{(\varpi_i^2 - \varpi_{Ai}^2)}{V_{Ai}^2}, \quad M_e^2 = -\frac{(\varpi_e^2 - \varpi_{Ae}^2)}{V_{Ae}^2},$$

for the internal and external regions, respectively. In purely mathematical terms the constants  $A_i$  and  $A_e$  should be considered to be arbitrary functions of  $t$  and  $z$ . However, to leading order in the WKB approximation this dependence can be neglected in comparison to the effect of the frequency and the vertical

wavenumber. This is a result of the WKB approximation reducing Equations (2.5) and (2.6) from coupled PDE's to coupled ODE's with respect to the radial component. Using equation (2.10) it is now possible to write an expression describing  $Q_\xi$ , i.e. the amplitude of the radial displacement. Application of the thin tube approximation and continuity across the boundary, i.e.  $[Q_\xi] = [Q_P] = 0$ , allows the dispersion relation to be written for  $m \geq 1$  modes, that is for the kink and fluting wave modes, (for full details see e.g. Goossens, Hollweg and Sakurai 1992b and Erdélyi and Goossens 1996),

$$\rho_i(\varpi_i^2 - V_{Ai}^2 K^2) + \rho_e(\varpi_e^2 - V_{Ae}^2 K^2) = 0. \quad (2.11)$$

We also note that equation (2.11) is in agreement with equation (21) of Ruderman (2010) for time-dependent waves in a loop of fixed length. Solving equation (2.11), using the definitions given in equation (1.47), permits the determination of the eikonal functions  $\Omega$  and  $K$  for two different approximate solutions.

## 2.3 Over-dense Loop Approximation

Application of the over-dense loop limit  $\rho_i \gg \rho_e$ , valid for dense coronal loops, allows for an analytic solution of equation (2.11). Equation (2.11) can be rewritten as

$$\begin{aligned} \varpi^2 - V_A^2 K^2 + \frac{\rho_e}{\rho_i} \Omega^2 - V_A^2 K^2 &= 0, \\ \varpi^2 &= 2V_A^2 K^2. \end{aligned}$$

Upon substitution of the differential forms of the dynamic frequency and wavenumber, the above expression becomes

$$\frac{\partial \theta}{\partial t} + (V_{0z} + \sqrt{2}V_A) \frac{\partial \theta}{\partial z} = 0,$$

which can be solved for an arbitrary function  $F$  with an argument given by

$$\theta = F \left[ (V_{0z} + 2\sqrt{2}V_A) \frac{\exp[-At]}{A} \right].$$

At this point the driven boundary condition can be applied and we require that

$$\theta(t, 0) = -\omega t,$$

where  $\omega$  is the driving frequency of the system. The full expression for the phase,  $\theta$ , is given by

$$\theta = \frac{2\omega}{A} \ln \left| \left( V_{0z} + 2\sqrt{2}V_A \right) \frac{\exp(-At)}{2\sqrt{2}V_{A0}} \right|. \quad (2.12)$$

Therefore,  $\Omega$  and  $K$  can be written as

$$\Omega = 2\omega \frac{V_{0z} + \sqrt{2}V_A}{V_{0z} + 2\sqrt{2}V_A}, \quad K = \frac{2\omega}{V_{0z} + 2\sqrt{2}V_A}. \quad (2.13)$$

As we can see from Figure 2.1,  $\Omega$  decays to the driving frequency  $\omega$  relatively

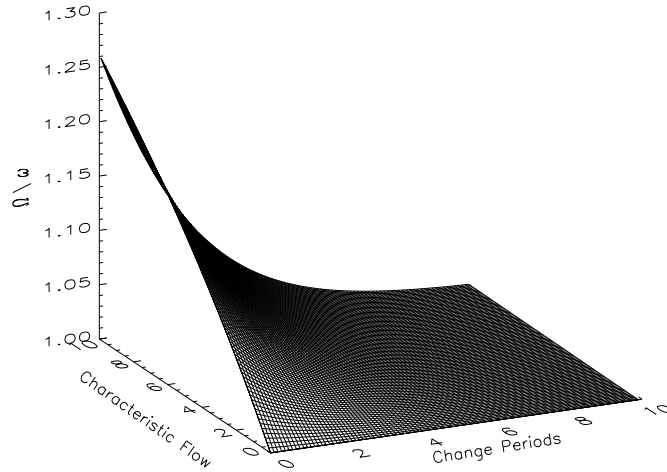


Figure 2.1:  $\Omega/\omega$  plotted for characteristic change periods ( $t/\tau_\rho$ ) against characteristic flow speeds ( $V_{0z}/V_{A0}$ ).

quickly in terms of characteristic times of density change, for background flows typical to quiet coronal loops, i.e. those in the nearby region of  $V_{0z}/V_{A0} < 1$ . However, an argument can be made that for wave propagation in coronal loops after a large eruption, e.g. a CME or a large solar flare, in the region of the coronal loop, the background flow can feasibly be of comparable order to the Alfvén speed itself and, thus, the impact could be much higher, see e.g. Terradas

et al. (2011). This could arguably increase the decay timescale indefinitely. As

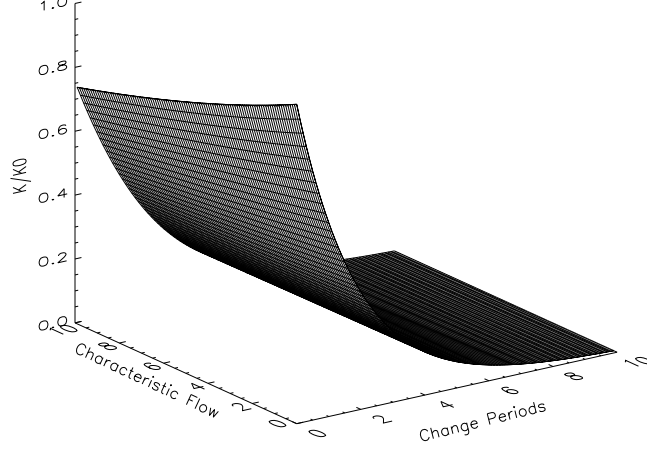


Figure 2.2:  $K/K_0$  ( $K_0 = K(t = 0)$ ) plotted for characteristic change periods ( $t/\tau_\rho$ ) against characteristic flow speeds ( $V_{0z}/V_{A0}$ ).

plotted in Figure 2.2, the wavenumber  $K$  tends to zero over 8 to 10 characteristic time periods, however, as the background flow increases the value of  $K$  tends to zero more swiftly. Using these expressions,  $Q_P$  can now be rewritten as

$$Q_{Pi} = A_i J_m \left( \frac{2\omega r}{V_{0z} + 2\sqrt{2}V_{Ai}} \right), \quad (2.14)$$

in the inner, over-dense region, while

$$Q_{Pe} = A_e K_m \left( \frac{2\omega r}{(V_{0z} \pm 2\sqrt{2}V_{Ai})V_{Ae}} \left[ V_{Ae}^2 - (V_{0z} + \sqrt{2}V_{Ai})^2 \right]^{1/2} \right), \quad (2.15)$$

in the exterior of the magnetic environment. As is to be expected from the assumption of evanescence made earlier, the exterior pressure perturbation decays radially away from the loop, as well as in time, as the interior Alfvén speed increases. The interior pressure perturbation also decreases in time and height for all  $m \geq 1$  modes.

Unfortunately, with the current level of observational technology we are unable to use this result as a diagnostic tool in its own right. However, with the total pressure now analytically determined we can make progress toward determining the radial displacement, a value that is measurable using today's

equipment.

### 2.3.1 Amplitude of the fast MHD wave

The amplitude of the fast MHD wave is given by the radial displacement of the cylinder, and can be found by rearranging equation (2.8) for  $Q_\xi$ . Now, that the frequency and wave function can be written explicitly, and therefore  $Q_P$  can equally be determined in an explicit form, the amplitude of the fast MHD wave can be obtained explicitly inside and outside the cylinder as

$$Q_{\xi i} = \frac{A_i \mu_0}{KB^2} \left[ \frac{m}{Kr} J_m(Kr) - J_{m+1}(Kr) \right], \quad (2.16)$$

and

$$Q_{\xi e} = \frac{A_e M_e}{\rho_e (\Omega^2 - V_{Ae}^2 K^2)} \left[ \frac{m}{M_e r} K_m(Kr) - K_{m+1}(M_e r) \right]. \quad (2.17)$$

By the assumption of no leaky modes, the exterior wave propagation is evanescent and decays sharply as the distance from the tube increases. Using these expressions, the propagation of the interior fast MHD wave can now be analysed for the temporal changes introduced with the variation in background density as well as the spatial changes brought about by the presence of the non-constant background plasma flow.

### 2.3.2 Temporal Dependency of Individual Wave Modes

Edwin and Roberts (1983b) (see Figure 4 of their paper) have shown that the axisymmetric sausage ( $m = 0$ ) mode has a cut-off frequency in the region of  $M_0 r$  being of order unity. Such a result is excluded by the application of the thin tube approximation and by the assumption of the zero- $\beta$  plasma. Therefore, only the kink and fluting modes remain, analysis of which can be conducted separately.

#### Kink Oscillations

It is commonly said that the most *interesting* of the oscillations in the thin loop approximation is the fast kink MHD oscillation. By *interesting* we refer

to the fact that this is the most easily observed of all the fast MHD wave modes, see e.g. Ofman and Wang (2008), and therefore the most useful tool for magneto-seismology. By considering the full expression given in equation (2.16) it is straightforward to show (see Figure 2.3) that the kink oscillation will have an exponentially growing amplitude with respect to the characteristic temporal change. This result, whilst interesting on its own, has obvious physical limitations, as a wave of infinite amplitude is a physically impossible notion. Hence, a limiting factor must be applied at the point where the linear analysis conducted above is no longer viable. The most obvious point for which this work can no longer be considered to be valid is when  $\rho_i$  and  $\rho_e$  of the same order of magnitude, and the solution for  $\theta$  as found in equation (2.12) is no longer valid.

### $|m| > 1$ Modes

The remaining fast MHD wave modes available for analysis are the *fluting* modes, which are of order  $m \geq 2$ . Whilst these modes will exist in both the thin tube approximation and under coronal conditions, unlike the  $m = 0$  sausage mode, the current resolution of the current cohort of observational tools means that we are yet to clearly determine these higher order wave modes. This analysis then, cannot be observationally verified at this point but may prove to be useful to explain future data.

The  $m = \pm 2$  mode can be shown to be amplified up to a saturation level, (see Figure 2.4) the continuing propagation of this mode is then independent of time. This analysis is true only for small values of the background flow when compared to the Alfvén speed, i.e.  $V_{0z}/V_{A0} \ll 1$ , as is true in the coronal approximation when the loop is not set in a region of high dynamic activity. For very thin tubes, i.e. those where the radial wavenumber,  $M_0 r$ , is of order less than unity, amplification is modest and can be considered to be negligible, hence the wave mode can be considered to have a constant amplitude in time.

For higher values of  $m$ , the various modes will be damped by half their initial amplitude after just a few (i.e. after approximately 2 and a half) elapses of the characteristic time of density variation, typical of the  $m = 3$  mode. Higher

order wave modes  $m$  will have increased rates of damping due to the density variation within the flux tube.

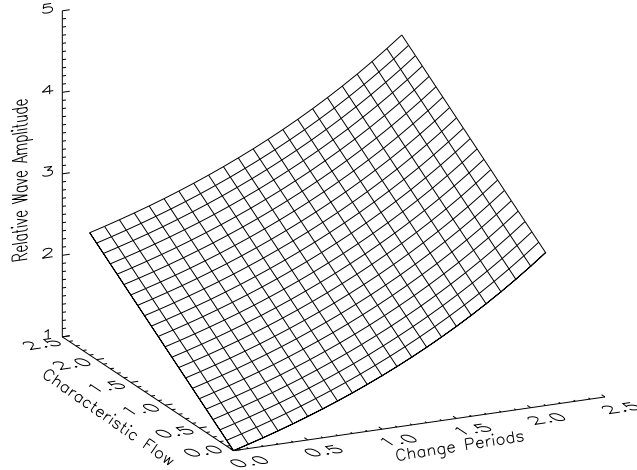


Figure 2.3: Relative change in wave amplitude of the fast MHD kink waves for a fixed loop radius ( $R = 1/K_0$ ).

### 2.3.3 Spatial Dependency of Wave Modes

The background time-dependent variation also plays a role in determining the amplitude of the fast MHD wave. The background bulk flow, as defined in section 2.2, has a linear relationship with height above the base of the loop.

For the results found above are obtained for values typical of coronal conditions, the background flow values can be limited to small changes in height above the driven point. This limiting factor implies that the changes introduced by a time-dependent background are mostly insignificant when compared not only to the Alfvén speed, but the change in Alfvén speed (due to the temporal evolution of the wave). Exceptions occur in the region of large seismic events on the solar surface, e.g. CME eruption (see e.g. Terradas *et al.* (2011) for details). Flows driven by a CME have been observed to be of the order of the Alfvén speed, therefore the generated flow may have a significant initial impact, of the same magnitude as the Alfvén speed. The temporal change in Alfvén speed, however, will have a greater impact upon the evolution in frequency, wavenumber and amplitude as the system is allowed to develop.

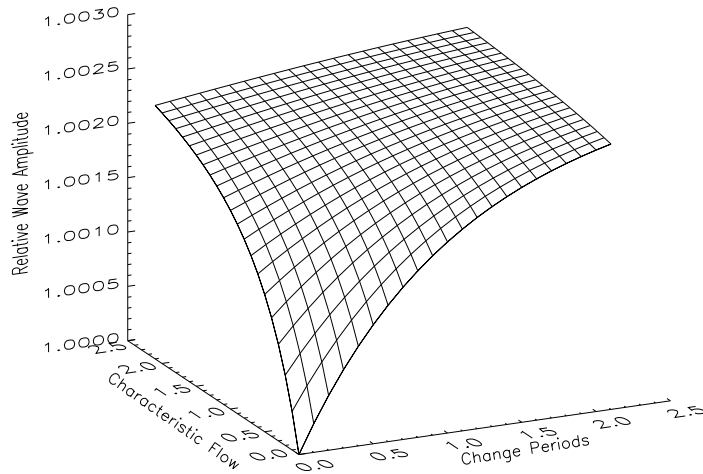


Figure 2.4: Relative change in wave amplitude of the  $m = 2$  wave for a fixed loop radius ( $R = 1/K_0$ ).

### 2.3.4 Increasing Density

Whilst the work outlined above is strictly relevant to a loop being evacuated of plasma, the reverse has a high likelihood of occurrence and applicability, e.g. due to plasma pumped into the corona via chromospheric evaporation, see e.g. Milligan *et al.* (2006). Under more restrictive conditions to those applied above, this result can be reversed in a straightforward manner. An increasing density within the loop would act as a natural damping mechanism to the fast MHD kink wave, albeit over large time with respect to the characteristic time of density change. Complications would occur when the inflow speed of the plasma becomes comparable to the decreasing Alfvén speed. When the two values are of comparable magnitude,  $K$  changes sign and from that point onwards the analysis of the Bessel functions present in section (1.7) must change. Further investigation of this problem is not considered here.

## 2.4 Moderate-Activity Approximation

Whilst the over-dense loop approximation is very useful in examining many of the structures found in the solar corona, the approximation does affect its widespread use. Photospheric MHD waves are an active area of research within

the solar community and this over-dense approximation will be of no use in the much denser photospheric regions. To this end we develop another solution which may well be applicable to more varied models. This approximation however, is less physically rigorous than the over-dense loop and as such may not give such an accurate model as found previously.

Within this section we apply a different approximation to the dispersion relation found in section 2.2. We can now investigate the effect of the changing density ratio, albeit in a system within which the background flow is much less than was considered in the previous section. Given that the background, bulk, flow is intrinsically linked to the temporal decay of the interior density, this approximation may not be entirely representative of the physics involved as a result of the decreasing density. However, the results gained herein are a good chance to check the results found in the earlier part of this chapter as well as provide a foundation for further work. It is also worth noting that the moderate-activity approximation will mean that the spatial variation in the vertical direction may be less accurate than the over-dense approximation, therefore, the focus from here will be on the temporal variation only.

We now revisit the dispersion relation for the fast MHD wave,

$$\rho_i(\varpi^2 - \varpi_A^2) + \rho_e(\Omega^2 - \varpi_{Ae}^2) = 0. \quad (2.18)$$

Previously the over-dense loop approximation was applied in order to make analytical progress. Here, however, we solve equation (2.18) in terms of the frequency,  $\Omega$  to arrive at

$$\Omega(1 + \chi) = V_{0z}K + \sqrt{2V_A^2(1 + \chi) - V_{0z}^2\chi}K, \quad (2.19)$$

where  $\chi$  is the density ratio,  $\rho_e/\rho_i$ . Now, we compare the relative sizes of the terms within the square root. By assuming a background flow much smaller than the Alfvén speed,  $V_{0z} \ll V_A$ , the above expression can be simplified into a more reasonable format, where the eikonals  $\Omega$  and  $K$  are written in their differential form,

$$\frac{\partial\theta}{\partial t} + \left[ \frac{V_{0z}}{1 + \chi} + \sqrt{2} \frac{V_A}{\sqrt{1 + \chi}} \right] \frac{\partial\theta}{\partial z} = 0. \quad (2.20)$$

Following the method developed for the over-dense loop case, equation (2.18) can be solved using the method of characteristics to give an expression for the wave phase in terms of an arbitrary function,  $F$ . Now,  $\theta$  can then be written as

$$\theta = F \left[ \frac{V_{0z}}{A} (1 + \chi) \exp[-At] + \frac{2\sqrt{2}V_{A0}}{A} \left( \sqrt{\exp[-At] + \chi_0} - \sqrt{\chi_0} \operatorname{arctanh} \left[ \frac{\sqrt{\chi_0 + \exp[-At]}}{\sqrt{\chi_0}} \right] \right) \right], \quad (2.21)$$

for an initial density ration,  $\chi_0 = \rho_e/\rho_{i0}$ . Before the boundary condition describing the constant driver can be applied, the above expression must be simplified into a more manageable solution. The only way to proceed is by approximating the *arctanh* function to two terms in the Taylor series the following is gained,

$$\theta = F \left[ \frac{V_{0z} \exp[-At]}{A} (1 + \chi) + 2\sqrt{2}V_A \frac{(1 + \chi)^{3/2}}{A\chi_0} \exp[-2At] \right], \quad (2.22)$$

However, the Taylor Series is not applicable in such a context as the argument of the *arctanh* function is always greater than 1. In order to make analytical progress, therefore, we return to equation (2.20) and the characteristics lines,  $C$ , of equation (2.20). By taking the binomial expansion to leading order we can write

$$\begin{aligned} C &= V_{0z}(1 + \chi) - \sqrt{2}V_{A0} \int \sqrt{1 + \chi} \exp \left[ -\frac{At}{2} \right] dt \\ &\approx V_{0z}(1 + \chi) - \sqrt{2}V_{A0} \int \left( 1 + \frac{\chi}{2} \right) \exp \left[ -\frac{At}{2} \right] dt. \end{aligned}$$

A full solution can now be found, applicable in the region where  $\chi < 1$ , i.e. for trapped waves. The wave phase can now be solved in terms of an arbitrary function  $F_2$

$$\theta = F_2(g) = F_2 \left[ \left( V_{0z}(1 + \chi) + 2\sqrt{2}V_A(1 - \chi/2) \right) \frac{\exp[-At]}{A} \right]. \quad (2.23)$$

We again apply the constant driver boundary condition, i.e.  $\theta(t, 0) = -\omega t$ , and can gain the full expression for the wave phase as

$$\theta = \frac{2\omega}{A} \ln \left| \frac{1}{4\sqrt{2}V_{A0}} \left( g + \sqrt{g^2 + 16V_{A0}^2\chi_0} \right) \right|, \quad (2.24)$$

Using this new expression for the wave phase, it is now possible to find new forms of the eikonal functions  $\Omega$  and  $K$ . Once again, we can write

$$-\frac{\partial\theta}{\partial t} = \Omega = \frac{2\omega}{A} \frac{V_{0z} + \sqrt{2}V_A(1 + \chi/2)}{\sqrt{g^2 + 16V_{A0}^2\chi_0}} \exp[-At], \quad (2.25)$$

and

$$\frac{\partial\theta}{\partial z} = K = \frac{2\omega}{A} \frac{(1 + \chi)}{\sqrt{g^2 + 16V_{A0}^2\chi_0}} \exp[-At]. \quad (2.26)$$

We can note at this point that in the limit of the density ratio being zero, this

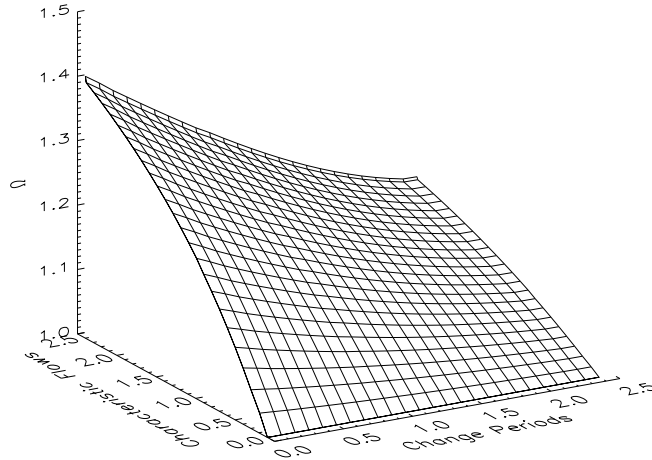


Figure 2.5: Temporal evolution of the wave frequency under the moderate activity approximation. All quantities are the same as detailed in Figure 2.1.

result reduces to the over-dense loop approximation made previously, despite both the approximations made to get to this point. In the same manner as before we investigate the dynamic frequency,  $\Omega$  (see Figure 2.5), and vertical

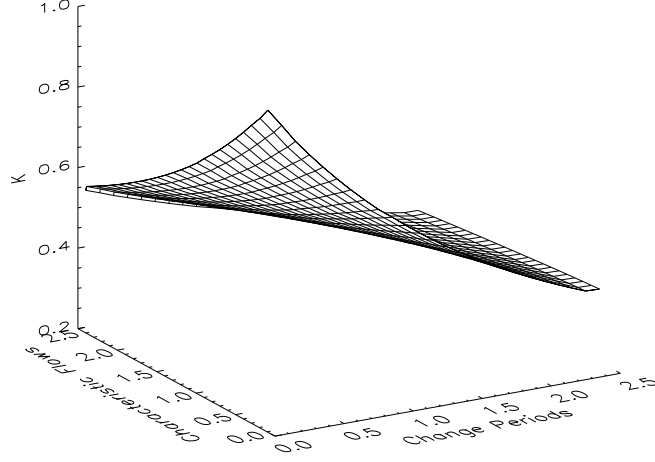


Figure 2.6: Temporal evolution of the vertical wavenumber under the moderate activity approximation. All quantities are the same as detailed in Figure 2.2.

wavenumber,  $K$  (see Figure 2.6). The dynamic frequency once again decreases in time with approximate exponential factor  $A/2$ , however, it now decreases to constant determined by the driving frequency and the initial density ratio instead of the driving frequency. The point at which the frequency can be considered to be zero is past the point at which the density ratio exceeds the limit of  $\chi < 1$  and therefore this asymptotic nature of the frequency is not relevant when taken to extreme points in time.

The dynamic wavenumber likewise evolves in the same way as in the case of the over-dense loop, however, the wavenumber now tends to a constant level. Once again this change is well beyond the point at which the interior and exterior densities will have reached the point of equality and hence gone beyond the limits imposed by the use of the binomial approximation. We can also note that the magnitude of the background plasma flow has an impact upon the constant value to which the wavenumber tends. However, we reiterate the point that the limitations imposed upon the flow mean that the analysis in the spatial component are likely to be less accurate than those conducted for the temporal evolution.

In the moderate-activity approximation the expression for the phase speed is given by

$$V_{ph} = \frac{\Omega}{K} = \frac{V_{0z} + \sqrt{2}V_A(1 + \chi/2)}{1 + \chi}, \quad (2.27)$$

which again can be shown to reduce to the same phase speed as the over-dense loop when  $\chi \rightarrow 0$ . The effect of the background flow now decreases as the density ratio increases and the increase in the Alfvén speed dominates the changing phase speed.

## 2.4.1 Temporal Evolution of the Individual Wave Modes

### $m = 1$ kink mode

Using the eikonal functions calculated in the previous subsection, the amplitude of the fast MHD wave can now be calculated using equation (2.8). Figure 2.7 describes the temporal evolution of the wave amplitude. The approximately exponential increase of the wave amplitude matches that found in the case of the over-dense loop. In the case of the moderate activity approximation, however, the wave propagation has an additional, limiting, factor. Were Figure 2.7 extended, it would show that the displacement amplitude tends to a constant limit at the point when the interior and exterior densities are equal, reinforcing the idea that this analysis is only valid up until the point where leaky wave propagation is likely.

### $m \geq 2$ mode

Comparison of Figure 2.4 and Figure 2.8 leads to a similar conclusion in that the wave is amplified over time to a constant level, however, this saturation point is reached after a shorter time period than in the over-dense loop approximation. The evolution of the higher order modes leads to the same conclusions as drawn in the previous section, namely that the  $m \geq 3$  modes are damped to nothing at increasing rates, dependent upon the azimuthal wave number  $m$ .

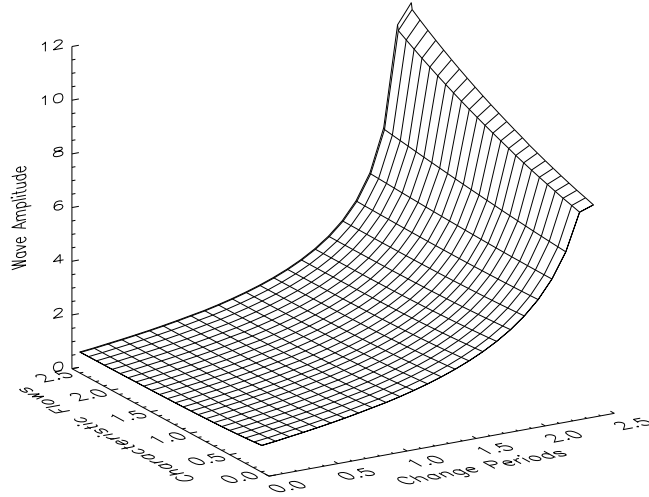


Figure 2.7: Relative change in the amplitude of the fast,  $m = 1$ , MHD wave under the moderate activity approximation.

## 2.5 Conclusion

This chapter has investigated the impact that a temporally decreasing density has upon the propagation of the kink and fluting fast linear MHD modes present in a coronal environment in a magnetic cylinder evolving dynamically. A set of two governing equations describing the evolution in total pressure,  $P$ , and the radial velocity,  $\xi_r$ , were found.

The assumption of a slowly varying plasma density allowed for the use of the WKB approximation by relating the slowly changing background to the period of oscillation of the fast MHD wave. By applying the WKB approximation to leading order the two governing equations were then solved for  $P$  and the radial displacement,  $\xi_r$ , for both the interior and exterior regions. The application of continuity of magnetic pressure and displacement at the flux tube boundary provided the general dispersion relation for MHD wave propagation in the dynamic magnetic cylinder and permitted a solution to be found for the two eikonal functions  $\Omega$  and  $K$ . Using the explicit forms for the evolution of the frequency and vertical wavenumber, the individual wave modes were investigated for the effects of time and spacial dependency.

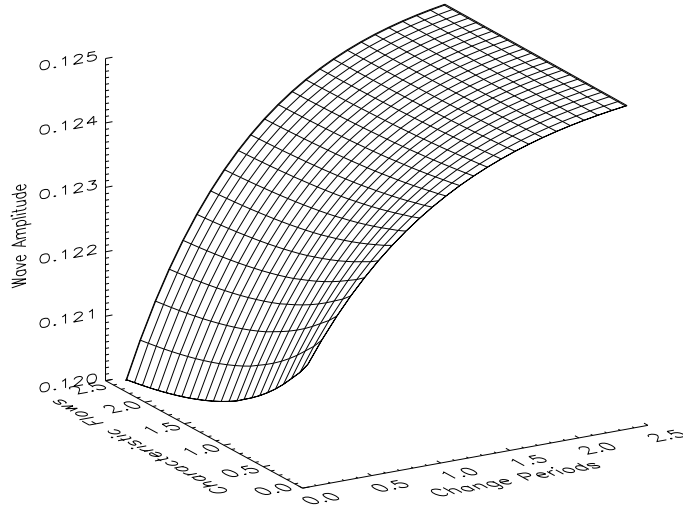


Figure 2.8: Relative change in the amplitude of the fast,  $m = 2$ , MHD wave under the moderate activity approximation.

The fast kink mode was found to be amplified exponentially. This result, whilst unphysical in the extreme limit, gives at least an indication of the propagation of fast kink waves under such conditions. The  $m = 2$  mode is likewise amplified, however, only to a saturation level after which the resulting wave is practically time-independent. All other modes, with  $m \geq 3$ , are damped to insignificance within a few times the characteristic time of density change. The non-constant flow acts in a similar manner to the decreasing density in that the flow helps drive the amplification or damping of the individual wave modes. However, in comparison with the effect of the increasing Alfvén speed this effect can be neglected for a cylinder of finite length.

In Section 2.4 the application of the moderate-activity approximation allowed a different form of solution to the dispersion relation. Analysis of this solution provided a different form of the dynamic frequency and wavenumber, however it can be shown that both quantities reduce to their counterparts in the over-dense approximation. The expression for the frequency in the moderate activity approximation gave a result similar to that found in the case of the over-dense loop, an approximately exponential decrease over the time for which

only trapped waves propagate. Likewise, the dynamic wavenumber decreases in the same manner, with the small alteration of tending to a constant value. These minor differences, however, create a limiting factor to the evolution in the overall wave amplitude. The amplitude of the kink (i.e. the  $m = 1$ ) wave is amplified to a constant level around the point where the densities equalise, much like in the manner of the  $m = 2$  wave in the over-dense loop approximation. Despite this difference, the initial amplification is in agreement and hence, for the region where the density ratio is low, would imply that both these results are consistent with the reality of wave propagation in the solar environment.

The main applications of this work done in this chapter, after its use as a tool for analysing observed propagating waves, will be on the forward modelling of standing wave observations in time dependent systems, by considering e.g. propagating waves traveling in opposite directions, and as an aid to further modelling in order to explain the observed damping in the corona. To aid in this, given the applicability and the simple nature of the calculations performed in the over-dense loop as well as the current level of observational data, the results from Section 2.3 should be preferred over those done in Section 2.4 which have more potential for chromospheric and photospheric wave propagation.

# Chapter 3

## MHD Wave Propagation in a Finite Plasma-beta

### 3.1 Introduction

The propagation of magnetohydrodynamic waves is an area that has been thoroughly studied for the idealised static and steady state magnetised plasma systems used in numerous theoretical models. By applying the generalisation of a temporally varying background density to an open flux tube further investigations into the propagation of both the fast and slow MHD waves can take place. The assumption of a zero-beta plasma was used in Chapter 2 and that assumption is now relaxed for further analysis here. The introduction of a finite thermal pressure to the magnetic flux tube equilibrium modifies the existence of fast MHD waves which are directly comparable to their counterparts found in Chapter 2. Further, as a direct consequence of the non-zero kinetic plasma pressure, the slow MHD wave now exists, and can be investigated in a similar manner to the fast MHD wave. Analysis of the slow wave shows that, similar to the fast MHD wave, wave amplitude amplification takes place in time and height that is analytically determined here. We conclude that for a temporally decreasing density both propagating the fast and slow MHD wave modes are amplified for over-dense magnetic flux tubes. Most of the work within this chapter is based upon the work done by Williamson and Erdélyi (Submitted

Solar Physics 2013b).

## 3.2 Background Plasma

A magnetic cylinder of radius  $R$  is embedded in a magnetic atmosphere in an equilibrium background analogous to those in Chapter 2 with pressure, density, flow and magnetic field denoted by  $p$ ,  $\rho$ ,  $\mathbf{V}$  and  $\mathbf{B}$ . A subscript ‘i’ indicates a value within the flux tube and an ‘e’ stands for exterior ones. From this point a subscript ‘0’ means a background value as opposed to the perturbed values defined in Section 3.3. The interior background density is assumed to decrease in time such that  $\rho_i = \rho_{i0} \exp[-At]$  where  $A$  is a positive constant and  $\rho_{i0}$  is the density at  $t = 0$ . In order to maintain conservation of mass, plasma will evacuate the flux tube, a background flow of  $V_{i0z} = Az$  is required. A constant exterior density,  $\rho_e$  is assumed. Both the interior and exterior magnetic fields are assumed to be constant but distinct from each other. Likewise, the interior and exterior kinetic pressures are constant but distinct in order to satisfy the radial pressure balance given by

$$p_i + \frac{B_{0zi}^2}{2\mu_0} = p_e + \frac{B_{0ze}^2}{2\mu_0}. \quad (3.1)$$

The assumption of constant kinetic pressure gives rise to an exponentially increasing sound speed, defined by

$$c^2 = \gamma \frac{p_0}{\rho_0},$$

where  $\gamma$  is the adiabatic gas index. The sound speed is noted to change in time at the same rate as the Alfvén speed. Once again we can write the total pressure as the sum of the thermal and magnetic pressures and therefore the background total pressure can be written as

$$P_0 = p_0 + \frac{B_{0z}^2}{2\mu_0}. \quad (3.2)$$

### 3.3 Governing Equations

Using the definitions as given in the previous Section, the perturbed, linearised and ideal MHD equations can be written as

$$\frac{\partial \rho}{\partial t} + \nabla \cdot (\rho_0 \mathbf{V} + \rho \mathbf{V}_0) = 0, \quad (3.3)$$

$$\rho_0 \left[ \frac{\partial \mathbf{V}}{\partial t} + \mathbf{V} \cdot \nabla \mathbf{V}_0 + V_{0z} \frac{\partial \mathbf{V}}{\partial z} \right] + \rho V_{0z} \frac{\partial \mathbf{V}_0}{\partial z} = -\nabla p + \frac{1}{\mu} (\nabla \times \mathbf{B}) \times \mathbf{B}_0, \quad (3.4)$$

$$\frac{\partial \mathbf{B}}{\partial t} = \nabla \times (\mathbf{V}_0 \times \mathbf{B}) + \nabla \times (\mathbf{V} \times \mathbf{B}_0) + (\nabla \times \mathbf{B}) \times \mathbf{B}_0, \quad (3.5)$$

$$\frac{\partial p}{\partial t} + \mathbf{V}_0 \cdot \nabla p = -\gamma \left( p \frac{\partial V_{0z}}{\partial z} + p_0 \nabla \cdot \mathbf{V} \right). \quad (3.6)$$

By splitting equations (3.3)-(3.6) into vector components, the perturbed variables are governed by

$$\hat{\omega} \rho = -\nabla \cdot (\rho_0 \mathbf{V}), \quad (3.7)$$

$$\left( \hat{\omega} + \gamma \frac{dV_{0z}}{dz} \right) p = -\gamma p_0 \nabla \cdot \mathbf{V} - \gamma p \frac{dV_{0z}}{dz}, \quad (3.8)$$

$$\left( \hat{\omega} + \frac{\partial V_{0z}}{\partial z} \right) B_r = B_{0z} \frac{\partial V_r}{\partial z}, \quad (3.9)$$

$$\left( \hat{\omega} + \frac{\partial V_{0z}}{\partial z} \right) B_\phi = B_{0z} \frac{\partial V_\phi}{\partial z}, \quad (3.10)$$

$$\hat{\omega} B_z = B_{0z} \frac{\partial V_z}{\partial z} - B_{0z} \nabla \cdot \mathbf{V} - \frac{dB_{0z}}{dr} V_r, \quad (3.11)$$

$$\rho_0 \hat{\omega} V_r = -\frac{\partial P}{\partial r} + \frac{B_{0z}}{\mu_0} \frac{\partial B_r}{\partial z}, \quad (3.12)$$

$$\rho_0 \hat{\omega} V_\phi = -\frac{1}{r} \frac{\partial P}{\partial \phi} + \frac{B_{0z}}{\mu_0} \frac{\partial B_\phi}{\partial z} \quad (3.13)$$

$$\rho_0 \left( \hat{\omega} + \frac{\partial V_{0z}}{\partial z} \right) V_z = -\frac{\partial P}{\partial z} + \frac{B_{0z}}{\mu_0} \frac{\partial B_z}{\partial z} + \frac{dB_{0z}}{dr} \frac{B_r}{\mu_0} - \rho V_{0z} \frac{dV_{0z}}{dz}, \quad (3.14)$$

where

$$\hat{\omega} = \frac{\partial}{\partial t} + V_{0z} \frac{\partial}{\partial z}. \quad (3.15)$$

Combination of these equations and the perturbed pressure balance equation, equation (3.2), will lead to a set of governing equations for linear MHD wave propagation for the perturbed variables  $P$ ,  $V_r$ ,  $\nabla \cdot \mathbf{V}$  and  $V_z$ . These governing equations are given by the following four expressions

$$\begin{aligned} \hat{\omega} \left( \hat{\omega} + \gamma \frac{dV_{0z}}{dz} \right) P = & -\rho_0 (c^2 + V_A^2) \hat{\omega} \nabla \cdot \mathbf{V} + \rho_0 V_A^2 \left( \hat{\omega} + \gamma \frac{dV_{0z}}{dz} \right) \frac{\partial V_z}{\partial z} - \\ & -\gamma \frac{dV_{0z}}{dz} \rho_0 V_A^2 \nabla \cdot \mathbf{V} - \frac{B_{0z}}{\mu_0} \frac{dB_{0z}}{dr} \gamma \frac{dV_{0z}}{dz} V_r, \end{aligned} \quad (3.16)$$

$$\begin{aligned} \rho_0 \left( \hat{\omega} \left[ \hat{\omega} + \frac{dV_{0z}}{dz} \right] - \hat{\omega}_A^2 \right) \nabla \cdot \mathbf{V} = & \rho_0 \left( \hat{\omega} \left[ \hat{\omega} + \frac{dV_{0z}}{dz} \right] - \hat{\omega}_A^2 \right) \frac{1}{r} \frac{\partial (rV_r)}{\partial r} - \\ & - \left( \hat{\omega} + 2 \frac{dV_{0z}}{dz} \right) \frac{1}{r^2} \frac{\partial^2 P}{\partial \phi^2} + \rho_0 \left( \hat{\omega} \left[ \hat{\omega} + \frac{dV_{0z}}{dz} \right] - \hat{\omega}_A^2 \right) \frac{\partial V_z}{\partial z}, \end{aligned} \quad (3.17)$$

$$\rho_0 \left( \hat{\omega} \left[ \hat{\omega} + \frac{dV_{0z}}{dz} \right] - \hat{\omega}_A^2 \right) V_r = - \left( \hat{\omega} + 2 \frac{dV_{0z}}{dz} \right) \frac{\partial P}{\partial r}, \quad (3.18)$$

$$\begin{aligned} \left( \hat{\omega} - \frac{dV_{0z}}{dz} \right) \rho_0 \left[ \hat{\omega} \left( \hat{\omega} + \frac{dV_{0z}}{dz} \right) - \hat{\omega}_A^2 \right] V_z = & - \left( \hat{\omega}^2 - \frac{dV_{0z}^2}{dz} \right) \frac{\partial P}{\partial z} - \\ & - \left( \hat{\omega} - \frac{dV_{0z}}{dz} \right) \rho_0 V_A^2 \frac{\partial}{\partial z} \nabla \cdot \mathbf{V} + V_{0z} \frac{dV_{0z}}{dz} \nabla \cdot (\rho_0 \mathbf{V}). \end{aligned} \quad (3.19)$$

The non-commutability of the various combinations of  $\hat{\omega}$  and  $\hat{\omega}_A$  inhibit further general progress. As a result, this work will now apply the WKB approximation to leading order. By applying equation (1.47) to equations (3.16)-(3.19) allows for leading order equations for  $V_r$  and  $P$  to be found. Then, using the expression for the plasma displacement,  $\mathbf{V} = -i\varpi \underline{\xi}$ , where  $\underline{\xi}$  is the displacement vector, three governing equations can be obtained as,

$$\rho_0 (\varpi^2 - \varpi_A^2) Q_r = \frac{\partial Q_P}{\partial r}, \quad (3.20)$$

$$\begin{aligned} \frac{\rho_0}{r} (c^2 + V_A^2) (\varpi^2 - \varpi_A^2) (\varpi^2 - \varpi_c^2) \frac{\partial (rQ_r)}{\partial r} = \\ = - \left[ \varpi^4 - (c^2 + V_A^2) (\varpi^2 - \varpi_c^2) \left( \frac{m^2}{r^2} + K^2 \right) \right] Q_P, \end{aligned} \quad (3.21)$$

describing the total pressure amplitude ( $Q_P$ ), radial component of the displacement vector ( $Q_r$ ) and for the longitudinal component of the displacement vector ( $Q_z$ )

$$\rho_0 \varpi^2 Q_z = iKP + iK \frac{B_{0z}^2}{\mu_0 r} \frac{\partial(rQ_r)}{\partial r}. \quad (3.22)$$

We can observe, that the equations for  $Q_P$  and  $Q_r$  are coupled but form a closed system. Once they are solved, equation (3.18) can be also solved to determine the longitudinal perturbation. The Alfvén and cusp frequencies are now in their standard form and are given by

$$\varpi_A^2 = V_A^2 K^2, \quad \varpi_c^2 = \frac{c^2 \varpi_A^2}{c^2 + V_A^2}.$$

Using equations (3.20) and (3.21), solutions inside and outside the flux tube can now be sought.  $Q_P$  and  $Q_r$  can be written as

$$Q_P = \begin{cases} A_i J_{|m|}(M_i r) & r < R, \\ A_e K_{|m|}(M_e r) & r > R, \end{cases} \quad (3.23)$$

where

$$M_i^2 = \frac{(\varpi^2 - c^2 K^2)(\varpi^2 - \varpi_A^2)}{(c^2 + V_A^2)(\varpi^2 - \varpi_c^2)}, \quad M_e^2 = -\frac{(\Omega^2 - \varpi_{Ae}^2)(\Omega^2 - c_e^2 K^2)}{(c_e^2 + V_{Ae}^2)(\Omega^2 - \varpi_{ce}^2)}.$$

Here  $J_m$  and  $K_m$  are the Bessel functions of the first kind and the modified Bessel function of the second kind of order  $m$ , respectively. The alternative solutions, i.e. the Bessel  $I$  function, represents surface waves and consequently are neglected. The individual  $M_{i,e}$  can be considered to be the wavenumbers in the radial direction for the interior and exterior regions. We once again neglect solutions which allow for energy losses to the exterior atmosphere and hence the wave propagation in the exterior region is expressed using the Bessel  $K$  function.

## 3.4 Fast Wave Propagation

### 3.4.1 Over-Dense Loop Approximation

Using the definition for  $Q_P$  in equation (3.23) the dispersion relation for the fast MHD wave modes can be found to be algebraically identical to that given in Chapter 2 and is given by

$$\rho_i(\varpi_f^2 - \varpi_A^2) + \rho_e(\Omega_f^2 - \varpi_{Ae}^2) = 0. \quad (3.24)$$

The solution of equation (3.20) is close to that of Chapter 2 for coronal conditions and can be written as

$$\theta_f = 2\frac{\omega}{A} \ln \left| \left( V_{0z} + 2\sqrt{\frac{B_i^2 + B_e^2}{\mu_0\rho_i}} \right) \frac{\exp[-At]\sqrt{\mu_0\rho_{i0}}}{2\sqrt{B_i^2 + B_e^2}} \right|. \quad (3.25)$$

Let us introduce the following notation,

$$\tilde{B} = \sqrt{\frac{B_i^2 + B_e^2}{\mu_0\rho_i}}, \quad \tilde{B}_0 = \sqrt{\frac{B_i^2 + B_e^2}{\mu_0\rho_{i0}}}.$$

Thus the wave phase can be rewritten as

$$\theta_f = 2\frac{\omega}{A} \ln \left| \left( V_{0z} + 2\tilde{B} \right) \frac{\exp[-At]\sqrt{\mu_0\rho_{i0}}}{2\tilde{B}_0} \right|.$$

Using the definitions for  $\Omega_f$  and  $K_f$ , as given in Section 1.7.3, will give the frequency and wavenumber as

$$\Omega_f = 2\omega \frac{V_{0z} + \tilde{B}}{V_{0z} + 2\tilde{B}}, \quad K_f = \frac{2\omega}{V_{0z} + 2\tilde{B}}. \quad (3.26)$$

These definitions for  $\Omega_f$  and  $K_f$  follow a similar temporal evolution as their counterparts in the zero plasma-beta environment and can be shown to reduce to their respective corresponding expressions. For more details refer to Figures 1 and 2 in Chapter 2. Applying the new form of  $\Omega_f$  and  $K_f$  into  $Q_P$ , given by

equation (3.19), gives

$$Q_P = \begin{cases} A_i J_{|m|}(M_i r) & r < R, \\ A_e K_{|m|}(M_e r) & r > R, \end{cases} \quad (3.27)$$

$$Q_{ri} = \frac{A_i M_i}{\rho_i V_A^2 K_f^2} J'_{|m|}(M_i r), \quad (3.28)$$

$$Q_{re} = \frac{A_e M_e}{\rho_e (\Omega_f^2 - V_{Ae}^2 K^2)} K'_{|m|}(M_e r), \quad (3.29)$$

where

$$M_i^2 = K_f^2 \frac{V_A^2 - c^2 + B_e^2 / \mu_0 \rho_i}{c^2 + V_A^2 (1 + B_i^2 / B_e^2)}, \quad M_e^2 = -\frac{(\Omega_f^2 - \varpi_{Ae}^2)(\Omega_f^2 - c_e^2 K^2)}{(c_e^2 + V_{Ae}^2)(\Omega_f^2 - \omega_c^2)}.$$

When comparing these expressions to those in Chapter 2 it is obvious to see that not only do the results gained for the fast MHD wave mode here reduce to those found under zero plasma-beta conditions, i.e. that  $p_i = p_e = 0$  and  $B_i = B_e$ . Therefore, the temporal and spatial dependence of the wave amplitude are of the same implicit form and, for the waves propagating inside the flux tube, merely scaled down by the presence of the evolving sound speed. Again, for details of the individual wave modes refer to Section 2.4.

### 3.4.2 Moderate-Activity Approximation

Like in the case of the over-dense loop, the moderate activity approximation for the fast MHD wave is merely a correction to the work done in the previous chapter. Using the governing equations for a magnetic flux tube with a constant thermal pressure, the dispersion relation can be rewritten in the form

$$(1 + \chi) \frac{\partial \theta}{\partial t} = V_{0z} K + \sqrt{(1 + \chi)} \tilde{B} K.$$

The solution to which is similar in nature to that found for equation (2.20), where

$$\theta = \frac{2\omega}{A} \ln \left| \frac{1}{2} \left( g + \sqrt{g^2 + 2\chi_0} \right) \right|, \quad (3.30)$$

but where  $g$  now has the form

$$g = \left( V_{0z}(1 + \chi) + 2\tilde{B}(1 - \chi/2) \right) \frac{\exp[-At]}{A}.$$

From this it can be easily seen that the evolution of the phase, and therefore the frequency, wavenumber and wave amplitudes, takes place in exactly the same fashion as shown in Figures 2.5, 2.6, 2.7 and 2.8 in Chapter 2. As such, we can write the following expressions for the frequency and vertical wavenumber for the fast MHD waves as

$$\Omega = \frac{2\omega}{A} \frac{V_{0z} + \tilde{B}(1 + \chi/2)}{\sqrt{g^2 + 16\tilde{B}_0\chi_0}} \exp[-At] \quad (3.31)$$

$$K = \frac{2\omega}{A} \frac{(1 + \chi)}{\sqrt{g^2 + 16\tilde{B}_0\chi_0}} \exp[-At], \quad (3.32)$$

which can, once again, be shown to reduce to their counterparts in the zero plasma- $\beta$  regime as well as to their counterparts in the over-dense loop approximation.

### 3.5 Slow Wave Propagation

With the addition of a finite background pressure the propagating slow wave is now enabled. Analysis of the slow MHD wave can be conducted in a similar manner as for the fast wave. The slow MHD wave components can be found by solving for the vertical velocity,  $V_z$ , or the vertical displacement,  $\xi_z$ . During this process we focus entirely upon the wave propagation within the flux tube as the exterior propagation is again considered to be evanescent. After the WKB approximation is applied to leading order it is possible to establish that

$$V_z = \frac{\varpi K c^2}{\rho_0(\varpi_s^2 - \varpi_c^2)(c^2 + V_A^2)} P \quad \xi_z = \frac{iK_s c^2}{\rho_0(\varpi_s^2 - \varpi_c^2)(c^2 + V_A^2)} P. \quad (3.33)$$

Whilst these equations govern the slow MHD wave amplitude, the frequency and wavenumber have to be determined via another route. By limiting the

slow MHD wave propagation to a rigid magnetic field, i.e.  $B_r \approx 0$ , allows for a modified version of the classical sound wave equation to be formed from the perturbed form of equation (3.1) and equations (3.8) and (3.14). As a consequence of the rigid magnetic field, we expect that only the symmetric  $m = 0$  sausage mode will propagate, such expectation is borne out by the following analysis. Application of the definitions for the frequency and wavenumber, from Section 1.7, allows the following governing PDE to be written for the wave phase

$$\frac{\partial \theta}{\partial t} + (V_{0z} \pm c) \frac{\partial \theta}{\partial z} = 0. \quad (3.34)$$

When the condition  $\theta(t, 0) = -\omega t$  is applied to equation (3.30), we gain

$$\theta = \frac{2\omega}{A} \ln \left| (V_{0z} + 2c) \frac{\exp[-At]}{2c_0} \right|, \quad (3.35)$$

here  $c_0$  is the initial sound speed. With such result the frequency and wavenumber can now be found in their explicit form, i.e.

$$\Omega_s = 2\omega \frac{V_{0z} + c}{V_{0z} + 2c}, \quad K_s = \frac{2\omega}{V_{0z} + 2c}. \quad (3.36)$$

Whilst such a result gives an indication of the evolution of a slow MHD wave in a time-dependent waveguide, the assumption of a rigid magnetic field has consequences for the various slow MHD wave modes that would be expected to propagate in a magnetic cylinder. When equation (3.36) is used to fully explore the evolution of the amplitude of the wave, as given in equation (3.33), all of the  $|m| \geq 1$  modes are removed from consideration by the lack of radial motion. This is immediately obvious when the amplitude of the vertical velocity component and the vertical displacement are written explicitly,

$$V_z = \frac{J_m(0)}{\rho_0 c}, \quad \xi_z = i \frac{V_{0z} + 2c}{\rho_0 c^2} J_m(0). \quad (3.37)$$

By considering the  $m = 0$  sausage mode, the temporal and spatial evolution of the slow wave is simple to read off. The velocity component does not vary with the position above the driving point and varies only in time with respect to

half the characteristic period of density change, i.e.  $\exp[-At/2]$ . The vertical displacement, however, varies linearly with respect to the background flow. The temporal evolution takes the same form as that of the velocity albeit with an increased initial value due to the presence of the background plasma flow.

### 3.6 Conclusion

This study has investigated the propagation of the magneto-sonic MHD waves in a pressurised magnetic flux tube with a time-dependent density. A set of four governing equations for wave action within the magnetic atmosphere is found. Applying the leading order in the WKB approximation, the governing equations for MHD wave propagation were found. By isolating the different directions of displacement the individual wave modes were isolated and investigated separately.

The first wave mode studied was the fast kink wave. Using the method of solution outlined in Chapter 2, generalised forms of the frequency and wavenumber were found and shown to correspond to their counterpart results found previously in zero plasma-beta. The presence of the sound speed introduces a scaling of absolute values, however, the temporal evolution of the eigenfunctions is unaltered. When compared to the counterparts values, i.e. in the time-independent system as investigated in Edwin and Roberts (1983a) the wave frequency  $\Omega$  tends to the driving frequency  $\omega$  over large time periods. However, when the time-dependent wavenumber,  $K$ , is compared to the time-independent wavenumber,  $k$ , the result is very different. The temporally evolving wavenumber becomes infinitely small over a large time period indicating a cessation of the wave propagation assumed in this model, i.e. non-leaky waves. The result conforms to current theory when the density decreases to that of the exterior density the wave propagation will tend to that of a uniform medium and the analysis performed here is no longer valid.

The fast MHD wave has an alternative solution for the moderate activity which can be performed in the same manner as in Chapter 2, the results are again algebraically similar to those found previously. As in the case of the overdense loop approximation, the presence of the sound speed induces a scaling

within the perturbed total pressure and the evolution of the various components of the propagating wave all evolve in the same manner as their counterparts in the zero plasma- $\beta$  regime.

In Section 3.5 we investigated the propagation and properties of the slow MHD wave within a waveguide with a temporally varying density. The introduction of a constant thermal pressure allows for the propagation of the slow wave that was previously excluded from Chapter 2 by the zero plasma-beta assumption. By finding the displacement parallel to the magnetic field the slow MHD wave amplitude was obtained in terms of the undetermined frequency and wavenumber. By considering the slow MHD wave as a propagating MHD wave in a rigid magnetic field, an expression to determine the frequency and vertical wavenumber was found simply. The frequency and wavenumber vary in a similar manner as their counterparts in the fast MHD wave and are found by solving the one-dimensional wave equation. With the explicit forms for  $\Omega_s$  and  $K_s$  the amplitude of the slow wave was revisited and evaluated. The rigidity assumption of the magnetic field reduced the number of potential slow wave modes to one, namely the longitudinal (i.e. sausage) MHD mode. The evolution of the slow sausage wave is then simply read off, for either the velocity or displacement of the wave. Note that the amplification of the slow MHD wave, for a temporally decreasing density, is again in disagreement with the current observational data and continues to emphasize the strong need for improved wave damping theories in particular in temporally evolving magnetised plasmas. On the other hand just as in the case of the propagating fast MHD wave an increasing density will cause a damping of the propagating wave.

# Chapter 4

## Leaky Wave Propagation in a Zero-beta Dynamic Plasma

### 4.1 Introduction

In this chapter we consider a system which supports the propagation of fast MHD waves with energy leakage into the magnetised atmosphere. In the previous chapters we discounted this possibility by constructing models based upon over-dense structures in the solar corona, for which it is well known that leaky waves do not propagate. The most simple system that would support leaky waves is an under-dense structure. These under-dense structures are typically found at lower atmospheric levels, e.g. in the photosphere, however, a possible coronal exception to this is the coronal hole. The coronal hole is an area of open magnetic field lines stretching from the solar surface out through the corona. Density levels within a coronal hole are generally thought to be of the order of three times less than the general surrounding coronal atmosphere. A coronal hole though is a difficult place to search for these leaky waves, mainly due to the very low density levels in both the interior and exterior regions. In this model we make the assumption of zero plasma- $\beta$ , perhaps less accurate for the leaky waves found in the low levels of the solar atmosphere, but useful as an initial step. We will use the governing equations found in Chapter 2 to explore the damping of the fast MHD wave mode through energy leakage into the surround-

ing atmosphere. After obtaining the analytical expressions for the amplitude of the leaky waves we determine the damping coefficient,  $\gamma$ . In order to fully explore the temporal evolution of these quantities our next step is to solve the real part of the dispersion relation in the moderate activity approximation and determine the wave phase, the dynamic frequency and wavenumber in terms of the Lambert W function. The frequency and wavenumber can be shown to decrease to a constant level, in approximately the same manner as found in the moderate-activity approximations as detailed in the previous chapters. The amplitude of the various wave modes behaves more like those in the over-dense loop approximation as there no longer exists a limiting factor that occurs when the densities become approximately equal.

The damping coefficient can be shown to decrease to zero in a relatively short time period, e.g. 2-3 characteristic density change periods.

## 4.2 Introduction to leaky waves

Whilst the introductory work into MHD wave propagation laid the foundations for the analysis of propagating waves, most of the early works restricted themselves to models with purely real  $\omega$ , representing conservation of energy. Complex frequencies were considered by Wilson (1979) for a magnetic field-free environment, whilst Spruit (1979), Goossens and Hollweg (1993) and Cally (1986) made some of the first rigorous investigations into the damping as a result of energy losses into the surrounding magnetic atmosphere. Further works have expanded upon the results found therein, perhaps the most relevant to this Thesis were the efforts into combining the damping through energy leakage and resonant absorption investigated by Stenuit *et al.* (1999) and Goossens *et al.* (2009). The following discussion is based upon the derivation as presented in Goossens *et al.* (2009).

In the previous chapters we have assumed that the wave propagation is trapped within the flux tube and hence the eigen-modes are unaltered. By relaxing this assumption or, alternatively, assume that some energy is lost to the magnetised atmosphere, we can find appropriate conditions under which this energy loss is important. If we analyse a stationary, vertical flux tube with

constant background parameters, equivalent to those detailed by Edwin and Roberts (1983a), we can construct the following governing equations:

$$\frac{dP}{dr} = \rho_0(\omega^2 - \omega_A^2)\xi_r, \quad (4.1)$$

$$\rho_0 V_A^2 \frac{1}{r} \frac{d(r\xi_r)}{dr} = -(\omega^2 - \omega_A^2)P. \quad (4.2)$$

These governing equations can then be solved for e.g. the total pressure perturbation,  $P$ . Now, instead of assuming that  $P \rightarrow 0$  as  $r \rightarrow \infty$  we allow for a non-zero exterior perturbation and as such we can write

$$P = \begin{cases} A_i J_{|m|}(m_i r) & r < R, \\ A_e H_{|m|}^1(m_e r) & r > R, \end{cases} \quad (4.3)$$

where  $H_m^1$  is the Hankel function of the first kind. We note that the  $H_m^2$  solution is neglected as this would represent an incoming wave that is of no interest to this work at present. Using equation (4.3) we can now write the radial displacement as

$$\xi_{ri} = \frac{A_i}{\rho_i(\omega^2 - \omega_A^2)} \frac{dJ_m(M_i r)}{dr}, \quad \xi_{re} = \frac{A_e}{\rho_e(\omega^2 - \omega_{Ae}^2)} \frac{dH_m^1(M_e r)}{dr} \quad (4.4)$$

The approach to solving for the wave propagation is mathematically identical up until the point at which we form the dispersion relation for the fast MHD wave. Again, making the assumption of continuity at the radial boundary of the flux tube, as detailed in Equation (1.14), we can write the dispersion relation as

$$\rho_i(\omega^2 - \omega_A^2) \frac{J_m(m_i R) H_m^{1'}(m_e R)}{J_m'(m_i R) H_m^1(m_e R)} \frac{m_e}{m_i} = \rho_e(\omega^2 - \omega_{Ae}^2). \quad (4.5)$$

Application of the thin tube approximation allows the dispersion relation to be reduced to

$$\rho_i(\omega^2 - \omega_A^2) + \rho_e(\omega^2 - \omega_{Ae}^2) = i \frac{\pi}{2} (m_e R)^2 \rho_i(\omega^2 - \omega_A^2). \quad (4.6)$$

The imaginary part of the dispersion relation indicates a damping of the kink frequency that was not present in the trapped wave calculation. At this point we make the assumption that  $\omega = \omega_r + i\gamma$  where  $\gamma \ll \omega_r$ , i.e., the damping rate is small. The real part of the complex eigen-frequency,  $\omega_r$ , describes the frequency of the waves in an undamped system and as such we can approximate the real part of the frequency by the kink frequency, as calculated in the case of trapped wave propagation, i.e.

$$\omega_k^2 = \frac{B_i^2 + B_e^2}{\mu_0(\rho_i + \rho_e)} k^2. \quad (4.7)$$

The damping coefficient,  $\gamma$ , can then be calculated by algebraically solving the dispersion relation, whilst ignoring a damping rate of order  $\gamma^2$  or higher.  $\gamma$  can therefore be written as

$$\gamma = \frac{\pi}{4} (m_e R)^2 \frac{\rho_i \rho_e}{(\rho_i + \rho_e)^2} \frac{\omega_{Ae}^2 - \omega_A^2}{\omega_k}, \quad (4.8)$$

The quantity  $\gamma$  is negative only if  $\omega_{Ae}^2 > \omega_A^2$ , in a zero plasma- $\beta$  this condition implies  $\rho_e > \rho_i$ . The damping coefficient can then be rewritten as

$$\gamma = -\frac{\pi}{8} \frac{(\rho_e - \rho_i)^2}{(\rho_e + \rho_i)^2} R^2 k_z^2 \omega_k, \quad (4.9)$$

which is always negative, and hence causes the wave to be damped. Whilst this condition is rarely satisfied high in the solar atmosphere, in the photosphere such magnetic structures are common. In the corona the magnetic structure most likely to satisfy this condition is a coronal hole, which does itself not satisfy the thin tube approximation. However, these investigations are useful for giving us some insight into the damping of MHD waves in these situations.

### 4.3 Governing Equations

For the purposes of this Thesis we wish to extend the analysis of leaky MHD waves into a time-dependent background. In the same manner that the derivation above was based upon the background as described in Edwin and Roberts

(1983b), the work here will be based upon a model similar to that discussed in Chapter 2, with the exception of an initial density ratio of approximate equality instead of the over-dense loop structure typical of coronal loops.

We construct a magnetic flux tube in a magnetised atmosphere of constant density, to which we again apply the zero plasma- $\beta$  approximation and as such we require that neither the interior region or the exterior region has finite plasma pressure. In both regions the magnetic fields are constant and vertical. The neglect of the plasma pressure directly implies that the magnetic fields are identical. In this chapter, however, we consider an exterior plasma density that is greater than or equal in magnitude to the initial interior density,  $\rho_{i0}$  allowing for the propagation of leaky MHD waves. We consider such solution as appropriate in the analysis of e.g. coronal holes, sunspots and magnetic pores. Given these parameters we can construct two governing equations under the assumption of ideal linearised MHD approximation for the radial displacement and perturbed total pressure. This analysis follows that performed in Chapter 2 and as such we merely state the two governing equations after the application of the WKB approximation to leading order. The two governing equations are

$$\rho_0(\varpi^2 - \varpi_A^2) \frac{1}{r} \frac{\partial(r\xi_r)}{\partial r} = - \left[ \varpi^2 - V_A^2 \left( K^2 + \frac{m^2}{r^2} \right) \right] P, \quad (4.10)$$

and

$$\frac{\partial P}{\partial r} = \rho_0(\varpi^2 - \varpi_A^2) \xi_r. \quad (4.11)$$

At this point we can, once again, solve the two governing equations for the perturbed total pressure and the radial displacement. The differential equation for the perturbed total pressure can therefore be written as

$$\frac{\partial^2 P}{\partial r^2} + \frac{1}{r} \frac{\partial P}{\partial r} + \left[ \frac{\varpi_{i,e}^2 - \varpi_{Ai,e}^2}{V_{Ai,e}^2} - \frac{m^2}{r^2} \right] P = 0, \quad (4.12)$$

where subscripts  $i, e$  indicates background variables in either the interior or exterior regions. The interior version of equation (4.12) can be solved in an identical fashion to that found previously. However, given the relaxation of the evanescent condition, the exterior solution will now take a very different form.

## 4.4 Leaky Wave Solution

At this point we no longer require that the exterior wave propagation is evanescent, indeed in the current regime of an under-dense flux tube it is far more likely that the exterior waves will carry energy away from the flux tube and into the surrounding magnetised atmosphere. Upon the relaxation of this assumption we find the mathematical solution to equation (4.12) now has more physical applications and therefore the perturbed total pressure, for body waves, can now be written as

$$Q_{Pi} = A_i J_m(M_i r), \quad Q_{Pe} = A_e H_m^1(M_e r), \quad (4.13)$$

where  $H_m^1$  is the Hankel function of the 1<sup>st</sup> kind of order  $m$ . We discard the Hankel function of the second kind for the reasons discussed in the previous section, i.e. it represents an incoming wave, and do not consider it further within this work. Using equation (4.13) and equation (4.11) we can therefore write the expression for the radial displacement as

$$\xi_{ri} = \frac{A_i}{\rho_i(\varpi^2 - \varpi_A^2)} \frac{\partial J_m(M_i r)}{\partial r}, \quad \xi_{re} = \frac{A_e}{\rho_e(\Omega^2 - \omega_{Ae}^2)} \frac{\partial H_m^1(M_e r)}{\partial r}. \quad (4.14)$$

We now require that the continuity in the radial displacement across the discontinuity in the magnetic field, as defined in Equation (1.14), still holds and using these conditions we can now write the dispersion relation for leaky waves in a time-dependent flux tube as

$$\begin{aligned} \rho_i(\varpi^2 - \varpi_A^2) J_m(M_i R) H_m^{1'}(M_e R) M_e = \\ = \rho_e(\Omega^2 - \omega_A^2) J_m'(M_i R) H_m^1(M_e R) M_i. \end{aligned} \quad (4.15)$$

The thin-tube approximation can once more be applied in order to make analytical progress. Again, the imaginary component of the Hankel function will represent damping of the propagating wave. Equation (4.15) can now be rewritten as

$$\rho_i(\varpi^2 - \varpi_A^2) + \rho_e(\Omega^2 - \omega_A^2) = i \frac{\pi}{2} (M_e R)^2 \rho_i(\varpi^2 - \varpi_A^2). \quad (4.16)$$

In order to determine the damping rate and the evolution of the damping rate we can follow one of two methods. In both cases we assume that the damping can be written as,  $\Omega = \Omega_r + i\gamma$  where  $\Omega_r$  is the real part of the frequency and can be obtained by solving the real part of equation (4.16), where we also assume that  $\Omega_r \gg \gamma$ . An algebraic approach would see us solve equation (4.16) for the damping coefficient  $\gamma$ , ignoring terms of order  $\gamma^2$ . For this work we will use the following differential approach, as detailed by e.g. Krall and Trivelpiece (1973). The quantity  $\gamma$  can, therefore, be written as

$$\gamma = -\frac{D_i}{\partial D_r / \partial \Omega} \Big|_{\Omega = \Omega_r = \Omega_k} = -\frac{\pi}{4} (M_e R)^2 \rho_i \frac{\varpi^2 - \varpi_A^2}{\rho_i \varpi + \rho_e \Omega} \Big|_{\Omega = \Omega_k}. \quad (4.17)$$

Whilst at this point other works have performed further analytically simplification in order to understand this result we will, instead, determine the explicit forms of the real parts of the frequency and the wavenumber in order to explore the evolution of the damping in time. The coronal approximation made in Section 2.3 can now no longer be applied due to the density ratio now being very large, therefore, the second of the approximation methods must be used. By making the assumption of moderate activity (i.e.  $V_{0z} \ll V_A$  as detailed in Chapter 2) we can reduce real part of the dispersion relation to

$$\frac{\partial \theta}{\partial t} + \left[ \frac{V_{0z}}{1 + \chi} + \frac{\sqrt{2} V_A}{\sqrt{1 + \chi}} \right] \frac{\partial \theta}{\partial z} = 0. \quad (4.18)$$

Previously, in the moderate activity approximation, we made the assumption that  $\chi < 1$ . Such an assumption will not allow for the propagation of leaky waves. Therefore we state that the density ratio,  $\chi$ , must fulfill the condition  $1 < \chi$  with an initial density ratio  $\chi_0$ , we can then, in a similar manner to Chapter

2, approximate the characteristic lines,  $C$ , using the binomial expansion, as

$$\begin{aligned} C &= \frac{V_{0z}(1+\chi)}{A} \exp[-At] - \sqrt{2}V_{A0} \int \sqrt{1+\chi} \exp[-At/2] dt, \\ &= \frac{V_{0z}(1+\chi)}{A} \exp[-At] - \sqrt{2\chi_0}V_{A0} \int \left( \sqrt{1+\frac{1}{\chi}} \right) dt, \\ &\approx \frac{V_{0z}(1+\chi)}{A} \exp[-At] - \sqrt{2\chi_0}V_{A0} \int \left( 1 + \frac{1}{2\chi} \right) dt. \end{aligned}$$

The general solution of equation (4.18) can then be shown to be given by the arbitrary function

$$\theta = F(g) = F\left( \frac{V_{0z}(1+\chi)}{A} \exp[-At] - 2\sqrt{2\chi_0}V_{A0} \left( t - \frac{1}{2A\chi} \right) \right). \quad (4.19)$$

After the application of the constant driver condition equation (4.19) will become

$$\theta = \frac{\omega}{A} \left[ \frac{A}{2\sqrt{2\chi_0}V_{A0}} g - W \left( \frac{1}{2\chi_0} \exp \left[ \frac{Ag}{2\sqrt{2\chi_0}V_{A0}} \right] \right) \right], \quad (4.20)$$

where  $W$  is the Lambert  $W$  function. The Lambert  $W$  function is defined as the function  $W$  where

$$W(x) \exp[W(x)] = x,$$

(further details on the Lambert Function can be found in, e.g. Lambert 1996).

From equation (4.20) we can now find the explicit forms of the dynamic frequency and wavenumber. The dynamic frequency,  $\Omega$ , is given by

$$\Omega = \frac{\omega}{2\sqrt{2\chi_0}V_{A0}} \frac{V_{0z} \exp[-At] + 2\sqrt{2}V_{A0}(1+(2\chi)^{-1})}{(1+W)}, \quad (4.21)$$

and the dynamic wavenumber is given by

$$K = \frac{\omega}{2\sqrt{2\chi_0}V_{A0}} \frac{1+\chi}{(1+W)} \exp[-At]. \quad (4.22)$$

The dynamic frequency,  $\Omega$ , evolves in the manner shown in Figure 4.1, the dynamic frequency can be shown to be decreasing in a manner comparable to that found in the moderate activity approximations performed in Sections

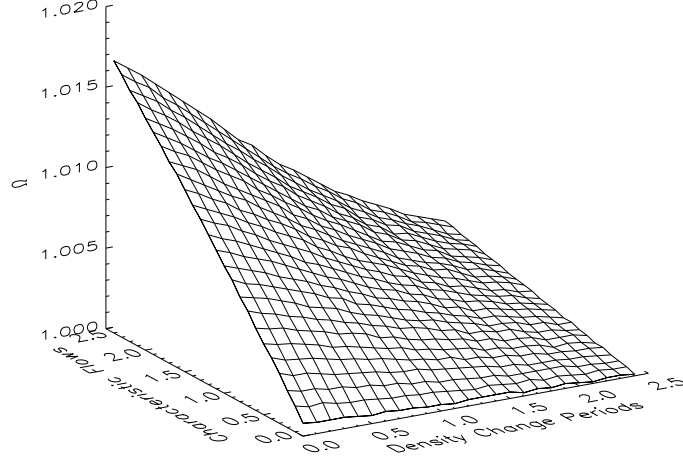


Figure 4.1: Dynamic frequency of propagating leaky waves. All quantities have the same description as given in Figure 2.1.

2.4 and 3.4.2. The point at which the frequency becomes approximately constant, i.e. past the point of rapid decrease, can be compared to the point at which the interior of the flux tube is largely evacuated of density and hence the change in frequency past that point is negligible. The same concept can be applied to the dynamic wavenumber (see Figure 4.2),  $K$ , in that there is the initial rapid decrease, again comparable to the moderate activity approximation, before tending to a constant limit after the point where the tube has been effectively evacuated.

Now that the dispersion relation has been solved for the real values of the dynamic frequency and wavenumber, the various wave modes can be explored. For MHD wave propagation inside the flux tube we return to Equation (4.14). Using the explicit forms of  $\Omega$  and  $K$  we plot the amplitude of the radial perturbation for the  $m \geq 1$  wave modes. The  $m = 1$  kink wave mode is shown in Figure 4.3 and has a similar initial amplification to that found in the over-dense loop approximation. In this model, however, there is no such restriction upon the time for which the wave can propagate and hence the wave can be amplified in this manner until the density within the flux tube is approximately zero. The

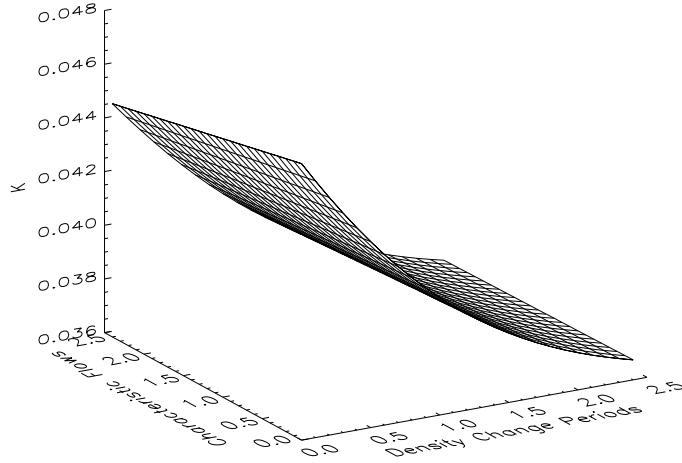


Figure 4.2: Dynamic wavenumber of propagating leaky waves. All quantities have the same description as given in Figure 2.2.

higher-order wave modes,  $m \geq 2$ , have the same evolution as their counterparts in the over-dense loop and hence we can say that all wave modes with,  $m \geq 3$  will be damped to zero without the need for the energy losses into the magnetic atmosphere. The amplitude of the  $m = 2$  wave mode is plotted in Figure 4.4 for comparison with the  $m = 1$  mode.

With the explicit forms of the frequency and wavenumber now determined, we can make analytical progress with the determination of the evolution of the damping coefficient,  $\gamma$ . Substitution of these values into equation (4.17) gives an expression which is difficult to clearly see the temporal changes as a result of the decreasing density, hence, we plot the evolution of the damping coefficient with respect to time and the height above the driving point. We also reiterate the point made in Chapter 2 that the moderate activity approximation does have potential implications for the evolution with respect to height and that most of the focus here will be on the temporal evolution. Figure 4.5 shows that the level of damping decreases approximately exponentially in time to a negligible level. Given the amplification of the  $m = 1$  kink mode this result would appear to defy the current theory of wave damping through leaky waves.

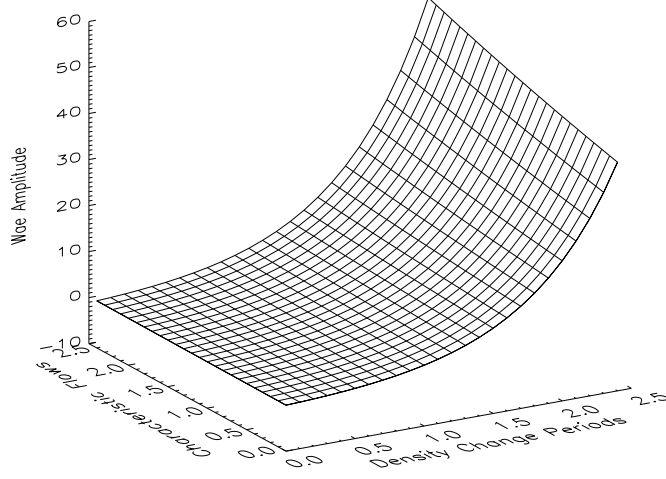


Figure 4.3: Relative change in the amplitude of the propagating  $m = 1$  body waves.

In order to check this we can contrast the result found in Figure 4.5 with the damping in the stationary model derived in Section 4.2 above. Equation (4.9) can be rewritten in terms of the density ratio and is given below,

$$\gamma = -\frac{\pi(\chi - 1)^2}{8(\chi + 1)^2} R^2 k^2 \sqrt{\frac{B^2}{\mu_0 \rho_e (1 + \chi)}}. \quad (4.23)$$

Plotting equation (4.23) for a fixed exterior density gives Figure 4.6 which clearly indicates an increase in the damping rate as the density ratio increases before decrease slowly to zero. However, this result presupposes a constant kink frequency and, as such, ignores the rate of damping due to density variation within the flux tube.

Whilst the dynamic result does seem to be in contradiction to the previous results found in static and stationary systems, the energy flux as a result of the damping is yet to be investigated and may allow for a full unification of these not completely inconsistent ideas.

At this point it is worth revisiting one of the points made previously, that as a result of the moderate-activity approximation the analysis with regard to the

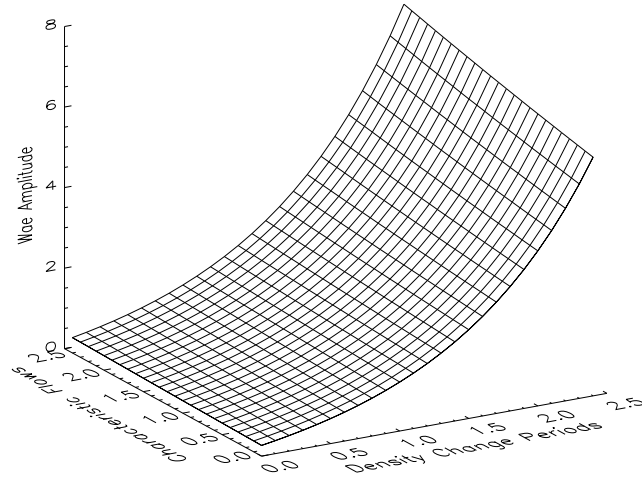


Figure 4.4: Relative change in the amplitude of the propagating  $m = 2$  body wave.

height above the driving point is suspect. Therefore, different ratios of the initial Alfvén speed and the background flow can change the initial evolution of the quantities discussed above. However, all the cases tend to the same limit and, therefore, we can consider them to be consistent. In several of these cases it is possible to obtain an initial increase in the damping such that the stationary and the dynamic damping coefficients follow the same, albeit over different time periods, evolution. However, most of the ratios considered produced results equivalent to those found above.

## 4.5 Conclusions

This chapter relaxed the assumption of evanescent wave propagation in the magnetised atmosphere. The algebraic form of both the interior and the exterior wave propagation, as well as the damping coefficient were determined and their evolution in time and height explored. The moderate activity approximation, in a different limit to that found in Chapters 2 and 3, was applied in order to find the real part of the frequency and the wavenumber. Using the

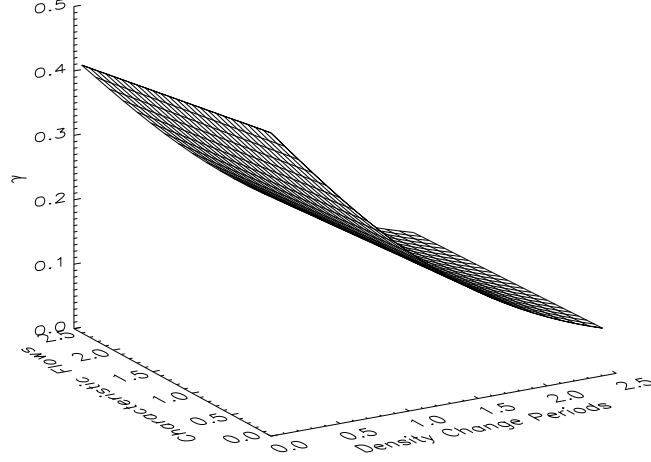


Figure 4.5: Evolution of dimensionless damping coefficient, i.e.  $\gamma/\gamma(t=0, z=0)$ .

expressions for the dynamic frequency and wavenumber, the full evolution of the propagating wave modes can be simply shown. The various wave modes all follow the same manner of propagation as found in Chapter 2 for the over-dense loop approximation. The  $m=1$  kink wave is amplified in an approximately exponential manner without any limiting factor as suggested in the case of the over-dense loop, beyond that of an empty flux tube. The  $m=2$  wave mode is amplified to a constant level after a small number of characteristic density change periods. The higher order,  $\geq 3$ , wave modes are damped after a small number of characteristic time periods of density change, with the damping rate increased for higher values of the azimuthal wavenumber,  $m$ .

The main focus of this chapter was on the damping coefficient  $\gamma$  and its evolution in time. The quantity  $\gamma$  is shown to decrease, approximately, exponentially in time as the flux tube evacuates. The damping as a result of leaky waves can therefore be considered to be negligible after a small number of characteristic density change periods.

Further investigations into expanding upon these findings are required, e.g. inclusion of a finite plasma pressure and relaxing of the thin tube approxima-

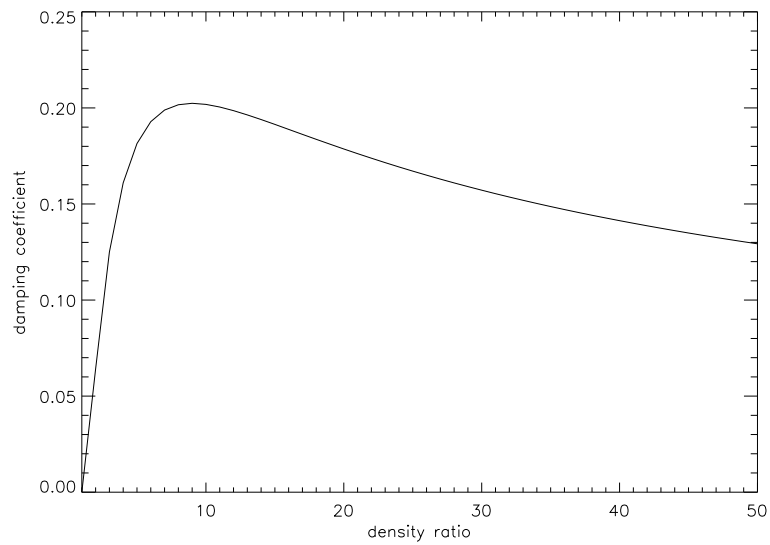


Figure 4.6: Damping coefficient in a static system plotted against density ratio.

tion, in order to make this an even more useful tool into magneto-seismology of photospheric structures.

# Chapter 5

## Resonant Damping of MHD Waves in a Zero-beta Plasma

### 5.1 Introduction

This work explores the notion of resonant absorption in a dynamic magnetised plasma background. A large number of studies have investigated resonance in the Alfvén and slow MHD continua under both ideal and dissipative MHD regimes. Jump conditions in static and steady systems have been found in previous studies connecting solutions at both sides of the resonant layer. Here, we derive the jump conditions in a temporally dependent, magnetised, inhomogeneous plasma background to leading order in the WKB approximation. Next we exploit the results found in Chapter 2 to describe the evolution of the jump condition in the dynamic model considered. The jump across the resonant point is shown to increase exponentially in time. Over the same time period the dissipation, as a result of the resonance, is determined and the temporal evolution of the dissipation itself is investigated. It is found that the dissipation coefficient decreases as the density gradient across the transitional layer decreases. This has the consequence that in such time-dependent systems resonant absorption may not be as efficient as time progresses.

## 5.2 Governing Equations

We consider an open-ended magnetic cylinder of radius  $R$  embedded in a magnetic atmosphere with magnetic field  $B_{0ze}\hat{\mathbf{z}}$ . A layer of thickness  $l$  smoothly connects the flux tube interior and magnetic exterior environment. A thin transition layer is assumed, i.e.  $l \ll R$ , which allows for an approximate solution for the eikonal functions  $\Omega$  and  $K$  to be applied later. The magnetic cylinder has a constant vertical magnetic field of strength  $B_{0z}\hat{\mathbf{z}}$ . The initial plasma density inside the cylinder,  $\rho_{0i}$ , is assumed to be an order of magnitude greater than the density in the exterior region,  $\rho_e$ . The density inside the flux tube is defined to decrease exponentially in time and can therefore be written as  $\rho_i = \rho_{0i} \exp[-At]$  where  $A$  is a positive constant equal to the reciprocal of the characteristic density change period,  $\tau_\rho$ , which is assumed to be large in relation to the characteristic oscillation period. Details of the WKB approximation, that has been used in this chapter, can be found in Section (1.7). Use of the mass conservation equation leads to an internal flow of  $V_{0z} = Az\hat{\mathbf{z}}$ . The cold-plasma approximation is applied, reducing the thermal pressure,  $p_0$ , to approximately zero, suitable for linear wave propagation under coronal conditions.

We assume that the wave propagation follows the style of that described in Chapter 2 for the perturbed, linearised MHD equations and the Eikonal functions  $\Omega$  and  $K$  as well as the full expression for the amplitude of the fast MHD wave, all the details in Chapter 2 and are reiterated later in this chapter. The linearised dissipative MHD equations can be written as

$$\begin{aligned} \frac{\partial \rho}{\partial t} + \nabla \cdot (\rho_0 \mathbf{V} + \rho \mathbf{V}_0) &= 0, \\ \rho_0 \left[ \frac{\partial \mathbf{V}}{\partial t} + \mathbf{V} \cdot \nabla \mathbf{V}_0 + V_{0z} \frac{\partial \mathbf{V}}{\partial z} \right] + \rho V_{0z} \frac{\partial \mathbf{V}_0}{\partial z} &= -\nabla p + \frac{1}{\mu} (\nabla \times \mathbf{B}) \times \mathbf{B}_0, \\ \frac{\partial \mathbf{B}}{\partial t} &= \nabla \times (\mathbf{V}_0 \times \mathbf{B}) + \nabla \times (\mathbf{V} \times \mathbf{B}_0) + \eta \nabla^2 \mathbf{B}, \\ \frac{\partial p}{\partial t} + \mathbf{V}_0 \cdot \nabla p &= -\gamma \left( p \frac{\partial V_{0z}}{\partial z} \right). \end{aligned}$$

At this point the perturbed total pressure of the system  $P$  is defined as

$$P = p + \frac{B_{0z}}{\mu} B_z \approx \frac{B_{0z}}{\mu} B_z.$$

For a model containing a finite plasma beta  $P$  is the combination of magnetic and thermal pressures, however, given the current zero plasma- $\beta$  approximation only the magnetic pressure plays a role. Applying the WKB approximation to leading order allows for all but two of the perturbed variables,  $P$  and the Lagrangian displacement,  $\xi_r = -i\varpi V_r$ , to be eliminated. The resulting governing equations can be written in the following form,

$$\frac{\partial P}{\partial r} = \rho_0(\varpi_\eta^2 - \varpi_A^2)\xi_r, \quad (5.1)$$

and

$$\rho_0(\varpi_\eta^2 - \varpi_A^2)V_A^2 \frac{1}{r} \frac{\partial \xi_r}{\partial r} = - \left[ \varpi^2 - V_A^2 \left( K^2 + \frac{m^2}{r^2} \right) \right] P \quad (5.2)$$

where

$$\varpi = \Omega - V_{0z}K, \quad \varpi_\eta^2 = \varpi^2 - i\eta\varpi \frac{\partial^2}{\partial r^2}, \quad \varpi_A^2 = V_A^2 K^2, \quad V_A^2 = \frac{B_{0z}^2}{\rho_0\mu}.$$

Equation (5.2) contains a potentially singular point in the region of the  $\varpi = \pm\varpi_A$ , called the Alfvén resonant point. In order to ensure a physical solution across this point it is necessary to evaluate wave action in the thin layer across the singularity.

To fully understand the results gained in later sections the decay of the MHD wave in environments with decreasing density must be considered. Applying the WKB approximation as stated above and then solving for the wave phase,  $\theta$ , gives the following solution.

$$Q_P = \begin{cases} A_i J_{|m|}(M_0 r), & r < R - l, \\ A_e K_{|m|}(M_e r), & r > R, \end{cases} \quad (5.3)$$

where

$$M_e^2 = - \frac{(\Omega^2 - \varpi_{Ae}^2)}{V_{Ae}^2}.$$

Equation (5.3) is comparable to and will reduce to, under time-independent conditions, those found by Edwin and Roberts (1983b) for evanescent waves in a static background, however, the eikonal functions  $\Omega$  and  $K$  must be determined from the dispersion relation for kink waves. The dynamic frequency and wavenumber as explicitly determined in Chapter 2, under the assumption of the over-dense loop, are a vital tool in the analysis of the resonant quantities. We recall

$$\Omega = 2\omega \frac{V_{0z} + \sqrt{2}V_A}{V_{0z} + 2\sqrt{2}V_A}, \quad K = \frac{2\omega}{V_{0z} + 2\sqrt{2}V_A}. \quad (5.4)$$

The fast wave frequency,  $\Omega$ , and the wavenumber,  $K$ , we derived in Chapter 2 and as such we do not expand upon their properties here. Within this chapter we are concerned with the change in the resonant quantities, i.e. jump condition, dissipative coefficient and magnitude of the dissipative layer.

### 5.3 Evaluation around the Alfvén Resonant Point

Evaluating wave action in the region of the Alfvén resonant point can lead to a solution for the wave amplitude across the dissipative region where the Doppler-shifter frequency is approximately equal to the local Alfvén frequency, i.e.  $\varpi \approx \pm\varpi_A$ . In order to simplify the calculation, a new variable  $s_A$  is introduced and it is defined as  $s_A = r - r_A$  where  $r_A$  is the radial point at which resonance occurs. Such a system is analogous to that analysed by Sakurai *et al.* (1991) for ideal jump conditions and Erdélyi *et al.* (1995b), Goossens *et al.* (1995) and Tirry and Goossens (1996) for dissipative jump conditions. The decreasing density of the cylinder will have an additional effect on the position of the point  $r_A$ . The position of  $r_A$  is dependent upon the density profile across the transitional layer. When the resonance was considered in a stationary system the density profile was considered to be a purely radial function and as such the position of the resonant point has been fixed. In the present model, the density profile is now a time-dependent function as well and varies its radial position within the transition layer. However, the thin boundary approximation allows us to write  $R \approx r_A \approx R - l$ , which in turn allows us to consider the point  $r_A$  to be constant in the leading order approximation. A Taylor-expansion around

$s_A$  reduces the governing equations to

$$\left( s_A \Delta_A - i\varpi\eta \frac{\partial^2}{\partial s_A^2} \right) \frac{\partial Q_\xi}{\partial s_A} = \frac{m^2}{\rho_A r_A^2} Q_P, \quad (5.5)$$

and

$$\left( s_A \Delta_A - i\eta\varpi \frac{\partial^2}{\partial s_A^2} \right) \frac{\partial Q_P}{\partial s_A} = 0, \quad (5.6)$$

where  $\Delta_A$  is given by

$$\Delta_A = \frac{d}{dr} (\varpi^2 - \varpi_A^2)|_{r=r_A}. \quad (5.7)$$

These equations can then be solved using the method given by e.g. Goossens et al. (1995) in terms of two functions  $G(\tau_A)$  and  $F(\tau_A)$ , where  $\tau_A$  is a radially scaled variable over the dissipative layer of thickness  $\delta_A$  and is expressed below. For the time-dependent model the dissipative layer is variable with respect to its time and spatial coordinate above the base of the flux tube. This reflects the change in the size of the dissipative layer due to the changing wave frequency.  $\tau$  and the dissipative layer thickness  $\delta_A$  are given by

$$\tau_A = \frac{s_A}{\delta_A}, \quad \delta_A = \left( \frac{\eta\varpi}{|\Delta_A|} \right)^{1/3}. \quad (5.8)$$

Applying the definitions for  $\Omega$  and  $K$  given by equation (5.4) it can now be shown, see Figure 5.1, that the thickness of the dissipative layer decreases to a constant as time evolves. Whilst this result may seem to be counterintuitive, it is plausible that the decrease in the density gradient across the transitional layer, which would otherwise lower the rate of dissipation, is in a more physically accurate system balanced by an increasing dissipation. Such a result could be countered by the inclusion of a non-constant dissipation, however, the analysis of such is not included in this work and is suggested as a topic to be investigated further. Another potential limiting factor may not be due to the dissipative layer itself as the transitional layer itself will be dynamic in its radial profile. After the application of the thin tube-thin boundary (TTTB) condition this change can be assumed to be negligible, but in a more physically accurate model this change may produce significant effects. The underlying physics that occurs

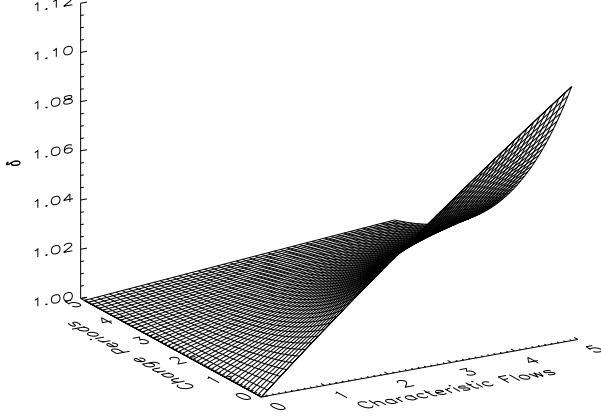


Figure 5.1: Evolution of the width of the dimensionless dissipative layer, i.e.  $\delta_A/\delta_A(t=0, z=0)$ .

when the width of the transitional layer and the dissipative layer approach equality will not be explored here and is again suggested as worthy of further investigation. It is noted that the impact of a thick transitional layer has been previously investigated, absent the changing dissipative layer, the results of which are useful to contrast with the potential dynamic transitional layer found here. The numerical studies undertaken by van Doorselaere *et al.* (2005) show that the damping can be underestimated by a factor of up to approximately 25%, thus rendering the analysis, here and below, an understatement of the physics involved at the resonant point.

By considering  $\tau_A$  as a purely radial parameter, a method analogous to that by Goossens *et al.* (1995) can be applied to solve equation (5.5) in an algebraically straightforward manner. The result is mathematically consistent with those gained by Goossens *et al.* (1995), and are given as

$$Q_\xi \approx \frac{m^2}{r_A^2 \rho_A \Delta_A} \left( \ln |\tau| + \frac{2\nu}{3} + \frac{1}{3} \ln 3 - i \frac{\pi}{2} \text{sign}(\Delta_A \tau) \right) Q_P + C_\xi, \quad (5.9)$$

where  $\nu$  is the Euler constant and  $C_\xi$  is an arbitrary constant of integration. The jump across the Alfvén resonant point can simply be read off from the

above solution. The jump in  $Q_\xi$  is therefore given by

$$[Q_\xi] = -i\pi \frac{m^2}{\rho_A r_A^2 |\Delta_A|} Q_P. \quad (5.10)$$

This jump condition must now be considered in the context of the amplified waves found in the case of an environment with no transitional layer. The solution to  $Q_P$  is given by equation (5.3) where  $\Omega$  and  $K$  are given by equation (5.4). When the explicit solution for  $Q_P$ , as given in equation (5.3), is considered, the time-dependent jump condition can be found to be

$$[Q_\xi] = -i\pi \frac{m^2}{r_A^2 \rho_A |\Delta_A|} A_i J_m \left[ \frac{2\omega r_A}{V_{0z} + 2\sqrt{2}V_A} \right]. \quad (5.11)$$

The time and height dependency of the jump are plotted in Figure 5.2, noting that the plot only shows the shape of the change and not the absolute values of the jump. This result, whilst indicating the importance of resonant absorption

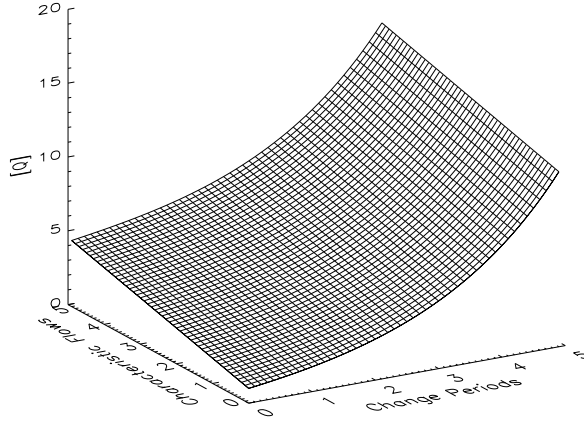


Figure 5.2: Evolution of the jump across the Alfvén resonant point as a function in time

in the solar corona, does hint at a potential flaw in the assumptions made if the results here are not considered carefully. The ever-increasing jump across the resonant point is obviously unphysical if the temporal evolution were to continue

under the assumptions made here. When the findings here are compared to the constant limit of the dissipative layer it is clear that there is a limit at which the jump condition becomes questionable or invalid, e.g. when leaky waves start to propagate.

## 5.4 Wave Dissipation

The dynamic background plasma has an additional effect, the change in the density gradient across the transitional layer should cause a change in the thickness of the layer itself, the decrease in density gradient, as specified here, will decrease the relative size of the transitional layer. Given that the thin-tube and the thin-layer approximations have already been made this provides no measurable difference to this model, however, when after a large period of time the transitional layer should tend to zero as the densities inside and outside the tube equalize. At this point the inhomogeneity that is the source of the resonance should disappear and the the jump should itself tend to zero. The jump condition above does not directly support this theory, however, using the results found in section (5.3) the dissipation due to the resonant point can still be found. The dissipative rate due to the presence of the resonance is calculated from the the general dispersion relation for  $\xi_r$ . The dispersion relation is attained by applying continuity across a thin transition layer for the eikonal functions  $\Omega$  and  $K$ . The dispersion relation is given by

$$\begin{aligned} \rho_i(\varpi^2 - \varpi_A^2) + \rho_e(\Omega^2 - V_{Ae}^2 K^2) = \\ = -i\pi \frac{\rho_i \rho_e}{\rho_A} (\varpi^2 - \varpi_A^2) (\Omega^2 - V_{Ae}^2 K^2) \frac{m}{r_A |\Delta_A|}. \end{aligned} \quad (5.12)$$

Then, making the assumption that for  $\Omega = \Omega_R + i\gamma$ ,  $\gamma \ll \Omega_R$  the following definition for  $\gamma$ , see e.g. Krall and Trivelpiece (1973), holds

$$\gamma = - \left. \frac{D_i}{\partial D_r / \partial \Omega} \right|_{r=\tau_A}, \quad (5.13)$$

where  $D_{i,r}$  is the imaginary/real part of the dispersion equation respectively. It is straightforward to show that

$$\gamma = -\frac{\rho_i^2(\varpi^2 - \varpi_A^2)^2\pi}{2(\rho_i\varpi + \rho_e\Omega)} \frac{|m|}{r_A\rho_A|\Delta_A|}. \quad (5.14)$$

Equation (5.14) is algebraically equivalent to equation (76) given by Goossens *et al.* (1992b), however, it is the time-dependent damping rate for a resonantly coupled fast MHD wave in a cylindrical tube with time-dependent, slowly varying (i.e. decreasing) density.

The time-dependency is plotted in Figure 5.3. The dissipation tends to zero as time evolves, which is to be expected as the over-dense plasma inside the loop tends to the value of the exterior density and the resonance disappears. Once again, Figure 5.3 is not representative of absolute values of the dissipation.

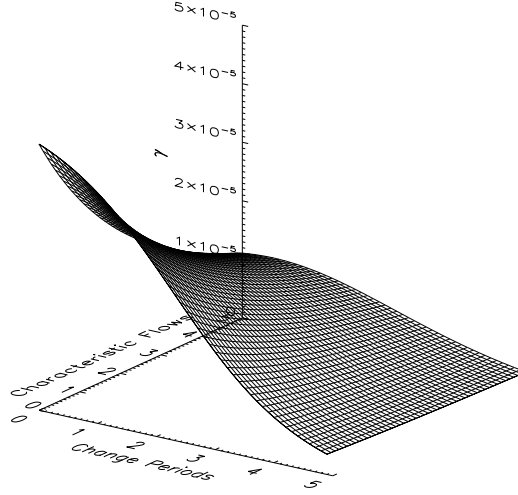


Figure 5.3: The evolution of the dimensionless wave dissipation, i.e.  $\gamma/\gamma(t=0, z=0)$ .

## 5.5 Resonance in the Moderate-Activity Approximation

Whilst wave damping in a quiet solar environment is of a lesser magnitude than in active regions, the theoretical problem still exists and can be solved in a similar manner to that above. The altered forms of the frequency and wavenumber, as calculated in section 2.4, can be substituted into equation (5.10) in order to calculate the jump condition under the assumption of moderate-activity. Given the more complicated nature of  $\Omega$  and  $K$  plotting the jump condition is the best way to examine the change in the jump across the resonant point, hence Figure 5.4 can be plotted. In this approximation we have a very different form of the

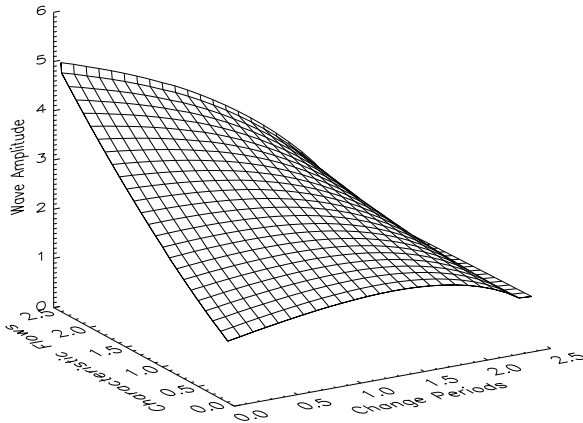


Figure 5.4: Jump condition under the moderate-activity approximation

jump condition. There is an initial amplification in the jump condition followed by a decrease to a constant level. The initial amplification can be considered to be in agreement with the amplification found in the case of the over-dense loop approximation, however, given that the density ratio has a finite value the decrease in the density gradient plays a large role in the decrease in the jump condition. This result coincides, again, with the change in the amplitude of the fast kink wave, now that the wave amplitude becomes constant the resonant jump must either become constant or disappear. Given that the saturation

level of the wave amplitude occurs at approximately the point of density equality we can say that the temporal evolution of the jump condition will be similar in nature, but occur at a lower rate, to that of the wave amplitude.

In the manner discussed previously we can also analyse the changing width of the dissipative layer and rate of dissipation. However, it must also be considered that in the moderate activity approximation, the amplitude of the fast kink wave does not increase for all time and as such the consequence of the matching densities will become more important.

Here, the dissipative layer decreases to a negligible amount during the pe-

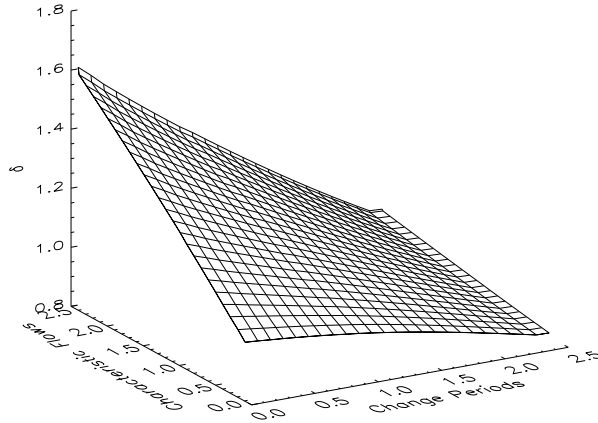


Figure 5.5: Evolution of the width of the dissipative layer under the moderate-activity approximation.

riod within which the density ratio is less than unity. When this result is put into the context of the decreasing density gradient and hence the disappearance of the transitional layer, this result would appear to be more representative of the physics involved.

The rate of dissipation, as calculated by equation (5.14), can be found and it is plotted in Figure 5.6. Once again there is a rapid decrease in the levels of damping, matching the decrease in the dissipative layer as well as the relative decrease in the effective resonant jump. Such a result is consistent with the equivalent calculations done in the over-dense loop approximation and there-

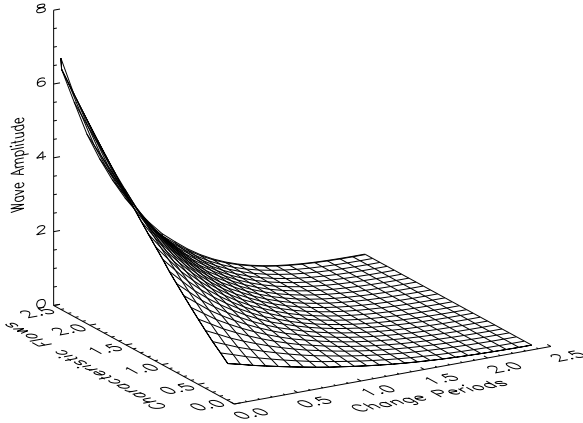


Figure 5.6: Evolution of the dimensionless dissipation coefficient under the moderate-activity approximation.

fore can be considered to be an accurate representation of resonance in coronal loops and other magnetic structures.

## 5.6 Conclusions

This work has investigated the impact of a time-dependent density (decreasing) upon the resonant coupling of a magnetic flux tube embedded in an external magnetised plasma environment. The first impact the time-dependent variation of background has is the need for a non-constant flow as a mechanism for removing the density. However, no physical mechanism for generating this flow has been considered here. The governing equations for a slowly changing background were discussed in Chapter 2 and have been recalled here in a different context. Using the seminal method laid down by Goossens *et al.* (1995) the jump conditions across the resonant layer were found in a time-dependent resonant flux tube. When the explicit expressions for the eikonals,  $\Omega$  and  $K$ , were introduced, the evolution of the jump condition was obtained. Whilst the jump condition is still a useful tool for analysis around the resonant point, for effects beyond the wave damping, i.e energy flux, the exponentially increasing jump is

seemingly unphysical in nature. However, when the rate of increase of the jump condition is put into the context of the increasing fast MHD wave amplitude, the relative size of the jump condition can be seen to decrease as the densities tend to comparable values between the flux tube interior and the magnetised exterior atmosphere.

The conclusion of a decreasing relative jump size is supported by the result found in section (5.4), the decreasing density results in a decreasing level of dissipation across the disappearing dissipative layer. Such a result is expected from the decreasing density profile across the transitional layer as defined during the initial construction of the problem. It is this prediction that allows for the use of the damping rate as not only a result on its own but as a check for the jump condition previously found.

It was noted in Chapter 2 that for an slowly increasing density, representing for example a mass enhancement due to e.g. in-flow, i.e.  $A < 0$ , the fast MHD kink wave is damped exponentially. If this notion is applied to the results found here the jump condition will decrease in size albeit at a slower rate than the damping of the propagating MHD wave. The resonance will then aid the damping rate instead of merely slowing the amplification, but if this idea is taken to extremes in time the jump will exist in a fully damped wave and can not occur in a physical system.

Under the consideration of moderate-activity in the Sun, the same analysis can be performed and it was shown that the same style of exponential growth in the jump conditions holds until the density gradient acts to limit the increase in the jump condition and causes a decrease to a constant level as the densities tend toward equality. In the same manner the relative size of the dissipative layer and the dissipative rate could be calculated. The dissipative layer displayed a more physical evolution than in the case of the over-dense loop. The decrease to a constant level is a much better match for the change in the jump condition than in the case of the over-dense loop and is hence is more consistent with the decrease in the dissipative rate,  $\gamma$ .

# Chapter 6

## Resonant Damping of MHD Waves in a Finite Plasma-beta

### 6.1 Introduction

This Chapter focuses on the impact of a time-dependent density on the resonance found in the slow continuum for a cylindrical flux tube. The introduction of a finite plasma pressure enables the propagation of, not only, the slow MHD wave but, with the introduction of an annular layer, the resonance in the slow continuum. Four coupled governing equations describing wave propagation in the flux tube are obtained, at which point the leading order in the WKB approximation is taken recovering an eikonal form of the familiar governing equations seen in many previous works. We briefly recall the resonance in the Alfvén continuum is briefly considered and, although a more general form of the results found previously are obtained, the temporal evolution can be shown to be similar. The jump condition in the slow continuum can be shown to, with respect to the temporal evolution, depend only upon the total pressure perturbation. By assuming that the slow MHD wave propagates in the limit of a low plasma-beta and rigid magnetic field, an investigation into the slow resonance can take place in a similar manner as the analysis performed in the previous chapter. The assumption of rigidity in the magnetic field only allows the  $m = 0$  slow sausage mode to propagate. Evaluation of the jump condition reveals that, to leading

order, the jump is constant in both time and height and hence becomes less important in the context of the amplification due to the density variation. The evolution of the dissipative layer is also investigated using the approximation derived in Chapter 3 and is shown to decrease in time to a constant level. This constant level is entirely dependent upon the magnitude of the initial sound speed and is compared to the dissipative layer in Chapter 5 for the over-dense loop.

## 6.2 Background

In a manner similar to Chapter 5, we consider a magnetic atmosphere with constant density and constant vertical magnetic field designated  $\rho_e$  and  $B_{ez}$ . To this a constant plasma pressure,  $p_e$  is introduced. A magnetic cylinder with constant vertical magnetic field  $B_{iz}$  is then embedded in the atmosphere, where the cylinder has a constant plasma pressure  $p_i$ . We introduce a time-dependent density and vertical flow inside the cylinder such that

$$\rho_i = \rho_0 \exp[-At], \quad V_{0z} = Az, \quad A = \tau_\rho^{-1}. \quad (6.1)$$

The characteristic time of density change,  $\tau_\rho$ , is considered to be large in comparison with the period of oscillation of the individual MHD waves. The cylinder is then driven at the base,  $z = 0$  at a constant frequency  $\omega$ . The total pressure can now be redefined as the sum of the plasma pressure and magnetic pressure, like in the finite-pressure case considered in Chapter 3, and it is written as

$$P = p + p_{mag} = p_0 + \frac{B_0^2}{2\mu_0}. \quad (6.2)$$

From here on a subscript ‘0’ indicates either the internal or external background variable.

### 6.3 Governing Equations

The linearised dissipative MHD equations are given by

$$\begin{aligned}\frac{\partial \rho}{\partial t} + \nabla \cdot (\rho_0 \mathbf{V} + \rho \mathbf{V}_0) &= 0, \\ \rho_0 \left[ \frac{\partial \mathbf{V}}{\partial t} + \mathbf{V} \cdot \nabla \mathbf{V}_0 + V_{0z} \frac{\partial \mathbf{V}}{\partial z} \right] + \rho V_{0z} \frac{\partial \mathbf{V}_0}{\partial z} &= -\nabla p + \frac{1}{\mu} (\nabla \times \mathbf{B}) \times \mathbf{B}_0, \\ \frac{\partial \mathbf{B}}{\partial t} &= \nabla \times (\mathbf{V}_0 \times \mathbf{B}) + \nabla \times (\mathbf{V} \times \mathbf{B}_0) + \eta \nabla^2 \mathbf{B}, \\ \frac{\partial p}{\partial t} + \mathbf{V}_0 \cdot \nabla p &= -\gamma \left( p \frac{\partial V_{0z}}{\partial z} \right).\end{aligned}$$

$\eta$  is the magnetic diffusivity and is considered to be important in narrow bands around the Alfvén and slow resonant points,  $\gamma$  is the adiabatic index. Combining Equations (6.3)-(6.3), allows for the following four equations to be written,

$$\begin{aligned}\hat{\omega} \left( \hat{\omega} + \gamma \frac{dV_{0z}}{dz} \right) P &= -\rho_0 (c^2 + V_A^2) \hat{\omega} \nabla \cdot \mathbf{V} + \rho_0 V_A^2 \left( \hat{\omega} + \gamma \frac{dV_{0z}}{dz} \right) \frac{\partial V_z}{\partial z} - \\ &\quad - \gamma \frac{dV_{0z}}{dz} \rho_0 V_A^2 \nabla \cdot \mathbf{V} - \frac{B_{0z}}{\mu_0} \frac{dB_{0z}}{dr} \left( \hat{\omega} + \gamma \frac{dV_{0z}}{dz} \right) V_r,\end{aligned}\quad (6.3)$$

$$\begin{aligned}\rho_0 \left( \hat{\omega} \left[ \hat{\omega}_\eta + \frac{dV_{0z}}{dz} \right] - \hat{\omega}_A^2 \right) \nabla \cdot \mathbf{V} &= \rho_0 \left( \hat{\omega} \left[ \hat{\omega} + \frac{dV_{0z}}{dz} \right] - \hat{\omega}_A^2 \right) \frac{1}{r} \frac{\partial (r V_r)}{\partial r} - \\ &\quad - \left( \hat{\omega} + 2 \frac{dV_{0z}}{dz} \right) \frac{1}{r^2} \frac{\partial^2 P}{\partial \phi^2} + \rho_0 \left( \hat{\omega} \left[ \hat{\omega} + \frac{dV_{0z}}{dz} \right] - \hat{\omega}_A^2 \right) \frac{\partial V_z}{\partial z},\end{aligned}\quad (6.4)$$

$$\rho_0 \left( \hat{\omega} \left[ \hat{\omega} + \frac{dV_{0z}}{dz} \right] - \hat{\omega}_A^2 \right) V_r = - \left( \hat{\omega} + 2 \frac{dV_{0z}}{dz} \right) \frac{\partial P}{\partial r},\quad (6.5)$$

$$\begin{aligned}\left( \hat{\omega} - \frac{dV_{0z}}{dz} \right) \rho_0 \left[ \hat{\omega} \left( \hat{\omega} + \frac{dV_{0z}}{dz} \right) - \hat{\omega}_A^2 \right] V_z &= - \left( \hat{\omega}^2 - \frac{dV_{0z}}{dz} \right) \frac{\partial P}{\partial z} - \\ &\quad - \left( \hat{\omega} - \frac{dV_{0z}}{dz} \right) \rho_0 V_A^2 \nabla \cdot \mathbf{V} + V_{0z} \frac{dV_{0z}}{dz} \nabla \cdot (\rho_0 \mathbf{V}).\end{aligned}\quad (6.6)$$

When comparing these equations to the ones found in the zero-beta model in Chapter 5, the shifted resonant point is no longer immediately obvious. The presence of the shifted Alfvén operator  $(\hat{\omega}_\eta^2 - \hat{\omega}_A^2)$  in Equation (6.3) indicated

that the shift still exists, however, the same idea of minimal difference due to this shift still holds. Upon the application of the WKB approximation, to leading order in  $\epsilon$ , the four governing equations can then be combined into the two familiar Hain-Lüst equations given by

$$\rho_0(\varpi^2 - \varpi_A^2)Q_\xi = \frac{\partial Q_P}{\partial r}, \quad (6.7)$$

$$\begin{aligned} & \frac{\rho_0}{r}(c^2 + V_A^2)(\varpi_\eta^2 - \varpi_A^2)(\varpi_\eta^2 - \varpi_c^2)\frac{\partial(rQ_\xi)}{\partial r} = \\ & = -\left[\varpi^4 - (c^2 + V_A^2)(\varpi^2 - \varpi_c^2)\left(\frac{m^2}{r^2} + K^2\right)\right]Q_P. \end{aligned} \quad (6.8)$$

From Equations (6.7) and (6.8) we can now deduce that, as in the zero-beta case, the Alfvén and slow singularities are recovered in the form established in previous works e.g. Goossens et al. (1992b), Erdélyi (1998) or Goossens et al. (2011). Having regained both the singular points investigations can take place in the regions around these points. For the sake of convenience we reintroduce the following notation in the following sections

$$\tilde{B}^2 = \frac{B_i^2 + B_e^2}{\mu_0\rho_i}, \quad \text{and} \quad \tilde{B}_0^2 = \frac{B_i^2 + B_e^2}{\mu_0\rho_{0i}}.$$

## 6.4 Alfvén Resonance

Although not the main focus of this chapter, the jump condition in the Alfvén continuum exists and can be found in the same manner as in Chapter 5. As previously derived, the jump condition can be shown to be

$$[Q_r] = -i\pi\frac{m^2}{r_A^2|\Delta_A|\rho_A}P. \quad (6.9)$$

When the frequency and wave-function for the propagating fast wave, as derived in Chapter 2 and given below, are substituted into equation (6.9) the evolution

of the jump condition for the fast wave can be written simply:

$$\Omega_f = 2\omega \frac{V_{0z} + \tilde{B}}{V_{0z} + 2\tilde{B}}, \quad K_f = \frac{2\omega}{V_{0z} + 2\tilde{B}}. \quad (6.10)$$

Although the form of  $\Omega$  and  $K$  are different from their counterparts in Chapter 5, the change due to the temporal dependency is identical to that found previously. This change carries over into the variation in the jump condition, where the sound speed introduces a slight scaling down from the value in the zero plasma-beta. For the full analysis of the jump condition of the fast MHD wave and the dissipation relating to the resonance see Chapter 5. For the purposes of investigating the slow resonance point the explicit expression for the total pressure is required. As can be shown in the calculation of the fast kink wave the total pressure perturbation can be written as

$$Q_P = A_i J_m \left( \frac{2\omega r}{V_{0z} + 2\tilde{B}} \left[ \frac{V_A^2 - c^2 + B_e^2/\mu_0\rho_i}{c^2 + V_A^2(1 + B_i^2/B_e^2)} \right]^{1/2} \right), \quad (6.11)$$

where  $A_i$  is an arbitrary constant,  $\omega$  is the driving frequency and  $J_m$  is a Bessel function of the first kind of order 'm'.

Likewise the Alfvén resonance under the moderate-activity approximation can be so examined. Analogue to in Chapter 3, the new expressions for the dynamic frequency and wavenumber are

$$\Omega = \frac{2\omega}{A} \frac{V_{0z} + \tilde{B}(1 + \chi/2)}{\sqrt{g^2 + 16\tilde{B}_0\chi_0}} \exp[-At], \quad (6.12)$$

$$K = \frac{2\omega}{A} \frac{(1 + \chi)}{\sqrt{g^2 + 16\tilde{B}_0\chi_0}} \exp[-At]. \quad (6.13)$$

Using these values, the temporal evolution of the jump condition, size of the dissipative layer and the dissipative coefficient can now be all be explored. The expressions for  $\delta_A$  and  $\gamma$  are, once again, given by

$$\delta_A = \left( \frac{\eta\varpi}{|\Delta_A|} \right)^{1/3},$$

and

$$\gamma = -\frac{\rho_i^2(\varpi^2 - \varpi_A^2)^2}{2(\rho_i\varpi + \rho_e\Omega)} \frac{|m|\pi}{r_A\rho_A|\Delta_A|}.$$

The constant values of the background magnetic fields imply that the temporal evolution of these quantities take a similar form as their counterparts in the zero-beta environment.

## 6.5 Slow Resonance

The addition of the constant plasma pressure enables the propagation of the slow wave and with the addition of the thin transition layer a resonance in the slow continuum. When the Doppler-shifted frequency is in the region of the cusp frequency we define a dissipative layer, labeled  $\delta_c$ , which removes the singularity. Within this dissipative layer the ideal MHD solutions found in Chapter 3 are no longer valid and a new description for the propagating slow wave must be investigated. Taylor expansion to leading order around the point  $\varpi = \pm\varpi_c$  of Equations (6.7) and (6.8) gives the following pair of equations:

$$\left(s|\Delta_c| - i\eta\varpi \frac{\varpi_c^2}{\varpi_A^2} \frac{\partial^2}{\partial s^2}\right) \frac{\partial Q_{rs}}{\partial s} = \frac{\varpi_c^4 \mu_0}{B^2 \varpi_A^2} Q_P, \quad (6.14)$$

$$\frac{\partial Q_P}{\partial s} = -\frac{\varpi_A^2 B^2}{(c^2 + V_A^2)\mu_0}, \quad (6.15)$$

where  $s$  is defined as  $s = r - r_s$ . From Equation (6.15) it is easy to spot that there is no resonance in the total pressure, i.e.  $[Q_P] \equiv 0$ . Further investigation into Equation (6.14) can now take place, using the SGRH-method of analysis. An analytic expression for the slow MHD wave in the dissipative layer can be shown to be

$$Q_{rs} = -\frac{\varpi_c^4}{\varpi_A^2 V_A^2 \rho_c |\Delta_c|} Q_P \left[ \ln|\tau| + \frac{2\nu}{3} + \frac{1}{3} \ln(3) - i\frac{\pi}{2} \text{sign}(|\Delta_c|\tau) \right]. \quad (6.16)$$

From equation (6.16) the jump condition can be simply read off as

$$[Q_{rs}] = -i\pi \frac{\varpi_c^4}{\varpi_A^2 V_A^2 \rho_c |\Delta_c|} Q_P. \quad (6.17)$$

The jump condition can be shown to be explicitly independent of the wave-function and frequency for the slow mode and is only dependent upon the constant plasma-beta, magnetic field and the total pressure which was defined in section (6.4). The complete time-dependence is contained within the evolving total pressure perturbation. The revised jump condition can be written as

$$[Q_{rs}] = -i\pi \frac{\beta \varpi_c^2 \mu_0}{(1 + \beta) B_0^2 |\varpi'_c|} Q_P, \quad (6.18)$$

where the ' indicates a radial derivative. Given that for the results derived in Chapter 3 are only valid for a propagating wave in a rigid magnetic field, only one slow wave mode can be considered to propagate in this model, the  $m = 0$  sausage mode. The lack of radial variation of the propagating slow sausage MHD wave implies that the total pressure is constant and therefore the jump across the resonant point is constant. Given that we expect the resonance to decrease as the density gradient decreases this result appears to be unphysical, however, in the context of the amplified slow MHD wave the relative jump in amplitude decreases rapidly. Investigations into the varying magnitude of the dissipative layer can show why the relative amplitude decreases.

## 6.6 Dissipative Layer

Given that the resonance is independent of the change to the propagating wave the question of why the resonance disappears must be addressed. In order to answer this we refer back to the Taylor-expanded governing equations, Equations (6.14) and (6.15), and the definition given there for the dissipative layer, and, more specifically the changing size of the dissipative layer.  $\delta_c$  can be written explicitly as

$$\delta_c = \left( \frac{\eta \varpi \varpi_c^2}{|\Delta_c| \varpi_A^2} \right)^{1/3} = \left( \eta \varpi \frac{c^2}{|\Delta_c| (c^2 + V_A^2)} \right)^{1/3}. \quad (6.19)$$

The dissipative layer changes therefore like  $(\varpi/|\Delta_c|)^{1/3}$ . In order to properly examine the changes in the size of the layer, the particular forms of the frequency and wave-function are required. By isolating the plasma displacement parallel to the magnetic field, i.e.  $\xi_z$ , the frequency, wave-function and the amplitude

of the propagating slow wave can be identified, with further details in Chapter 3. The frequency,  $\Omega_s$ , and the wave-function,  $K$ , are given by

$$\Omega = 2\omega \frac{V_{0z} + c}{V_{0z} + 2c}, \quad K = \frac{2\omega}{V_{0z} + 2c}. \quad (6.20)$$

Using these expressions the evolution of the dissipative layer can be plotted and is shown in Figure 6.1. Examining Figure 6.1 it is clear that the overall trend is of an exponential decrease in the size of the dissipative layer to a constant level defined by the plasma-beta of the model. The background plasma flow acts as a linear amplifier for the dissipative layer and determines the time taken for the constant magnitude to be achieved. However, the relative size of the flow, in comparison to that of the Alfvén and sound speeds, is assumed to be low in order to avoid potential instabilities.

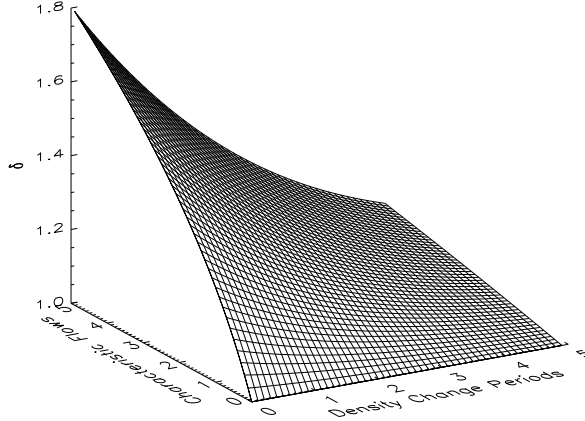


Figure 6.1: Evolution of the dimensionless dissipative layer,  $\delta_c/\delta_c(t = 0, z = 0)$ .

## 6.7 Conclusion

This work has investigated the effect of a time-dependent density on the resonant point found in the slow continuum. Four governing equations for the resistive MHD equations were constructed in operator form. Application of the

WKB approximation to leading order enables the derivation of the two familiar governing equations with both the Alfvén and slow resonance points. The Alfvén resonance was explored only to the point of similarity with the work done in the previous chapter. In the manner of Erdélyi (1998), investigations into the slow resonant point took place. Examining the wave propagation within the region, where dissipation can be considered to be important, leads to an analytic expression for the jump across the resonant point. Such a result can be easily shown to be independent of the propagation of the slow wave and dependent only upon the total pressure. Applying the model for the frequency and wavenumber of the slow MHD wave, as calculated in Chapter 3, it becomes clear that under the low- $\beta$  approximation, not only does the jump become constant across all time, but only exists for the  $m = 0$  sausage mode.

# Chapter 7

## Discussion and Further Work

### 7.1 Overview of Thesis and Summary of Results

The aims of the study presented in this Thesis were to investigate the effects of a time-dependent background density upon the propagation and damping of MHD waves in the solar corona. Recent observations have detailed the temporal variation in plasma density within coronal loops and the current level of theoretical investigations have not yet addressed this issues. In order to understand this observed change in the rate of damping of MHD waves, the propagation of the MHD waves in a time-dependent background needed to be investigated and the temporal evolution of the dynamic frequency, wavenumber and amplitude explored. Chapter 2 focused on the propagating fast MHD wave in a pressureless environment, mimicking coronal conditions. The typical plasma-beta in the corona is estimated to be in the region of 0.01 and, hence, the zero plasma-beta approximation is a good initial step into investigating the corona. Analytic expressions for the dynamic frequency, dynamic wavenumber and amplitude of the fast MHD wave were found and upon further investigation it was shown that the propagating fast kink waves were amplified exponentially in time. The higher-order modes were damped to negligible levels, with the exception of the  $m = 2$  mode which was amplified to a constant level. In the limit of a small background flow, in relation to the Alfvén speed (moderate activity), the am-

plification of the  $m = 1$  kink mode was found to be limited in the region where the interior and exterior densities are approximately equal. However, the initial amplification occurred in a similar manner to that found in the over-dense loop and hence both results can be considered to be in agreement with each other.

Chapter 3 expanded upon the work done in Chapter 2 by introducing a constant, finite plasma pressure to the environment, in an attempt to mimic the environment in the chromosphere and lower corona. The sound speed, now a finite quantity as a result of the presence of the plasma pressure, introduced a scaling for the analytical expression for the fast MHD wave. The temporal evolution, as a result of the dynamic background, is shown to take the same form as the fast MHD wave as calculated in Chapter 2. The second part of the chapter examined the slow MHD wave by modelling a longitudinally propagating sound wave in a dynamic waveguide. The sound wave can then be shown to have a similar form to that of the fast MHD wave and hence evolves in the same manner.

Chapter 4 examined leaky wave modes in a zero plasma- $\beta$  environment with an initial density ratio more typical of photospheric environments, although the lack of plasma pressure would refute this. Leaky wave modes are an important part of MHD wave theory as the energy leakage results in a damping of the propagating MHD waves. With the many observations of damped MHD waves, such investigations are important to aid in the understanding of MHD waves propagating under varied background conditions. Applying an altered version of the moderate activity assumption, expressions describing the frequency, wavenumber, wave amplitude and damping coefficient were found and the evolution of these quantities explored. It was shown that when the density ratio,  $\chi = \rho_e/\rho_i$ , is of the order of 1, all the dynamic quantities were amplified. However, rapid damping of all the quantities then followed as the density ratio grew, implying a cessation of wave propagation in the flux tube.

MHD waves in the corona have been observed to be damped within a mere handful of periods of oscillation, resonant absorption has been shown to be an effective means of explaining this damping. Previous investigations into resonant damping have been confined to static and steady systems, however, given the temporal density variation in coronal loops the current analytical models

need to be enhanced. To this end, Chapter 5 introduced a thin annular layer to the flux tube, allowing for an examination of the resonant damping within such a system. By studying the resonance in the Alfvén continuum, for a flux tube in a zero- $\beta$  environment, analytic expressions were found for the jump condition and the damping coefficient. Such expressions were then applied in the context of the evolving fast MHD wave as discussed in Chapter 2. Although the jump condition could be shown to increase in an exponential fashion, the amplification of the wave can be shown to outstrip this increase and hence the damping as a result of the resonance will vanish. In the case of a flux tube in a region of moderate activity the resonance was initially amplified in the same manner before decreasing to a constant level as the interior and exterior densities equalised. The other quantities evolved similarly to their counterparts derived in the over-dense loop approximation.

In the same manner as for the resonance in the Alfvén continuum, the resonance in the slow continuum has been previously modelled in static and stationary systems. The effect of the temporal density variation had not yet been examined, therefore, Chapter 6 introduced a finite plasma pressure and evaluated the resonant damping of the slow MHD wave. The expression for the jump condition was shown to be constant and, in light of the exponentially growing slow wave amplitude, can be considered to become negligible in a short period of time. A more accurate expression for the jump conditions and the damping coefficient in the Alfvén continuum were also found and shown to have the same temporal evolution as shown in Chapter 5 for their zero- $\beta$  counterparts.

## 7.2 Further Work

The work presented here makes a good first step in explaining the variation in linear wave propagation due to a time-dependent density. However, such first steps are necessarily limited in how they explore the new concepts they introduce. The first potential area this work could be extended into could explore the propagation of the longitudinal wave mode into an arbitrary plasma- $\beta$  system. Whilst the low plasma- $\beta$  assumption made in chapters 3 and 5 is a good approximation for slow MHD wave propagation in the corona, time-dependent

wave can propagate in many different environments in the solar region. The slow MHD wave is known to be an effective means of transferring energy from the photosphere up into the corona and, therefore, further investigations are required in order to explain the high temperature levels in the solar corona, as well as improving our ability to perform solar magneto-seismology.

As mentioned in Chapter 4, there exists, under certain conditions, a turning point in the damping coefficient. Investigations into identifying this turning point have not yet given an analytical answer and should be investigated further. Also, in order to properly model the photospheric and chromospheric conditions typical of the situations in which leaky waves propagate, additional physics must be included. The first such inclusion should be a finite plasma pressure and the extension into a thick tube, in order to more accurately represent structures such as pores, sunspots, etc.

For more complicated models mathematical issues may arise, solving the dispersion relation for the thin-tube required a physical reduction from the vastly more complicated dispersion relation. The hidden problems of the TTTB approximations are discussed in e.g. Zhugzhda and Goossens (2001). Although, the thin-flux-tube is a good approximation of coronal structures, magnetic structures in different arenas of study are not so accommodating of this reduction. Similar problems will occur even in the thin-tube limit for a twisted magnetic field, as found in e.g. Erdélyi and Fedun (2010a), even in the, relatively, simple case of studying the  $m = 0$  sausage modes the increased detail will make explicit solutions difficult to find. The dispersion relation is difficult to solve unless multiple approximations are made and as such important elements of the physics may be missed from the resulting solution.

Another avenue of exploration is MHD wave propagation in different geometries, e.g. infinite slab or elliptical loops. Mathematical problems will still occur in such systems as can be shown in the infinite slab configuration. Whilst most of the observed loops are currently modelled as cylindrical flux tubes, the physical systems are not perfectly regular and, hence, elliptic tubes are a more realistic description of coronal loops. Infinite slabs are a geometry used to investigate MHD waves propagating in quiescent prominences which, despite their long lifetimes, still contain time-dependent plasma density. The theory of

MHD waves in a slab in an equilibrium setting is detailed in Roberts (1981b), and the time-dependent equivalent of the kink wave in stationary equilibrium can be considered to be algebraically similar and, for a system analogous to the cylinder configuration in chapter 2, is given by

$$\rho_i(\varpi^2 - \varpi_A^2)M_e x_0 + \rho_e(\Omega^2 - \varpi_{Ae}^2) = 0. \quad (7.1)$$

Here  $M_e$  is the wave number in the  $x$ -direction and  $x_0$  is the width of the slab. For a model containing no shear perturbations, i.e.  $k_y = 0$  equation (7.1) reduces to

$$\rho_i(\varpi^2 - \varpi^2)x_0 = \rho_e V_{Ae} \sqrt{(\Omega^2 - \varpi_{Ae}^2)}. \quad (7.2)$$

The non-linearity of the dispersion relation makes the solution for the wave phase to be difficult to find, further efforts should be made into solving this for solutions constant with a constant driver. Furthermore, for any resonant effect to be included the shear perturbation must be non-zero and, hence, the dispersion relation becomes even more complicated and difficult to solve. Details of the formulation and the attempted solutions can be found in Appendix B.

Many of the observations of oscillations within coronal loops show that the MHD wave amplitudes are large in comparison to the background values. Therefore, the linear MHD wave theory is not an effective explanation for the observed waves and non-linear wave theory is required to accurately determine the properties of such oscillations. It is also feasible that non-linear effects in a time-dependent system could be responsible for limiting the exponential growth in wave amplitude found in the work that was analysed earlier in this Thesis.

Further efforts into expanding upon both the Alfvén and slow resonant damping mechanisms should take place in the same manner as the proposed investigations into the wave propagation discussed above, namely the twisted magnetic field or slab geometry. Otherwise, alternative damping mechanisms, e.g. phase mixing, should be considered in the context of the propagating waves discussed in chapters 2 and 3 in order for comparisons to be drawn with the resonant damping discussed here.

# Appendix A- SGRH Method of Asymptotics

The Sakurai, Goossens, Ruderman, and Hollweg (1995) method of analytically determining the jump conditions across the resonant point is explored below. This was first constructed in Goossens et al. (1995) for a stationary system, directly comparable to that discussed in Section 1.3.2. The two differential equations that describe the wave propagation in the dissipative layer, Equations (1.24) and (1.25), are rewritten here

$$\left( s\Delta - i\eta\omega \frac{d^2}{ds^2} \right) \frac{d\xi_r}{ds} = \frac{g_B}{\rho_A B_0^2} C_A(s), \quad (7.3)$$

and

$$\left( s\Delta - i\eta\omega \frac{d}{ds} \right) \frac{dP}{ds} = 2 \frac{f_B B_{0\phi} B_{0z}}{\mu_0 r_A \rho_A B_0^2} C_A(s). \quad (7.4)$$

We now introduce a scaling variable,  $\tau$ , across the dissipative layer such that

$$\tau = \frac{s}{\delta_A}.$$

It is clear that  $\tau$  is less than 1 when  $s$  is within the dissipative layer, and tends to  $\pm\infty$  when  $s \rightarrow \pm s_A$ , for  $s_A$  defined by

$$s_A = \left| \frac{2(\omega_A^2)'}{(\omega_A^2)''} \right|,$$

given that the Taylor-series is valid in the region  $[-s_A, s_A]$ . Using the new scaled variable, Equations (7.3) and (7.4) can be rewritten as

$$\left(\frac{d^2}{d\tau^2} + i\text{sign}(\Delta)\tau\right)\frac{d\xi_r}{d\tau} = i\frac{g_B}{\rho_A B_0^2 |\Delta|} C_A \quad (7.5)$$

and

$$\left(\frac{d^2}{d\tau^2} + i\text{sign}(\Delta)\tau\right)\frac{dP}{d\tau} = 2i\frac{f_B B_{0\phi} B_{0z}}{\rho_A B_0^2 \mu_0 r_A |\Delta|} C_A. \quad (7.6)$$

In addition, similar differential equations can be sought for  $C_A$  and  $\xi_\perp$ . Whilst the  $\xi_\perp$  solution is relevant for twisted magnetic fields, the work performed within this Thesis will focus on models with  $B_{0\phi} = 0$  and hence we only note that a solution can be sought in the same manner. The equation for  $C_A$ , however, is required for the calculation of the jump conditions for the radial displacement and total pressure. By taking a linear combination of Equations (7.5) and (7.6) we can write

$$\left(\frac{d^2}{d\tau^2} + i\text{sign}(\Delta)\tau\right)\frac{dC_A}{d\tau} = 0. \quad (7.7)$$

In order to progress we can seek solutions to the following second order differential equations

$$\left(\frac{d^2}{d\tau^2} + i\text{sign}(\Delta)\tau\right)\Psi(\tau) = 0, \quad (7.8)$$

and

$$\left(\frac{d^2}{d\tau^2} + i\text{sign}(\Delta)\tau\right)F(\tau) = -1. \quad (7.9)$$

For convenience we assume the following ansatz

$$F_i = \int_b^a \exp\left(iu\tau\text{sign}(\Delta) - \frac{u^3}{3}\right) du, \quad (7.10)$$

which, when substituted into equation (7.9) gives

$$\exp\left(iu\tau\text{sign}(\Delta) - \frac{u^3}{3}\right)\Big|_b^a = -1. \quad (7.11)$$

A series of solutions to Equation (7.11), if the lower limit,  $b$ , is assumed to be the origin in the complex plane, can be shown to be

$$\begin{aligned} F_1(\tau) &= \int_0^\infty \exp\left(iu\tau\text{sign}(\Delta) - \frac{u^3}{3}\right) du = -\pi Bi(i\pi\text{sign}(\Delta)), \\ F_2(\tau) &= \int_{\Gamma_2} \exp\left(iu\tau\text{sign}(\Delta) - \frac{u^3}{3}\right) du = -i\pi Ai(i\pi\text{sign}(\Delta)), \\ F_3(\tau) &= \int_{\Gamma_3} \exp\left(iu\tau\text{sign}(\Delta) - \frac{u^3}{3}\right) du = i\pi Ai(i\pi\text{sign}(\Delta)), \end{aligned}$$

where  $\Gamma_{2,3}$  are the lines in the complex plane starting at the origin and go to  $\infty$  along the rays  $\exp(\pm 2\pi i/3)$  and  $Ai$  and  $Bi$  are the Airy Functions of the first and second kind, respectively. Such solutions were found by finding values that sent the dominant term in the exponential expression ( $u^3/3$ ) to  $\infty$ . From these 3 solution a solution for equation (7.8) can be found using linear combinations of  $F_i$ 's. Therefore, we can write solutions for  $\Psi_{1,2}$  as

$$\Psi_1(\tau) = F_3(\tau) - F_1(\tau), \quad \Psi_2(\tau) = F_3(\tau) - F_2(\tau).$$

$\Psi$  can therefore be written as the sum of these linearly independent solutions and is given by

$$\Psi = A_1(F_3 - F_1) + A_2(F_3 - F_2). \quad (7.12)$$

For a physical solution we require that both  $\Psi$  and  $F$  are finite for all  $\tau$ , hence the solutions  $F_{1,2,3}$  can be tested for their boundedness. Details are not given here, but it can be shown that only the  $F_1$  solution is bounded at  $\tau \rightarrow \pm\infty$ . Therefore, the two constants,  $A_1$  and  $A_2$ , must be 0 and hence

$$\begin{aligned} \Psi(\tau) &\equiv 0, \\ F(\tau) &\equiv F_1(\tau). \end{aligned}$$

With these solution we return to Equation (7.7) and can therefore write

$$\frac{dC_A}{d\tau} = 0, \quad (7.13)$$

which directly implies that the quantity  $C_A$  is conserved across the dissipative layer. Now that  $C_A$  is known to be constant within the dissipative layer we can return to Equations (7.5) and (7.6) and apply the solution found for Equation (7.9), thus we can write

$$\begin{aligned}\frac{d\xi_r}{d\tau} &= -i\frac{g_B}{\rho_A B_0^2 |\Delta|} C_A F(\tau), \\ \frac{dP}{d\tau} &= -i\frac{2f_B B_{0\phi} B_{0z}}{\mu_0 r_A \rho_A B_0^2 |\Delta|} C_A F(\tau).\end{aligned}$$

Integration with respect to the scaling variable  $\tau$  produces

$$\begin{aligned}\frac{d\xi_r}{d\tau} &= -\frac{g_B}{\rho_A B_0^2 \Delta} C_A G(\tau) + C_\xi, \\ \frac{dP}{d\tau} &= -\frac{2f_B B_{0\phi} B_{0z}}{\mu_0 r_A \rho_A B_0^2 \Delta} C_A G(\tau) + C_P,\end{aligned}$$

where  $C_\xi$  and  $C_P$  are constants of integration and  $G(\tau)$  is given by

$$G(\tau) = \int_0^\tau F(\tau') d\tau' = \int_0^\infty \frac{e^{-u^3/3}}{u} (\exp[iu\tau \text{sign}(\Delta)] - 1) du,$$

for the dummy variable  $\tau'$ . Now, in order to evaluate these functions at the resonant point,  $\tau = 0$ , we rewrite  $G(\tau)$  as

$$G(\tau) = \int_0^\infty \frac{1 - \cos(u\tau)}{u} \exp\left[\frac{-u^3}{3}\right] du + i \text{sign}(\Delta) \int_0^\infty \frac{\sin(\tau u)}{u} \exp\left[\frac{-u^3}{3}\right] du. \quad (7.14)$$

By examining the real and imaginary parts of equation (7.14) separately, an asymptotic expression for  $G(\tau)$  as  $\tau \rightarrow \infty$  can be determined, i.e. in the points where dissipative and real solutions are bounded and are equal. The imaginary part of the solution will result in the jump condition and can be derived as follows

$$\text{sign}(\Delta) \int_0^\infty \frac{\sin(\tau u)}{u} \exp\left[\frac{-u^3}{3}\right] du = \text{sign}(\Delta \tau) \int_0^\infty \frac{\sin(u|\tau|)}{u|\tau|} \exp\left[\frac{-u^3}{3|\tau|^3}\right] d(u\tau), \quad (7.15)$$

$$\begin{aligned}
&= \text{sign}(\Delta\tau) \int_0^\infty \frac{\sin(u|\tau|)}{u|\tau|} d(u\tau) + o(1), \\
&= -i\frac{\pi}{2}\text{sign}(\Delta\tau) + o(1),
\end{aligned}$$

where  $o(1)$  is a function whose values tend to 0 as  $|\tau| \rightarrow 0$ . The real part of equation (7.14) can be explored as follows, whilst making the substitution  $u|\tau| \rightarrow u$  where appropriate,

$$\begin{aligned}
\int_0^\infty \frac{1 - \cos(u\tau)}{u} \exp\left[\frac{-u^3}{3}\right] du &= \left( \int_0^{\tau^{-2}} + \int_{\tau^{-2}}^\infty \right) \frac{1 - \cos(u\tau)}{u} \exp\left[\frac{-u^3}{3}\right] du, \\
&= \int_0^{1/|\tau|} \frac{1 - \cos(u)}{u} e^{-u^3/3|\tau|^3} du + \int_{\tau^{-2}}^\infty \frac{e^{-u^3/3}}{u} du - \int_{1/|\tau|}^\infty \frac{\cos(u)}{u} e^{-u^3/3|\tau|^3} du, \\
&= -\frac{1}{3} \int_{-\infty}^{-1/3\tau^6} e^u \frac{du}{u} - \int_{1/|\tau|}^\infty \frac{\cos(u)}{u} du + o(1), \\
&= \frac{1}{3} Ei\left(\frac{-1}{3\tau^6}\right) + Ci\left(\frac{1}{|\tau|}\right) + o(1).
\end{aligned} \tag{7.16}$$

Here, Ei is the integral exponent and Ci is the integral cosine functions as detailed in e.g. Abramowitz and Stegun (1972). The asymptotic expansions of these functions as their arguments tend to 0 are well known and are given by

$$\begin{aligned}
Ei(y) &= \ln(-y) + \nu + O(y), & \text{for } y \rightarrow -0, \\
Ci(y) &= \ln(y) + \nu + O(y), & \text{for } y \rightarrow +0,
\end{aligned}$$

where  $\nu$  is the Euler constant and  $\pm 0$  designated limits taken from above and below 0. Thus, the real part of equation (7.14) can be written as

$$\int_0^\infty \frac{1 - \cos(u\tau)}{u} \exp\left[\frac{-u^3}{3}\right] du = -\ln(\tau) - 2\frac{\nu}{3} - \frac{1}{3}\ln(3) + o(1), \tag{7.17}$$

and the expression for  $G(\tau)$  can therefore be expressed, in an asymptotic manner, as

$$G(\tau) = -\ln(\tau) - 2\frac{\nu}{3} - \frac{1}{3}\ln(3) + i\frac{\pi}{2}\text{sign}(\Delta\tau) + o(1). \tag{7.18}$$

# Appendix B- Slab Geometry

As mentioned in Section 7.2, an attempt has been made into describing the propagation of the fast MHD wave with a time-dependent density in a slab geometry, suitable for quiescent prominences in the solar atmosphere. However, no progress into solving this problem analytically has been made, numerical solutions could be sought but are beyond the scope of this work. A geometry similar in nature to that found in the cylindrical case discussed in Chapter 2 is constructed and explored to the point of solving the dispersion relation.

## 7.3 Background Geometry

A slab of high-density plasma is considered, for the purposes of this investigation we assume that the slab is infinite with respect to the  $y$  and  $z$  co-ordinates and has thickness  $2x_0$  centered on  $x = 0$ . The slab is embedded in a region with a constant vertical magnetic field,  $B_{0z}\hat{\mathbf{z}}$ . The interior density of the slab is designated  $\rho_i$  and is decreasing in time with a constant exponential factor  $A$ . The cold-plasma approximation is applied, the thermal pressure,  $p_0$  of the slab can be discarded. The exterior atmosphere can be considered to be a static system and all quantities are designated by a subscript 'e'. The slab is excited at the point  $z = 0$  with a driving frequency  $\omega$ .

The ideal perturbed, linearised MHD equations can be written as

$$\frac{\partial \rho}{\partial t} + \nabla \cdot (\rho_0 \mathbf{V} + \rho \mathbf{V}_0) = 0, \quad (7.19)$$

$$\rho_0 \left[ \frac{\partial \mathbf{V}}{\partial t} + \mathbf{V} \cdot \nabla \mathbf{V}_0 + V_{0z} \frac{\partial \mathbf{V}}{\partial z} \right] + \rho V_{0z} \frac{\partial \mathbf{V}_0}{\partial z} = -\nabla p + \frac{1}{\mu} (\nabla \times \mathbf{B}) \times \mathbf{B}_0, \quad (7.20)$$

$$\frac{\partial \mathbf{B}}{\partial t} = \nabla \times (\mathbf{V}_0 \times \mathbf{B}) + \nabla \times (\mathbf{V} \times \mathbf{B}_0), \quad (7.21)$$

$$\frac{\partial p}{\partial t} + \mathbf{V}_0 \cdot \nabla p = -\gamma \left( p \frac{\partial V_{0z}}{\partial z} \right). \quad (7.22)$$

Equations (7.20)-(7.22) can be combined in such a way as to eliminate all the perturbed variable except for the perturbed total pressure,  $P \approx B_{0z}B_z/\mu$ , and the perturbed velocity in the  $x$ -direction,  $V_x$ . Equations (7.20) and (7.21) can be combined to give equation (7.23). The remaining equation can be found by solving for  $P$  in terms of  $V_x$ . The two governing equations are given by

$$\left( \hat{\omega} + \frac{dV_{0z}}{dz} \right) \frac{\partial P}{\partial x} = -\rho_0(\hat{\omega}^2 - \hat{\omega}_A^2)V_x, \quad (7.23)$$

and

$$\rho_0 V_A^2 (\hat{\omega}^2 - \hat{\omega}_A^2) \frac{\partial V_x}{\partial x} = - \left[ \hat{\omega}^2 - V_A^2 \left( \frac{\partial^2}{\partial z^2} + \frac{\partial^2}{\partial y^2} \right) \right] P, \quad (7.24)$$

where

$$V_A^2 = \frac{B_0^2}{\mu \rho_0}, \quad \hat{\omega} = \frac{\partial}{\partial t} + V_{0z} \frac{\partial}{\partial z}, \quad \hat{\omega}_A^2 = V_A^2 \frac{\partial^2}{\partial z^2}.$$

## 7.4 Application of the WKB Approximation

Now, the WKB application, as detailed in Section (1.7), is applied and the two governing equations can be further explored in an analytical manner. Using the definitions for  $\Omega$  and  $K$ , as given in equation (1.45), equations (7.23) and (7.24) can be rewritten as

$$\frac{\partial P}{\partial x} = \rho_0(\varpi^2 - \varpi_A^2)\xi_x, \quad (7.25)$$

and

$$\rho_0 V_A^2 (\varpi^2 - \varpi_A^2) \frac{\partial \xi_x}{\partial x} = - \left[ \varpi^2 - V_A^2 (K_z^2 + k_y^2) \right] P, \quad (7.26)$$

where

$$\varpi = \Omega - V_{0z}K_z, \quad \varpi_A^2 = V_A^2 K_z^2, \quad -i\varpi \xi_x = V_x.$$

Solving equations (7.25) and (7.26) in the interior and exterior regions gives the solution for  $Q_P$  as

$$Q_P = \begin{cases} A_{e1} \exp(M_e(x + x_0)) & x < -x_0, \\ A_1 \cosh(M_0 x) + A_2 \sinh(M_0 x) & |x| < x_0 - l, \\ A_{e2} \exp(-M_e(x - x_0)) & x > x_0, \end{cases} \quad (7.27)$$

for  $M_0^2$  and  $M_e^2$  written as

$$M_0^2 = \frac{V_A^2 k_y^2 - \varpi^2 + \varpi_A^2}{V_A^2}, \quad M_e^2 = \frac{V_{Ae}^2 k_y^2 - \Omega^2 + V_{Ae}^2 K_z^2}{V_{Ae}^2}. \quad (7.28)$$

The dispersion relation for the infinite slab can be found by combining equations (7.23), (7.24) and (7.27). The resulting equation, equation (7.30), can be shown to be algebraically similar to equation (11) in Edwin and Roberts (1983b).

$$\rho_i(\varpi^2 - \varpi_A^2)M_e + \rho_e(\Omega^2 - V_{Ae}^2 K_z^2)M_0 \left\{ \begin{array}{l} \tanh \\ \coth \end{array} M_0 x_0 \right\} = 0, \quad (7.29)$$

where the  $\tanh$  solution represents the sausage mode and the  $\coth$  solution represents the kink mode. To further progress we apply the thin slab approximation, reducing equation (7.30) to

$$\rho_i(\varpi^2 - \varpi_A^2)M_e + \rho_e(\Omega^2 - V_{Ae}^2 K_z^2)M_0 \left\{ \begin{array}{l} M_0 x_0 \\ (M_0 x_0)^{-1} \end{array} \right\} = 0. \quad (7.30)$$

## 7.5 Analysis of Kink Wave Mode with Different $k_y$

In the thin-slab approximation the axis-symmetric sausage mode will not propagate, under coronal conditions, and hence only the propagating kink mode is left. Solutions can be sought, depending on the wavenumber in the  $y$ -direction, which is necessary for further investigations into resonant absorption or other damping mechanisms.

### 7.5.1 $k_y = 0$

In the limit of  $k_y=0$  we can perform the following investigation. The dispersion relation is given by

$$\rho_0(\varpi^2 - \varpi_A^2)M_e x_0 + \rho_e(\Omega^2 - V_{Ae}^2 K^2) = 0. \quad (7.31)$$

In the limit of  $k_y = 0$  the exterior wavenumber is reduced and the following equation can be formed from equation (7.31)

$$x_0(\varpi^2 - \varpi_A^2) = V_A \left[ \varpi_A^2 - \frac{\rho_e}{\rho_i} \Omega^2 \right]^{1/2}. \quad (7.32)$$

Under coronal conditions, i.e. we assume that  $\rho_i \gg \rho_e$ , this result can be reduced to

$$\Omega = V_{0z}K + V_A \sqrt{K^2 + \frac{K}{x_0}}, \quad (7.33)$$

to which no rigorous solution has yet been found.

### 7.5.2 $k_y \neq 0$

Now, we examine a model containing a finite wavenumber in the  $y$ -direction. Equation (7.30) can now be written as

$$\rho_i(\varpi^2 - \varpi_A^2)x_0 \left( k_y^2 - \frac{\Omega^2 - \omega_A^2}{V_{Ae}^2} \right)^{1/2} + \rho_e(\Omega^2 - \omega_A^2) = 0. \quad (7.34)$$

Analytical progress can only be made in the assumption that  $O(k_y) \approx O(M_e)$  such that the binomial expansion can be applied to equation (7.30). In this limit and after several steps of algebra the following can be written,

$$(\varpi^2 - \varpi_A^2)x_0 k_y + \frac{\rho_e}{\rho_i} \left( \Omega^2 - \omega_A^2 + \frac{\Omega^4 + \omega_A^4 - 2\Omega^2 \omega_A^2}{2k_y^2 V_{Ae}^2} \right) = 0. \quad (7.35)$$

To which the coronal approximation can be applied, reducing equation (7.31) to

$$(\varpi^2 - \varpi_A^2)x_0 k_y - \varpi_A^2 + \frac{\varpi_A^2}{2k_y^2} K^2 = 0, \quad (7.36)$$

for which, again, no rigorous solution can be found.

### 7.5.3 Solution Attempt

Equations (7.39) and (7.32) can be solved in general terms using the following ansatz,

$$\theta(t, z) = V_{0z} \frac{\exp[-At]}{x_0 A} + f(t), \quad (7.37)$$

i.e. attempting to mimic the solutions found in the cylindrical coordinate system. However, neither of these solutions produces an  $f(t)$  such that the constant driver boundary condition can be satisfied.

# Appendix C-Application of the WKB Approximation

In this Thesis we repeatedly used the WKB approximation to leading order, in this appendix we will show the details of the the application to the governing equations derived in the earlier chapters. Section 1.7.3 detailed the notation to be used upon application of the WKB approximation and is revisited here.

$$F = Q_F \left( \frac{r}{\epsilon}, z, t \right) \exp \left[ \frac{i}{\epsilon} \left( \theta(t, z) + m\phi \right) \right]$$

$$\Omega = -\frac{\partial \theta}{\partial t}, \quad K = \frac{\partial \theta}{\partial z}, \quad \varpi = \Omega - V_{0z}K. \quad (7.38)$$

Such expressions can be applied to the operator forms of the governing equations as derived in Chapter 3. Firstly we recall equation (3.16), the first of the governing equations to be analysed,

$$\hat{\omega} \left( \hat{\omega} + \gamma \frac{dV_{0z}}{dz} \right) P = -\rho_0 (c^2 + V_A^2) \hat{\omega} \nabla \cdot \mathbf{V} + \rho_0 V_A^2 \left( \hat{\omega} + \gamma \frac{dV_{0z}}{dz} \right) \frac{\partial V_z}{\partial z} -$$

$$-\gamma \frac{dV_{0z}}{dz} \rho_0 V_A^2 \nabla \cdot \mathbf{V} - \frac{B_{0z}}{\mu_0} \frac{dB_{0z}}{dr} \gamma \frac{dV_{0z}}{dz} V_r \quad (7.39)$$

Upon application of the WKB approximation, equation (7.39) can be written as

$$-i\varpi \left( -i\varpi + \epsilon \gamma \frac{dV_{0z}}{dz} \right) P = -\rho_0 (c^2 + V_A^2) (-i)\varpi \nabla \cdot \mathbf{V} + \rho_0 V_A^2 \left( (-i)\varpi + \epsilon \gamma \frac{dV_{0z}}{dz} \right) (iK) V_z -$$

$$-\epsilon\gamma\frac{dV_{0z}}{dz}\rho_0V_A^2\nabla\cdot\mathbf{V}-\frac{B_{0z}}{\mu_0}\frac{dB_{0z}}{dr}\epsilon\gamma\frac{dV_{0z}}{dz}V_r \quad (7.40)$$

Gathering together terms of equal order in  $\epsilon$  allows for the following to be written

$$\begin{aligned} & -\varpi^2P - i\rho_0(c^2 + V_A^2)\varpi\nabla\cdot\mathbf{V} - KV_A^2\varpi V_z = \\ & +\epsilon\left(i\varpi\gamma\frac{dV_{0z}}{dz}P + i\rho_0V_A^2\gamma\frac{dV_{0z}}{dz}KV_z - \gamma\rho_0V_A^2\frac{dV_{0z}}{dz}\nabla\cdot\mathbf{V} + i\frac{B_{0z}}{\mu_0}\frac{dB_{0z}}{dr}\varpi V_r - \gamma\frac{B_{0z}}{\mu_0}\frac{dB_{0z}}{dr}\frac{dV_{0z}}{dr}V_r\right) \end{aligned} \quad (7.41)$$

It is clear that to lowest order, in the small parameter,  $\epsilon$ , equation (7.41) reduces to

$$-\varpi^2P = i\rho_0(c^2 + V_A^2)\varpi\nabla\cdot\mathbf{V} + KV_A^2\varpi V_z$$

We can note that all the temporal and vertical derivatives of the background quantities have now been reduced to lower order effects and only the derivatives of the perturbed quantities remain. This reduction is attributed to the slowly varying nature of the background plasma, i.e. the constant  $A$  is small. The radial derivatives of the background quantities remain as a result of the stretching of the radial coordinate. A similar simplification can be seen from the other four governing equations and they also reduce to

$$\rho_0(\varpi^2 - \varpi_A^2)\nabla\cdot\mathbf{V} = \rho_0(\varpi^2 - \varpi_A^2)\frac{1}{r}\frac{\partial(rV_r)}{\partial r} + i\varpi\frac{m^2}{r^2}P - i\rho_0(\varpi^2 - \varpi_A^2)KV_z \quad (7.42)$$

$$\rho_0(\varpi^2 - \varpi_A^2)V_r = -i\varpi\frac{\partial P}{\partial r} \quad (7.43)$$

$$i\varpi\rho_0(\varpi^2 - \varpi_A^2)V_z = i\varpi^2KP - \varpi\rho_0V_A^2K\nabla\cdot\mathbf{V} \quad (7.44)$$

At this point we have a series of expressions which can now be algebraically combined into the two governing equations, as stated in equations (3.20) and (3.21). The same analysis can be applied to the third of the governing equations discussed in Chapter 3, giving equation (3.22).

# Bibliography

Abramowitz M and Stegun I A 1972 Handbook of Mathematical Functions New York: Dover Publications.

Andries J, Goossens M, Hollweg J V, Arregui I and Van Doorselaere T 2005 Astron. Astrophys. **430**, 1109–1118.

Andries J, Van Doorselaere T, Roberts B, Verth G and Verwichte, E Erdélyi R 2009 Space Science Review **149**, 3–29.

Arregui I, Oliver R and Ballester J L 2012 Living Reviews in Solar Physics **9**, 2.

Arregui I, Van Doorselaere T, Andries J, Goossens M and Kimpe D 2005 Astron. Astrophys. **441**, 361–370.

Aschwanden M J 2004 Physics of the Solar Corona. An Introduction Praxis Publishing Ltd.

Aschwanden M J and Title A M 2004 in A. K Dupree and A. O Benz, eds, ‘Stars as Suns : Activity, Evolution and Planets’ Vol. 219 of IAU Symposium p. 503.

Ballai I and Erdélyi R 1998 Sol. Phys. **180**, 65–79.

Ballai I and Ruderman M S 2011 Space Sci. Rev. **158**, 421–450.

Banerjee D, Gupta G R and Teriaca L 2011 Space Sci. Rev. **158**, 267–288.

Bender C M and Orszag S A 1978 Advanced Mathematical Methods for Scientists and Engineers, New York: McGraw-Hill.

- Berghmans D and Clette F 1999 Sol. Phys. **186**, 207–229.
- Cadez V M and Ballester J L 1996 Astron. Astrophys. **305**, 977.
- Cally P S 1986 Sol. Phys. **103**, 277–298.
- Corless R, Gonnet G, Hare D, Jeffrey D and Knuth D 1996 Advances in Computational Mathematics **5**, 329–359.
- Csík A, Erdélyi R and Cadez V M 1997 Sol. Phys. **172**, 61–68.
- de Moortel I 2009 Space. Sci. Rev. **149**, 65–81.
- De Moortel I, Ireland J and Walsh R 2000 Astron. Astrophys. **457**, L23–L26.
- De Moortel I and Nakariakov V M 2012 Royal Society of London Philosophical Transactions Series A **370**, 3193–3216.
- Defouw R J 1976 Astrophysical Journal **209**, 266–269.
- Dymova M and Ruderman M 2006 Astron. Astrophys. **457**, 1059–1070.
- Edwin P and Roberts B 1983a Sol. Phys. **88**, 179–191.
- Edwin P and Roberts B 1983b Sol. Phys. **76**, 239–259.
- Erdélyi R 1998 Sol. Phys. **180**, 213–229.
- Erdélyi R and Ballai I 1999 Sol. Phys. **186**, 67–97.
- Erdélyi R and Ballai I 2007 Astronomische Nachrichten **328**, 726–733.
- Erdélyi R and Fedun V 2010a Sol. Phys. **263**, 63–85.
- Erdélyi R and Fedun V 2010b Sol. Phys. **263**, 63–85.
- Erdélyi R and Goossens M 1994 Astrophys. Space Sci. **213**, 273–298.
- Erdélyi R and Goossens M 1996 Astron. Astrophys. **313**, 664–673.
- Erdélyi R, Goossens M and Ruderman M 1995a Sol. Phys. **161**, 123–138.

- Erdélyi R, Goossens M and Ruderman M S 1995b Sol. Phys. **161**, 123–138.
- Erdélyi R and Verth G 2007 Astron. Astrophys. **462**, 743–751.
- Goedbloed H and Poedts S 2004 Principles of Magnetohydrodynamics Cambridge University Press.
- Goossens M, Andries J and Aschwanden M J 2002 Astron. Astrophys. **394**, L39–L42.
- Goossens M, ed. 2003 Vol. 294 of Astrophysics and Space Science Library.
- Goossens M, Erdélyi R and Ruderman M 2011 Space Science Review **158**, 289–338.
- Goossens M and Hollweg J V 1993 Sol. Phys. **145**, 19–44.
- Goossens M, Hollweg J V and Sakurai T 1992a Solar Phycis **138**, 233–255.
- Goossens M, Hollweg, J V and Sakurai T 1992b Sol. Phys. **138**, 233–255.
- Goossens M, Ruderman M and Hollweg J 1995 Sol. Phys. **157**, 75–102.
- Goossens M, Terradas J, Andries J, Arregui I and Ballester J L 2009 Astron. Astrophys. **503**, 213–223.
- Hasan S S 2008 Advances in Space Research **42**, 86–95.
- Hasegawa A and Chen L 1974 Physical Review Letters **32**, 454–456.
- Hollweg J V 1978 Sol. Phys. **56**, 305–333.
- Hollweg J V 1988 Astrophys. J. **335**, 1005–1014.
- Hollweg J and Yang G 1998 Geophysical Research **93**, 5423–5436.
- Ionson, J A 1978 The Astrophysical Journal **226**, 650–673.
- Krall N A and Trivelpiece A W 1973 Principles of plasma physics New York: McGraw-Hill.

- Mathioudakis M, Jess D and Erdelyi R 2012 Space Sci. Rev. .
- Milligan R O, Gallagher P T, Mathioudakis M, Bloomfield D S, Keenan F P and Schwartz R A 2006 Astrophys. JI **638**, L117–L120.
- Nakariakov V M and Verwichte E 2005 Living Reviews in Solar Physics **2**, 3.
- Narayanan A S 1991 Plasma Physics and Controlled Fusion **33**, 333–338.
- Ofman L and Wang T J 2008 Astron. Astrophys. **482**, L9–L12.
- O’Shea E, Banerjee D, Doyle J, Fleck B and Murtagh F 2001 Astron. Astrophys. **368**, 1095–1107.
- Parnell C E and De Moortel I 2012 Royal Society of London Philosophical Transactions Series A **370**, 3217–3240.
- Roberts B 1981a Sol. Phys. **69**, 27–38.
- Roberts B 1981b Sol. Phys. **69**, 39–56.
- Roberts B 2000 Sol. Phys. **193**, 139–152.
- Roberts B 2006 Royal Society of London Philosophical Transactions Series A **364**, 447–460.
- Ruderman M 2010 Sol. Phys. **267**, 377–391.
- Ruderman M 2011 Sol. Phys. **271**, 41–54.
- Ruderman M and Erdélyi R 2009 Space Science Review **149**, 199–228.
- Ruderman M S and Roberts B 2002 Astrophysical Journal **577**, 475–486.
- Sakurai T, Goossens M and Hollweg J 1991 Sol. Phys. **133**, 227–245.
- Spruit H C 1979 Sol. Phys. **61**, 363–378.
- Spruit H C 1982 Sol. Phys. **75**, 3–17.

- Stenuit H, Tirry W J, Keppens R and Goossens M 1999 Astron. Astrophys. **342**, 863–866.
- Tataronis J and Grossmann W 1973 Z. P. **261**, 203–216.
- Terra-Homem M, Erdélyi R and Ballai I 2003 Sol. Phys. **217**, 199–223.
- Terradas J 2009 Space Sci. Rev. **149**, 255–282.
- Terradas J, Arregui I, Verth G and Goossens M 2011 Astrophys. J **729**, L22.
- Terradas J, Goossens M and Verth G 2010 Astronomy and Astrophysics **524**, A23.
- Tirry W J and Goossens M 1996 Astrophys. J. **471**, 501.
- van Doorselaere T, Arregui I, Andries J, Goossens M and Poedts S 2005 Space Science Rev. **121**, 79–89.
- Verth G and Erdélyi R 2008 Astron. Astrophys. **486**, 1015–1022.
- Verth G, Terradas J and Goossens M 2010 Astrophysical Journal **718**, L102–L105.
- Wang T 2011 Space Science Review **158**, 397–419.
- Williamson A and Erdélyi R 2013-in Press Sol. Phys. .
- Wilson P R 1979 Astron. Astrophys. **71**, 9–13.
- Zhugzhda Y D and Goossens M 2001 Astron. Astrophys. **377**, 330–342.